2023

Investigation of Microbiome Metabolites and Mitochondrial Function in a model of Non-Alcoholic Fatty Liver Disease

Boeira, Paula

COPYRIGHT STATEMENT

UNIVERSITY OF PLYMOUTH

INVESTIGATION OF MICROBIOME METABOLITES AND MITOCHONDRIAL FUNCTION IN A MODEL OF NON-ALCOHOLIC FATTY LIVER DISEASE

by

PAULA BOEIRA

A thesis submitted to the University of Plymouth

in partial fulfilment for the degree of

DOCTOR OF PHILOSOPHY

Peninsula Medical School

May 2023

ACKNOWLEDGEMENTS

I am extremely lucky to be surrounded by so many amazing people who supported me throughout this process. First, I would like to express my immense gratitude to my mom, even far away she always supported me regardless. This is for you and I hope I made you proud.

All my awesome friends in Brazil, thank you for keeping me sane during the most challenging times and always making me laugh.

I had so much great support at the laboratory, I would like to thank Dr. Jane Carré for all the help with the endless seahorses and Dr. Paul Waines for keeping everyone in line.

All my colleagues from the Hepatology Research Group. I am so thankful for this research group who helped me so much! I have no words to express my gratitude to Dr. Matthew Cramp who had my back during the most difficult times.

And last but not least my supervisory team. Dr. Daniel Felmlee for all the lifts and laughter. Dr. Charles Affourtit whose passion for science is a true inspiration.

And finally, my director of studies, Dr. David Sheridan. I could not have asked for a better DoS. You were always there to help me and encourage me when I was frustrated with failed experiments. I could not have done it without your support.

"DE CAXIAS PARA O MUNDO"

AUTHOR DECLARATION

At no time during the registration for the degree of Doctor of Philosophy has the author been registered for any other University award without prior agreement of the Doctoral College Quality Sub-Committee.

Work submitted for this research degree at the University of Plymouth has not formed part of any other degree either at the University of Plymouth or at another establishment.

This study was financed with the aid of a studentship from the University of Plymouth, Faculty of Health: Medicine, Dentistry and Human Sciences and a grant from the Northcott Devon Medical foundation.

Word count of main body of thesis: 19821

Signed 

Date 09/05/2023

IMPACT OF COVID-19 PANDEMIC

The Covid-19 pandemic has been an extremely challenging time. Due to the virus outbreak our research laboratory closed their doors for four months. This closure caused a great delay to my experiments since to obtain fully differentiated HepaRG cells for my study it takes up to two months. During this difficult period, I joined the study named Immune Biomarkers of Outcome from COVID-19 (IBOC) where we looked for markers of immune function in 46 COVID patients.

(*Dhanda AD, Felmlee D, Boeira P, et al. Patients with moderate to severe COVID-19 have an impaired cytokine response with an exhausted and senescent immune phenotype. Immunobiology. 2022;227(2):152185. doi:10.1016/j.imbio.2022.152185*)

ABSTRACT

INVESTIGATION OF MICROBIOME METABOLITES AND MITOCHONDRIAL FUNCTION IN A MODEL OF NON-ALCOHOLIC FATTY LIVER DISEASE

PAULA BOEIRA

Several dietary metabolites produced by gut bacteria have been linked to disease including non-alcoholic fatty liver disease (NAFLD). Trimethylamine N-oxide (TMAO) and phenylacetic acid (PAA) are microbiome-derived metabolites that have been associated with early onset of NAFLD. Hypothesising that these metabolites contribute to lipid deposition in the liver by altering hepatic mitochondrial function, we assessed how TMAO and PAA affect hepatocyte bioenergetics in cell models of liver steatosis.

Proliferative and differentiated HepaRG cells were cultured under standard conditions, and steatosis was established by 48h exposure to oleate and palmitate (2:1 molar ratio). Lipid accumulation was assessed by BODIPY™ staining and quantified by CellProfiler software. To gain insight into HepaRG mitochondrial respiration, we measured a number of bioenergetic parameters with the Seahorse extracellular flux analyser in control cells and cells exposed to PAA (100 µM and 200 µM) or TMAO (20 µM, 50 µM, 100 µM and 200 µM).

PAA and TMAO led to an increase in lipid deposition in HepaRG cells. TMAO caused a 42% increase in lipid accumulation in proliferative cells and 1.6% in differentiated HepaRG cells while PAA exacerbated intracellular lipid droplets by 54% in proliferative HepaRG and by 10% in fully differentiated cells. The same effects were seen in mitochondrial function. PAA and TMAO lowered spare respiratory capacity dose-dependently, maximal respiration and

basal oxygen consumption in HepaRG cells. In addition, the decline in mitochondrial function preceded lipid accumulation. Our data indicate that microbiome-derived compounds decrease mitochondrial capacity significantly and exacerbate lipid deposition suggesting a potential link between microbiome metabolite driven mitochondrial dysfunction and NAFLD onset.

TABLE OF CONTENTS

CONTENTS

LIST OF FIGURES

LIST OF TABLES

LIST OF ABBREVIATIONS

2D Two dimensional

3D Three dimensional

AASLD American Association for the Study of Liver Diseases

ADP Adenosine di-phosphate

ALT Alanine aminotransferase

ANOVA Analysis of variance

ASK-1 Apoptosis signal-regulating kinase 1

AST Aspartate transaminase

ATP Adenosine triphosphate

BAM15 N5,N6-Bis(2-fluorophenyl)[2,1,3]oxadiazolo[4,5-b]pyrazine-5,6-diamine

BCA Bicinchoninic acid assay

BMI Body max index

BSA Bovine serum albumin

CAT2 Category two

CO_2 Carbon dioxide

COVID Coronavirus

CPT1 Carnitine palmitoyltransferase I

CT Cycle threshold

CYP Cytochrome

DAMPs Damage-associated molecular patterns

DAPI 4’,6-diamidino-2-phenylindole

DMEM Dulbecco's modified eagle medium

DMSO Dimethyl sulfoxide

DNA Deoxyribonucleic acid

EASL European Association for the Study of the Liver

ECAR Extracellular acidification rate

EMA European Medicines Agency

ER Endoplasmic reticulum

EUK Eukarion

FBS Faetal bovine serum

FCCP Carbonyl cyanide p-trifluoromethoxyphenylhydrazone

FDA Food and Drug Administration

FFAs Free fatty acids

FMO Flavin-containing monooxygenases

FXR Farnesoid X receptor

HCC Hepatocellular carcinoma

HEPES 4-(2-hydroxyethyl)-1-piperazineethanesulfonic acid

HNF4a Hepatocyte nuclear factor 4 Alpha

HPRT1 Hypoxanthine phosphoribosyltransferase 1

IL Interleukin

K Thousand

KCl Potassium chloride buffer

MDR1 Multidrug resistance 1

MRP2 Multi-drug resistance protein 2

mtDNA Mitochondrial deoxyribonucleic acid

NAFLD Non-alcoholic fatty liver disease

NAS NAFLD Activity Score

NASH Non-alcoholic steatohepatitis

NHS National Health Service

OCR Oxygen consumption rate

OXPHOS Oxidative phosphorylation

PA Phenylalanine

PAA Phenylacetic acid

PBS Phosphate-buffered saline

PCLS Precision cut liver slices

PCR Polymerase chain reaction

PHH Primary human hepatocyte

PMOL picomole

PNPLA3 Patatin-like phospholipase domain containing 3

PPARs Peroxisome proliferator-activated receptors

RNA Ribonucleic acid

ROS Reactive oxygen species

SAF Steatosis, activity and fibrosis

SD Standard deviation

SGLT Sodium-dependent glucose cotransporter

SS Szeto-schiller

TCA Tricarboxylic acid cycle

TMA Trimethylamine

TMAO Trimethylamine N-oxide

TM6SF2 Transmembrane 6 Superfamily Member 2

TNF α - tumour Necrosis Factor alpha

UK United Kingdom

US United States

USA United States of America

VLDL Very-low-density lipoprotein

VS Versus

WEM William's E medium

CHAPTER 1.

INTRODUCTION

1.1 DEFINITION OF NON-ALCOHOLIC FATTY LIVER DISEASE (NAFLD)

Non-alcoholic fatty liver disease (NAFLD) was first described in 1980 and represents a spectrum of liver disease, ranging from steatosis to more progressive forms of non-alcoholic steatohepatitis (NASH), fibrosis, cirrhosis and ultimately hepatocellular carcinoma (HCC) and liver failure, in the absence of a history of excess alcohol consumption (Anstee, McPherson & Day, 2011). NAFLD is the most common cause of liver disease worldwide (Rinella, 2015). Most patients with NAFLD are asymptomatic and when symptoms occur, they are commonly nonspecific. When symptoms are present, they usually include fatigue and discomfort in the upper right side of the abdomen (Day, 2011). People who are overweight or obese are the most affected by NAFLD. It is estimated up to 1 in every 3 people in the UK has the early stages of NAFLD, steatosis, where small amounts of fat start to accumulate in the liver (Figure 1.1) (Williamson *et al.*, 2011).

A small percentage of NAFLD patients will develop NASH. NASH is a more severe state, and it differs from simple steatosis by hepatocellular ballooning, lobular inflammation and fibrosis. NASH prevalence worldwide ranges from 2% to 10%, and it is estimated that approximately 5% of the UK population has NASH. Cirrhosis occurs in a minority of NASH patients, around 5% to 12% of people with NASH will progress to cirrhosis. In addition, cirrhosis associated to NASH accounts for nearly 13% of all cases of HCC (Delgado, 2008). The percentage of patients receiving a liver transplant due to NASH is progressively increasing in Europe from 1% in 2007 to 6% in 2017 (Durand, 2019).

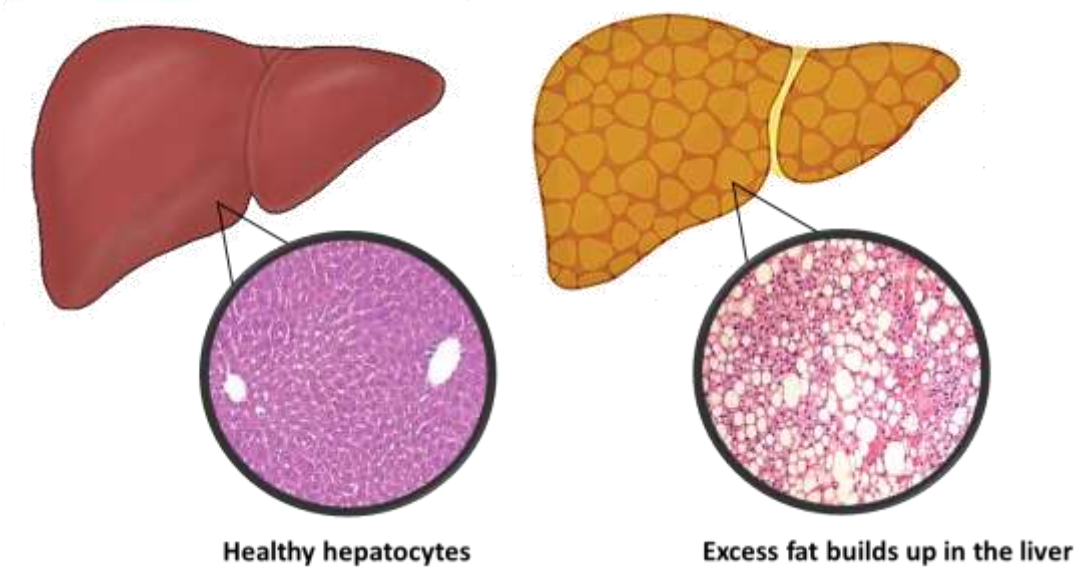

Figure 1.1. Representative images of a healthy liver and a liver with NAFLD. Histological images stained with haematoxylin and eosin show healthy liver with uniform arrangements of hepatocytes (left) in contrast with NAFLD liver with macrovesicular steatosis (right).

1.2 GLOBAL EPIDEMIOLOGY OF NAFLD

Globalisation has led to an increase in office jobs, rapid changes in diet and high levels of physical inactivity resulting in a more sedentary lifestyle with an excess of caloric intake in many parts of the world (Popkin, 2012). This phenomenon represents a significant negative impact on the overall health of populations, especially in developing countries and those experiencing fast socioeconomic transition. Emerging economies, such as India and China, have experienced a dramatic increase in sedentary lifestyle combined with dietary excess and shift to western diet. These factors are the main drivers of obesity, metabolic syndrome and NAFLD in most parts of the world (Misra & Khurana L, 2008).

NAFLD is one of the most significant causes of liver disease and is projected to be the primary cause of end-stage liver disease in the coming years, with the disease affecting both adults and children (Younossi *et al.*, 2018). Driven by the obesity epidemic, the global prevalence of NAFLD is currently estimated to be 24%. NAFLD is a worrying and growing burden on European healthcare (Schattenberg & Ekstedt, 2019). A study published in 2016 reported an average prevalence of 24% in Europe, varying from 5% to 44% in different countries. Approximately 15 million people have NAFLD in the UK, while it is estimated that 12 million people are affected by NAFLD in Germany, 14 million in France and 10 million in Italy (O'Hara, 2020).

1.3 NATURAL HISTORY

The natural history of NAFLD is variable. A number of risk factors are associated with NASH development and include presence of type 2 diabetes, hypertension, dyslipidaemia, and obesity (Fazel *et al.*, 2016). Most patients with NAFLD will not progress to NASH; however a significant percentage will develop hepatocellular injury (ballooning), inflammation and progressive liver fibrosis, the features of NASH. 20–30% of the patients with steatosis alone can progress to NASH over 3 years (Anstee, McPherson & Day, 2011). In addition, patients with a severe stage of NASH may develop cirrhosis. Cirrhosis is then a major risk for patients developing HCC. It is estimated that NAFLD and NASH will become the most common risk factors for HCC and liver transplantation in the coming years (Tateishi & Koike, 2017). Even in the absence of fibrosis and cirrhosis, NASH patients may develop HCC, with studies showing a 2–20% 5-year cumulative HCC incidence (Onzi et al., 2019).

1.4 DIAGNOSIS

Diagnosing fatty liver disease is a major challenge since NAFLD and NASH are frequently silent diseases. Consequently, NASH patients remain unacquainted of their condition until the disease develops into a more severe and life-threatening stage. 0.6% of NAFLD is diagnosed when they are symptomatic in a more advanced stage of liver disease (Pheasant, 2019). The presumptive diagnosis of NAFLD is made through a liver function blood test, where patients show persistent elevated serum aminotransferases with a positive imaging scan for hepatic steatosis and no history of excessive alcohol use. However, these routine tests are not sufficient on their own to be used as consistent diagnostic tools for NASH. In order to confirm NASH and exclude other coincident liver diseases, the current gold standard for NASH diagnosis is a liver biopsy (Chalasani *et al.*, 2018). Liver biopsy is an invasive, costly diagnostic tool and sampling errors can result in misdiagnosis and staging inaccuracies. Yet liver biopsies are essential to provide an assessment of hepatic steatosis, hepatocellular ballooning, inflammation and fibrosis. The presence of hepatocyte ballooning in association with steatosis is the main histological feature that differentiates NASH from simple steatosis (Figure 1.2) (Dyson, Anstee & McPherson, 2014).

The 'NAFLD activity score' (NAS) is the most used grading and staging system for NAFLD in histological samples. NAS represents the sum of scores for steatosis, lobular inflammation, and ballooning, and ranges from 0-8 (Brunt *et al.*, 2011). The SAF score has been introduced more recently and is a more accurate way to identify NASH. The SAF score comprises of an assessment of steatosis (S), activity (A) and fibrosis (F) (Hagström, 2017). The majority of patients with NAFLD can be diagnosed and staged adequately using non-invasive

approaches. However, the only feature that can predict liver-related mortality is hepatic fibrosis determined by liver histology (Angulo *et al.*, 2015).

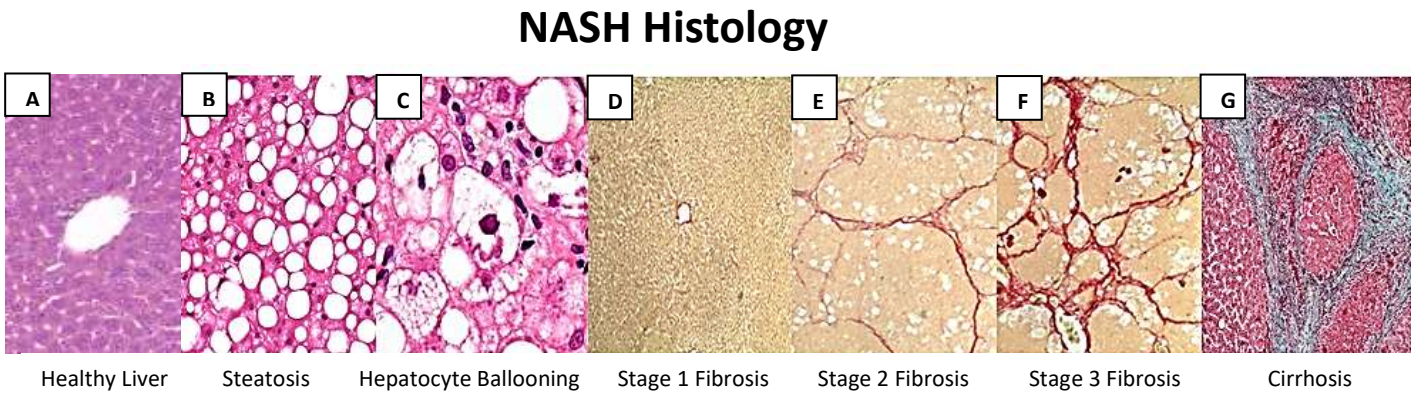

Figure 1.2. NASH Histology. Haematoxylin and eosin staining shows uniform healthy hepatocytes (A), simple liver steatosis (B) and hepatocyte ballooning (C). Sirius red staining shows fibrosis at stage 1 (D), stage 2 (E) and stage 3 (F). Trichrome staining shows cirrhotic liver with fibrosis, nodular regeneration and distortion of hepatic architecture (G).

1.5 PATHOGENESIS OF NASH

1.5.1 LIPOTOXICITY

Lipotoxicity is defined as an imbalance in the intracellular lipid composition, causing accumulation of lipids, which can cause organelle dysfunction, cell injury, and apoptosis. Emerging data indicate that toxic lipids cause hepatocyte injury displayed as endoplasmic reticulum (ER) stress, inflammation, apoptosis, and hepatocyte ballooning (Neuschwander-Tetri, 2010). Hepatic lipotoxicity will trigger several pathways which will activate an inflammatory cascade (Figure 1.3) (Marra & Svegliati-Baroni, 2018). In addition, the production of lipotoxic lipids typically occurs alongside with the accumulation of triglyceride droplets (steatosis), resulting in a NASH phenotype where steatosis and features of

hepatocellular injury are present together (Neuschwander-Tetri, 2010). The activation of lipotoxic pathways can be considered a critical event in the pathogenesis of NAFLD and NASH (Ibrahim, Hirsova & Gores, 2018). The pathogenesis of NASH is far from being fully understood, the model describing toxic lipids implies that mitochondrial damage occurs as a consequence of lipotoxicity. However, the sequence of events remains unknown and further investigation is needed.

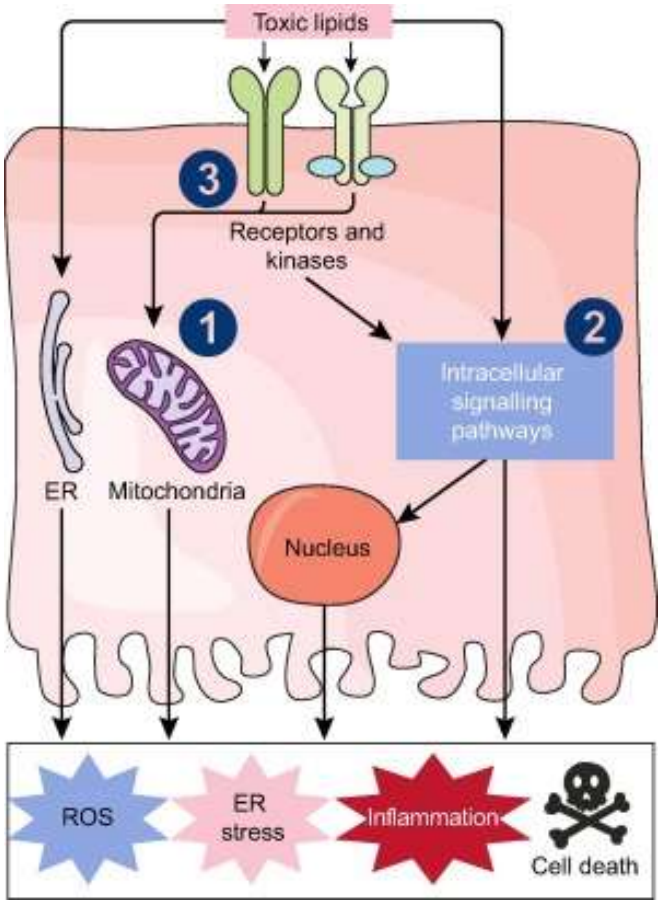

Figure 1.3. Putative Mechanisms of lipotoxicity. (1) Toxic lipids may directly disturb organelles like ER and mitochondria. (2) Alteration in intracellular signalling pathways by toxic lipids may affect metabolic and inflammatory pathways. (3) Interaction between lipids and kinases indirectly changes signalling, leading to ROS, ER stress, cell death and inflammation. Adapted from (Marra & Svegliati-Baroni, 2018).

1.5.2 PATHOGENESIS HYPOTHESES

The factors and sequence of cellular injury leading to progressive NASH and inflammation are not completely understood. A generally used working model describes that multiple “pathogenic hits” are required for the progressive development of fatty liver disease (Ganz *et al*., 2015). The historic “two hit” hypothesis involves numerous insults occurring at the same time on genetically predisposed subjects to induce NAFLD and offers a more precise explanation of NAFLD pathogenesis.

Dietary habits, environmental and genetic factors (e.g. PNPLA3 and TM6SF2) can trigger the development of insulin resistance and changes in gut microbiome (Anstee & Day, 2015). Altered gut microbiome leads to further production of fatty acids in the gut raising circulating levels of molecules which induce inflammatory pathways and release proinflammatory cytokines (Figure 1.4). In subjects predisposed by genetic factors, all these insults affect hepatocyte lipid content and liver inflammation, consequently leading to chronic hepatic inflammation via upregulation of cellular injury pathways, with possible progression to hepatocellular death (Buzzetti, Pinzani & Tsochatzis, 2016). Furthermore, injured hepatocytes secrete damage-associated molecular pattern molecules (DAMPs) that trigger inflammation leading to the recruitment of neutrophils and macrophages (Magee, Zou & Zhang, 2016).

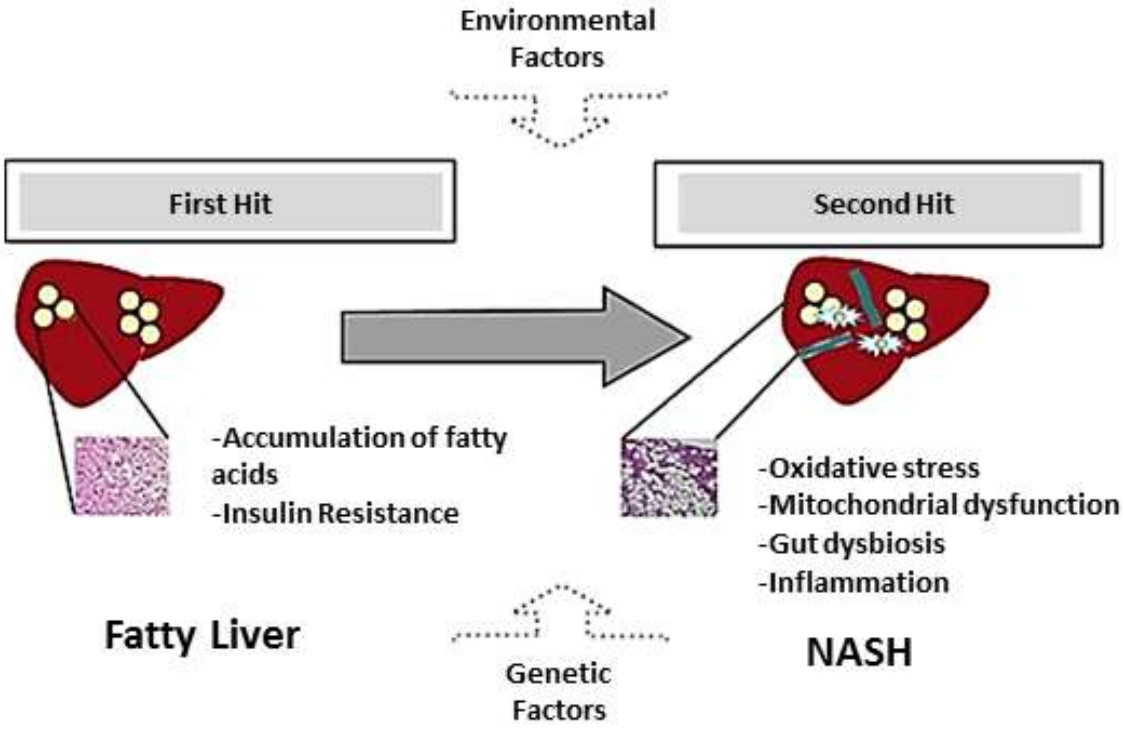

Figure 1.4. Two hit hypothesis. The first hit comprises of intrahepatic build-up of fatty acids, which is linked to insulin resistance, and leads to hepatocytes becoming more susceptible to secondary injuries (oxidative stress, mitochondrial dysfunction, gut dysbiosis and production of pro-inflammatory cytokines). Adapted from (Alisi *et al.*, 2011).

1.6 MITOCHONDRIA

Mitochondria dysfunction has recently been implicated in NASH pathogenesis. Mitochondria serve as the powerhouse of the cells generating ATP or heat by using substrates originated from fat and glucose. Most of the energy obtained from the breakdown of carbohydrates or fats is derived by oxidative phosphorylation (OXPHOS). OXPHOS is a fundamental mitochondrial process, linking the tricarboxylic acid (TCA) cycle to the production of ATP (Wilson, 2017). OXPHOS is a highly efficient method of producing large amounts of ATP as energy, however the liver primarily uses fatty acid oxidation as its energy

source (Wilson, 2017). Hepatocytes are normally rich in mitochondria and each hepatocyte contains approximately 800 mitochondria occupying about 18% of the entire liver cell volume (Nassir & Ibdah, 2014). Mitochondria play a key role in hepatocyte metabolism, being the main site for fatty acid β-oxidation (Osellame, Blacker & Duchen, 2012).

β-oxidation is a process by which fatty acids are broken down by different tissues generating energy. Fatty acids are removed from the cytosol and then transferred to the mitochondria where β-oxidation occurs (Schulz, 1991). Mitochondrial β-oxidation is the main oxidative pathway for the clearance of fatty acids under physiologic conditions and consists of the oxidation of short-chain, medium-chain, and long-chain free fatty acids (FFAs). Short-chain and medium-chain FFAs freely enter the mitochondria, while long-chain FFAs require carnitine palmitoyltransferase I enzyme (CPT1) to be translocated across the mitochondrial membrane (Wan *et al*., 2008). Impaired β-oxidation and a reduction in mitochondrial quality, have been suggested to play a key role in NAFLD onset and progression to NASH (Ramanathan *et al*., 2022).

1.7 GUT MICROBIOME

The human intestinal microbiome plays a key role in regulating metabolic and immune functions, and alterations in microbiome composition (dysbiosis) have been linked to several human diseases including inflammatory bowel disease, obesity, type 2 diabetes, Alzheimer, obesity, and colorectal cancer (Wieland *et al*., 2015; Baptista *et al*., 2020). The link of the liver and gut starts from early embryology with the liver maturing directly from the foregut. This connection is maintained in adult life with the liver obtaining 75% of its blood flow directly from the intestinal portal circulation. Because of the strong anatomical link between the

intestines and the liver, it is hypothesised that gut dysbiosis may affect hepatic function and contribute to the pathogenesis of NAFLD (Wieland *et al*., 2015). It has been shown that in patients with NAFLD, the microbiome's abundance and diversity is altered. A significant increase of bacterial species, such as *Proteobacteria*, *Enterobacteria*, E*scherichia* and *Bacteroides* was found in patients with NASH when compared to matched healthy individuals (Zhu et al, 2013; Boursier et al, 2016). Faecal transplantation from mice with NAFLD into wild-type mice caused NAFLD in mice that received the microbiome (Le Roy *et al.*, 2013). Studies also suggest a role for the gut microbiome in the progression of NAFLD to NASH. Miele *et al*. found a higher prevalence of small intestinal bacteria overgrowth in NAFLD patients, correlated with the severity of steatosis (Miele *et al.*, 2009). One of the potential mechanisms linking microbiome to NAFLD is altering the efficiency of energy harvest from food, with description of an obesogenic gut flora that can be transmitted in germ free mice. However, there are also potential metabolic perturbations resulting from secondary metabolites, such as methylamines (Figure 1.5) (Zelber-Sagi *et al.*, 2018).

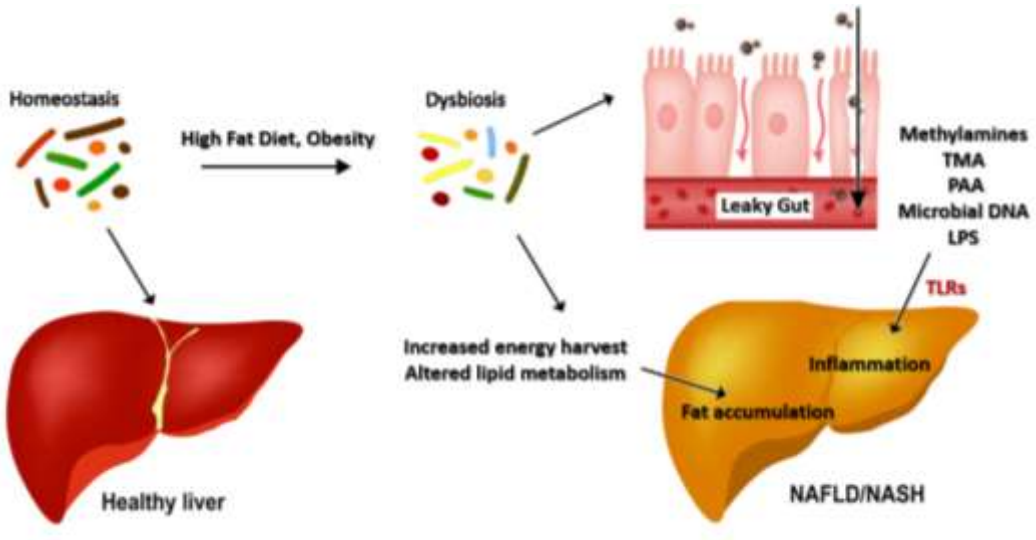

Figure 1.5. Schematic representation of the proposed mechanisms between gut dysbiosis and NAFLD/NASH development. Gut microbiome imbalance leads to higher energy harvest, altered lipid metabolism and increased gut permeability. Leaky intestinal tight junction barrier

allows bacteria metabolites and microbial DNA translocation driving inflammation via Toll-like receptors.

1.8 GUT MICROBIOME METABOLITES

Several metabolites produced by the gut microbiome from our diet have been associated to pathologies such as atherosclerosis, hypertension, heart failure, chronic kidney disease, NAFLD, obesity, and type 2 diabetes mellitus (Tang *et al*., 2017). These findings suggest that the gut microbiome can produce bioactive metabolites that can directly or indirectly affect host homeostasis and health (Clarke *et al*., 2014).

1.9 METHYLAMINES

Choline is an essential component of biological membranes and necessary for lipid export into very low-density lipoprotein (VLDL) from the liver. Feeding mice a choline deficient diet is a commonly used nutritional model of NASH. This diet mimics the pathological findings of severe human NASH, however also leads to acute weight loss (Lau, Zhang & Yu, 2017). Gut microbiome is essential for catalysing the conversion of dietary choline to methylamines (Corbin, Schwarz & Sonnichsen, 1997). Toxic methylamines will activate inflammatory pathways leading to hepatic inflammation and injury. The conversion of choline to methylamines also reduces the bioavailability of choline, leading to impaired VLDL export and promoting steatosis (Figure 1.6) (Zelber-Sagi *et al*., 2018). Methylamines also prompt hepatotoxicity and hepatocarcinogenicity in rats (Lin & Ho, 1992). These findings taken together suggest that the gut microbiome may play a critical role in NAFLD progression by

causing relative choline deficiency and by increasing toxic methylamines (Williams & Taylor-Robinson, 2016).

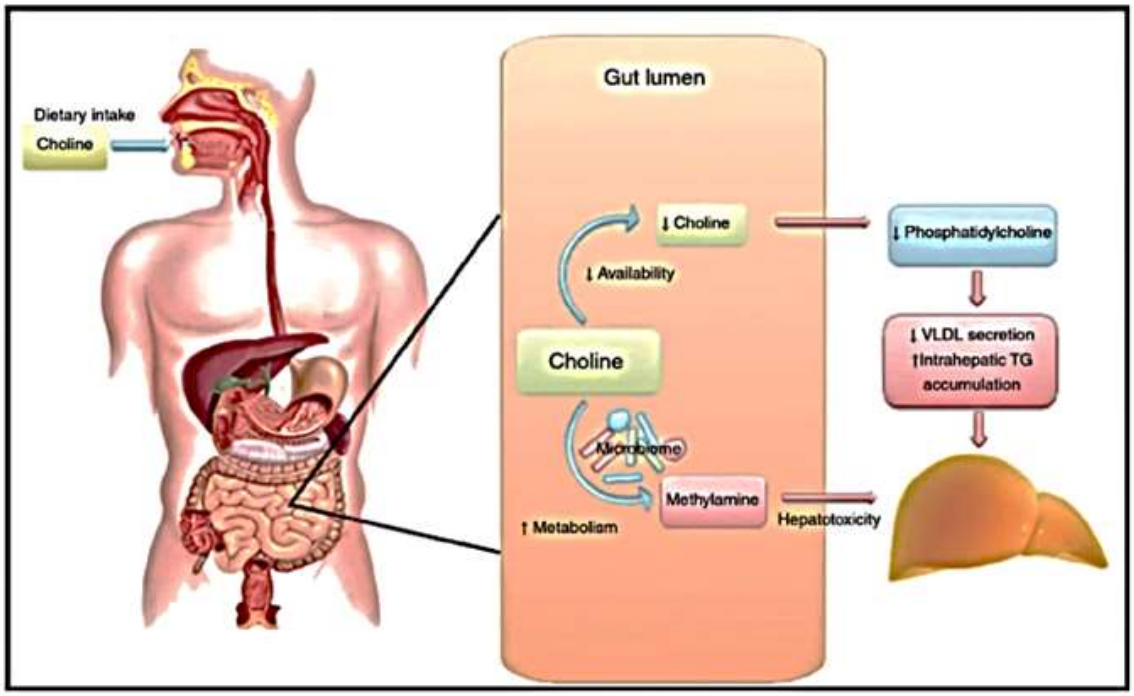

Figure 1.6. Gut microbiome shifts can lead to NAFLD. The gut is responsible for converting choline from our diet into methylamines, which enter the portal circulation and trigger hepatocellular damage. Choline conversion decreases choline availability leading to lower VLDL secretion and increased steatosis. Adapted from (Williams & Taylor-Robinson, 2016).

1.9.1 TRIMETHYLAMINE N-OXIDE

Trimethylamine N-oxide (TMAO) is a product of the oxidation of trimethylamine (TMA). Sources of TMA are foods containing choline, lecithin, and L-carnitine (mainly fish, meat, egg, and dairy). Gut bacteria metabolizes these dietary components forming TMA. TMA in the gut is oxidized by hepatic flavin containing monooxygenases (FMO) FMO3 and

FMO1 (Zhu *et al*., 2018). FMOs main function is to add molecular oxygen to lipophilic compounds, making them soluble to ensure rapid excretion. In humans, FMOs are primarily expressed in the liver, lungs, and kidneys, where most of the metabolism of xenobiotics occur. FMO1 has a lower specific activity in the liver compared to FMO3, FMO3 is the main enzyme responsible for the conversion of TMA into TMAO (Fennema *et al*., 2016).

In most studies, TMAO is measured in urine and plasma samples although it is can also be measured in serum (Burton *et al*., 2020; Lombardo *et al*. 2021). Circulating levels of TMAO are highly variable and are determined by different factors, such as diet, gut microbiome diversity, liver FMO enzymes and kidney function. High levels of TMAO have been linked to increased risk of cardiovascular disease and all-cause mortality (Mahdieh, 2020). Roncal *et al*. observed that people with elevated TMAO levels have 60% higher risk of major adverse cardiovascular events when compared to lower TMAO blood levels (Roncal *et al*., 2019). TMAO has also been linked to heart failure and chronic kidney disease (Figure 1.7) (Janeiro *et al*., 2018).

Besides cardiovascular disease, high TMAO levels have also been associated with elevated risk of developing NAFLD. Mice fed a high-fat diet containing TMAO developed impaired liver function (high AST levels) and increased hepatic triglyceride deposition. TMAO supplementation also significantly increased liver weight and liver/body weight ratio after 18-week TMAO supplementation (Tan *et al*., 2019). In humans, TMAO and choline levels were significantly linked with NAFLD histology and increased NASH risk. A study showed that Chinese adults with higher circulating levels of TMAO presented a greater severity of NAFLD (Chen *et al*., 2016). While other study demonstrated that serum TMAO levels were

approximately 4 times greater in NAFLD patients than in the controls. The link between TMAO and NAFLD remains poorly explored (León-Mimila *et al*., 2021).

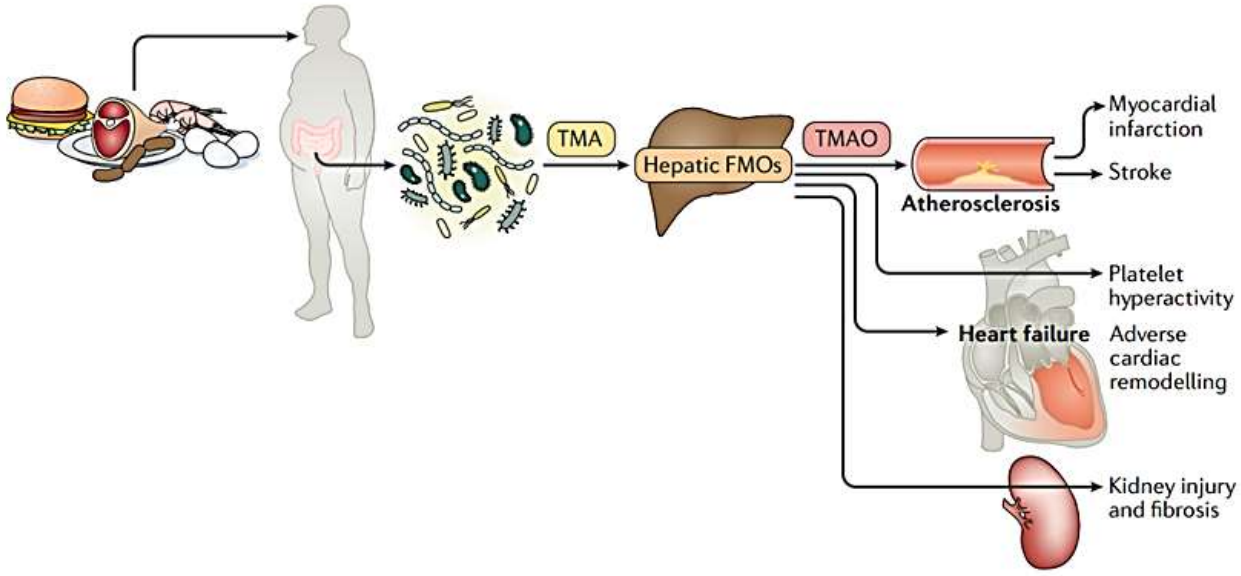

Figure 1.7. TMAO is a product of the oxidation of TMA. The gut microbiome metabolizes dietary choline, L-carnitine, and betaine to form TMA, TMA is oxidized by hepatic FMOs into TMAO. TMAO has been linked to higher risk of developing atherosclerosis, heart failure and kidney injury. Adapted from (Metaboprofile Biomart, 2020).

1.9.2 PHENYLACETIC ACID

Phenylacetic acid (PAA) is a metabolic product of phenylalanine (PA) after its conversion to phenylpyruvate. Phenylalanine is found in milk, eggs, cheese, chicken, beef, pork, beans, and fish (Figure 1.8). Gut bacteria are responsible for metabolizing phenylalanine into PAA (Wagner *et al*., 2019). High levels of PAA have been associated to kidney disease and liver steatosis (Jankowski *et al*., 2003; Hoyles *et al*. 2018).

In obese women, plasma PAA levels were positively correlated with steatosis severity. In primary human hepatocytes, treatment with PAA induced lipid build-up and modified the expression of genes involved in lipid and glucose metabolism. Likewise, mice fed a chow diet supplemented with PAA showed increased hepatic triglyceride levels and hepatic lipid accumulation (Hoyles *et al*. 2018).

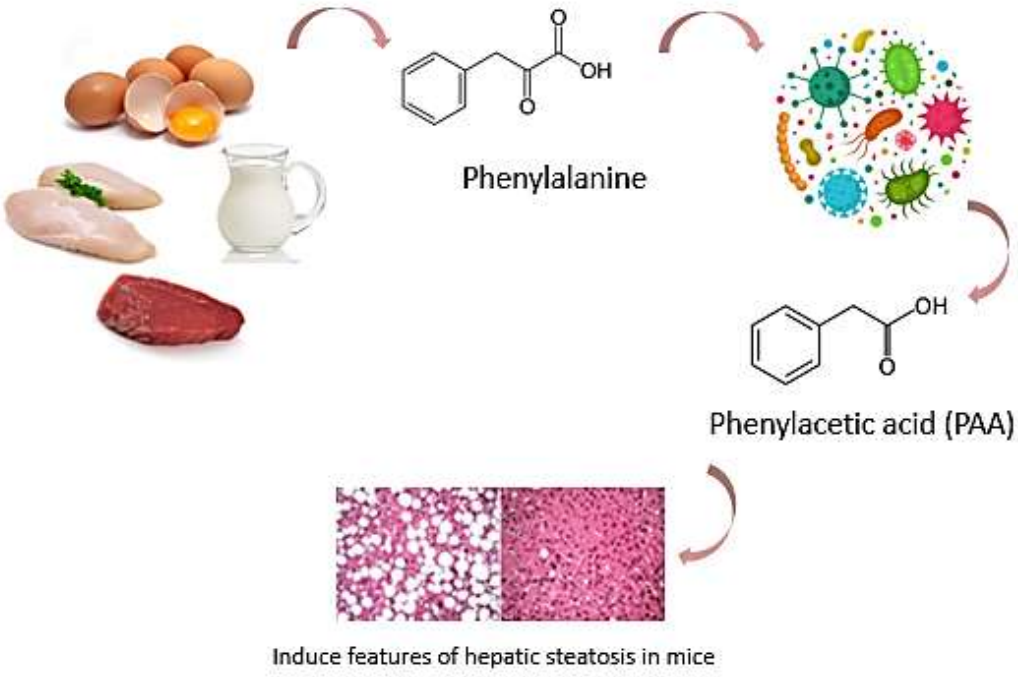

Figure 1.8. PAA is a metabolic product of PA. Phenylalanine is an amino acid found in several foods, including meat, poultry, fish, and cheese. PAA is a microbial product of phenylalanine that has been linked to inducing hepatic lipid accumulation in mice.

1.10 ANIMALS MODELS OF NAFLD AND NASH

There is an urgent need to more completely understand the pathogenetic mechanisms responsible for NAFLD and NASH development and progression. This requires the development of experimental models that fully resemble the human condition. Available animal models of NASH have different utility and clinical translatability. Rodent models are

widely used in NASH research due to their ability to mimic the aetiology, natural history and histopathology of this complex disease (Takahashi, Soejima & Fukusato, 2012). The pathogenesis of NASH is extremely complex and involves crosstalk between various organs (brain-gut-liver-adipose tissue). For this reason, NASH is no longer considered an exclusively hepatic disease, as many different systems are implicated in the pathogenesis of liver inflammation (Van Herck, Vonghia & Francque, 2017). Animal models have become important tools to study progression from simple steatosis to NASH, fibrosis, and HCC (Table 1). These animal models do not replicate the complex spectrum of NASH in humans; however, they can be used in testing hypotheses on the pathogenesis of NASH and in carrying out interventional studies. NASH models which more precisely mimic the histopathology and pathophysiology of the disease in humans still need to be developed in the coming years (Takahashi, Soejima & Fukusato, 2012).

Table 1. Most common animal models of NAFLD

Animal Models of Non-Alcoholic Fatty Liver Disease							
	Model	**Summary**	**Obesity**	**Steatosis**	**Inflammation**	**Fibrosis**	**NASH**
Dietary Models	MCD diet	Diet is high in sucrose and fat and if deficient in methionine and choline	no	yes	yes	yes	yes
	HF diet	High fat diet with 60% energy from fat, 20% from carbohydrate and 20% from protein	yes	yes	no	yes	yes (mild)
	Cholesterol and cholate	High cholesterol diet (21% milk butter, 0.2% cholesterol)	no	yes	yes	yes	yes
	Fructose	High-fructose diet (70%)	yes	yes	yes	no	yes
Genetic Models	ob/ob mice	Lack functional leptin due to a spontaneous mutation in the leptin gene	yes	yes	no	no (resistant to fibrosis)	no (does not develop spontaneously)
	db/db mice	Spontaneous mutation in the leptin receptor gene	yes	yes	no	no (does not develop spontaneously)	no (does not develop spontaneously)
	SREBP-1 c transgenic mice	Transgenic mice overexpressing nuclear SREBP-1c	no	yes	yes	yes	yes
	KK-A^y mice	Heterozygous mutation in the agouti gene	yes	yes	yes (mild)	no (does not develop spontaneously)	no (does not develop spontaneously)
	PTEN null mice	Hepatocyte-specific PTEN deficiency	no	yes	yes	yes (mild)	yes

1.11 NASH CELL CULTURE

1.11.1 2D CELL CULTURE VS. 3D CELL CULTURE

The mechanisms and signalling pathways involved in the progression of NAFLD were first observed using animal models and confirmed with clinical studies. However, recent studies have utilized *in vitro* cultures to investigate the molecular mechanisms involved in the progression of the disease (Kanuri & Bergheim, 2013). Cell culture has become an essential tool to help understanding fundamental mechanisms by which cell function becomes disrupted in disease. Two-dimensional (2D) cell culture has been the main method used to investigate NASH, often this means that the culture will only last for a few days as primary hepatocytes rapidly lose their metabolic features when cultured for longer (Duval *et al.*, 2017). Furthermore, the cellular environment in a monolayer 2D culture that is important for differentiation, proliferation and cellular functions *in vivo* are lost which directly affects gene expression profile and cellular physiology (Ravi *et al.*, 2015).

In vitro studies investigating steatosis in human hepatocytes are still scarce. Exposure to oleate and palmitate has been shown to trigger intracellular lipid build-up in primary human hepatocytes (PHH). These studies are performed in 2D monolayer cell cultures where fatty acids are added for a short incubation period usually 12-48 h (Kostrzewski *et al.*, 2017).

In general, primary cell cultures and immortalized cell lines are broadly used as *in vitro* models. Primary human hepatocytes, and non-parenchymal cells including Kupffer cells, stellate cells and sinusoidal endothelial cells are physiologically relevant to mimic clinical conditions; however, cell viability, ethical issues, and a limited number of human liver samples make it extremely challenging to obtain primary human cell cultures (Kanuri & Bergheim,

2013). To overcome these issues an alternative to primary cell cultures are immortalized cell lines. Immortalized cell lines offer several advantages such as extended replicative capacity, stable phenotype, cost effectiveness, and bypass of ethical concerns associated with the use of animal and human tissue (Kaur & Dufour, 2012). In addition, cultivation of immortalized cell lines is simpler and easier to standardize (Kanuri & Bergheim, 2013). The main disadvantage of immortalized cell lines is that these cells are not 'normal', as they divide indefinitely and can express genes that are not usually found in any cell type *in vivo* (Kaur & Dufour, 2012), and exhibit proliferative mitochondrial bioenergetics, that is altered from the differentiated state.

Recent research has shifted toward culture using three-dimensional (3D) structures. 3D cell culture is closer to the complex *in vivo* conditions, therefore 3D culture models have proven to be more realistic for translating the study findings for *in vivo* applications (Edmondson *et al.*, 2014). Numerous 3D cell culture models that preserve the differentiated phenotype of primary cells and provide more complex tissue organisation are now being developed and tested (Kostrzewski *et al.*, 2017) (Table 2). However, many challenges remain in 3D cell culture, including the tissue-tissue crosstalk, the mechanical microenvironment, and complex distributions of oxygen and nutrients to closely replicate the *in vivo* tissue (Duval *et al.*, 2017).

Table 2. Advantages and disadvantages of 2D and 3D cell culture

	Type of Culture	Advantages	Disadvantages
2D	Primary cell culture	Mimic in vivo settings	Limited culture time Isolation problems Ethical issues
	Immortalized cell lines	Easy to culture Continuous growth Stable phenotype	Lack of function and characteristics of normal cells
	Co-culture	Mimic in vivo architecture Important for cross talk studies	Difficult to cultivate High variability
3D	Spheroids	Heterotypic cell-to-cell contact Similar environment to in vivo Inexpensive 3D method	Simplified architecture Limited culture time High variability
	Organoids	In-vivo like complexity Similar environment to in vivo Long term culture	High variability Need for specific growth conditions
	Precision-cut liver slices	Retain tissue organization Cell–to-cell matrix interactions High reproducibility	Short culture time Limited availability Special equipment needed
	Liver-on-chips	Long term culture Dynamic microenvironment Retain tissue organization	Microbial contamination Difficult to operate Specific cells needed

1.11.2 LIVER SPHEROIDS AND ORGANOIDS

Liver spheroids are 3D systems that typically involve co-culture of primary human hepatocytes, stellate and Kupffer cells. Liver spheroids have great potential to become a robust liver model. Liver spheroids maintain differentiated hepatocyte phenotypes and extended viability up to 5 weeks. Kozyra *et al*. showed that liver spheroids are a good model for steatosis and insulin resistance, while several authors described that spheroids are a suitable 3D model for liver injury and toxicity studies (Kozyra *et al.*, 2018; Ingelman & Lauschke, 2021; Fey & Wrzesinski, 2012; Feng *et al*., 2019). Liver organoids are clusters of cells

similar to spheroids. The main difference is that organoids require an extracellular matrix and are mainly developed from induced pluripotent stem cells (Prior *et al.*, 2019).

1.11.3 PRECISION CUT LIVER SLICES

Precision cut liver slices (PCLS) represent an *ex vivo* tissue culture technique that retains all heterogeneity of cells in their natural environment where intercellular connections remain intact (Palma *et al*., 2019). Murine slices are more commonly used, but human liver slices can also be cultured and are obtained from liver resections. Slices have a wet weight of around 5 mg and are approximately 250 µm thick corresponding to 10–15 cellular layers. PCLS have been used extensively to investigate drug metabolism and toxicity. PCLS quickly deteriorate when cultured under static conditions, therefore alternatives are being developed such as bioreactor-cultured PCLS that remain stable up to 6 days (Paish *et al*., 2019).

1.11.4 LIVERCHIP

The Liverchip is a device that allows maintenance of three-dimensional primary human liver cells for longer period of times (> 1month) (Dehne, Hasenberg & Marx, 2017). It consists of twelve wells that contain scaffolds for cells to attach to and culture in perfused conditions (Figure 1.9). The scaffolds' dimensions recreate the hepatic capillary structures of the liver sinusoids such as including bile canaliculi and cell polarization (Kostrzewski *et al.*, 2017). To model the organization of hepatocytes on liver sinusoids, cells are seeded into the scaffold and are pressed by fluidic flow against a filter encouraging cell adherence to the insides of channels of collagen coated scaffolds. After 8 hours the flow is reversed, and the cells are allowed to form microtissues. Differently than conventional 2D cultures, 3D fluidic

systems are able to deliver nutrients and oxygen to the cultures at constant levels (Ortega-Prieto *et al.*, 2018).

In addition, cells seeded in the Liverchip maintain stable high levels of albumin secretion and CYP450 activity. Cells seeded in the Liverchip remain viable and maintain stable morphology for at least 40 days when compared to conventional static 2D hepatocyte cultures where cells present de-differentiation over 10–13 days (Ortega-Prieto *et al.*, 2018). Primary human hepatocytes seeded in the Liverchip form viable microtissues and produce 10-fold higher levels of albumin when compared to 2D after 2 weeks of culture. Therefore, the Liverchip device has the potential to recapitulate the physiological and mechanical microenvironment of the liver and could be an alternative to animal experimentation (Ortega-Prieto *et al.*, 2018).

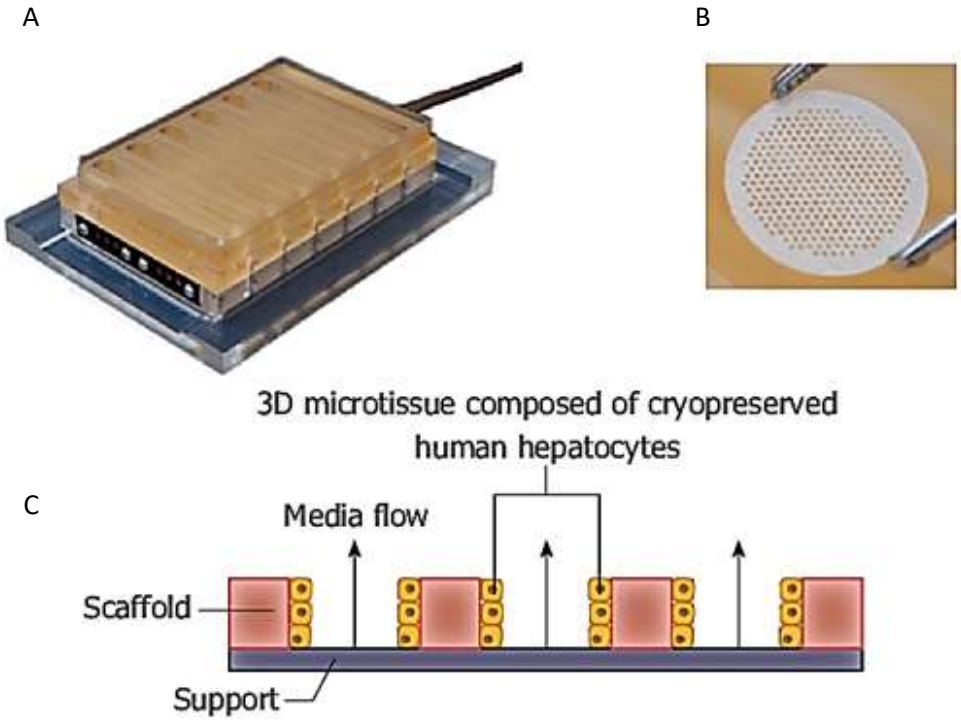

Figure 1.9. Liverchip 3D cell culture platform. A: The Liverchip plate comprises of 12 isolated wells for hepatocyte culture; B: Hepatocytes form microtissues in a collagen coated scaffold that is placed in each individual Liverchip well; C: Schematic illustration of media flowing through the channels of each Liverchip scaffold. The speed and direction of flow are adjustable. Adapted from (Kostrzewski *et al.*, 2017).

1.12 AIMS & HYPOTHESIS OF PROPOSED PHD STUDY

Many questions remain about NASH pathogenesis and whether NAFLD and NASH are mitochondrial diseases. There is accumulating evidence that mitochondrial dysfunction plays a key role in the physiopathology of NASH. Furthermore, microbiome metabolite levels such as TMAO were found to be higher in NASH patients and levels were positively correlated to disease severity. Currently there are no studies showing whether there is a link between microbiome metabolites and mitochondrial dysfunction in NAFLD/NASH. Our hypothesis is that the microbiome metabolites TMAO and PAA alter mitochondrial function contributing to lipid deposition leading to NAFLD development.

AIMS

1. Establish if TMAO and PAA contribute to lipid deposition in liver-derived cells in lipid-rich and lipid-poor environments.
2. Investigate if and how TMAO and PAA alter mitochondrial bioenergetics, and how this may contribute to exacerbated lipid deposition.
3. Assess the temporal and mechanistic link between increased lipid deposition and decreased mitochondrial function and determine if this effect is reversible.

OBJECTIVES

1. Optimise primary human hepatocyte isolation from human liver resections.

2. Develop a 3D cell culture model to study the effects of TMAO and PAA on mitochondrial bioenergetics and steatosis onset.

3. Develop 2D cell culture models to mimic progenitor ‘unhealthy’ hepatocytes and differentiated ‘healthy’ hepatocytes to assess the effects of TMAO and PAA on mitochondrial bioenergetics and steatosis onset.

CHAPTER 2.

MATERIAL AND METHODS - 3D CELL CULTURE: LIVERCHIP

This chapter describes the methods used for the data presented in Results Chapter 3 – 3D cell culture: LiverChip

2.1 PRIMARY MOUSE HEPATOCYTE ISOLATION

Mice livers were obtained from CD1 mice aged at minimum P30. Procedures were performed according to local ethical guidelines and conformed to the UK Animals (Scientific Procedures) Act 1986. All mice livers were retrieved from discarded carcasses used by other research groups at Derriford Research Facility. Mice were euthanised by carbon dioxide inhalation and livers were obtained within 30 minutes of death. The liver was dissected and dissociated using manual force in warm PBS, macerated tissue was then incubated in digestion solution containing 1mg/ml Collagenase A at 37°C for 30 minutes. After tissue digestion, cell suspension was centrifuged with percoll at 50g speed for 10 minutes, percoll was used for density separation of viable hepatocytes from dead hepatocytes and cell debris (Figure 2.1). Trypan blue was used to calculate cell viability.

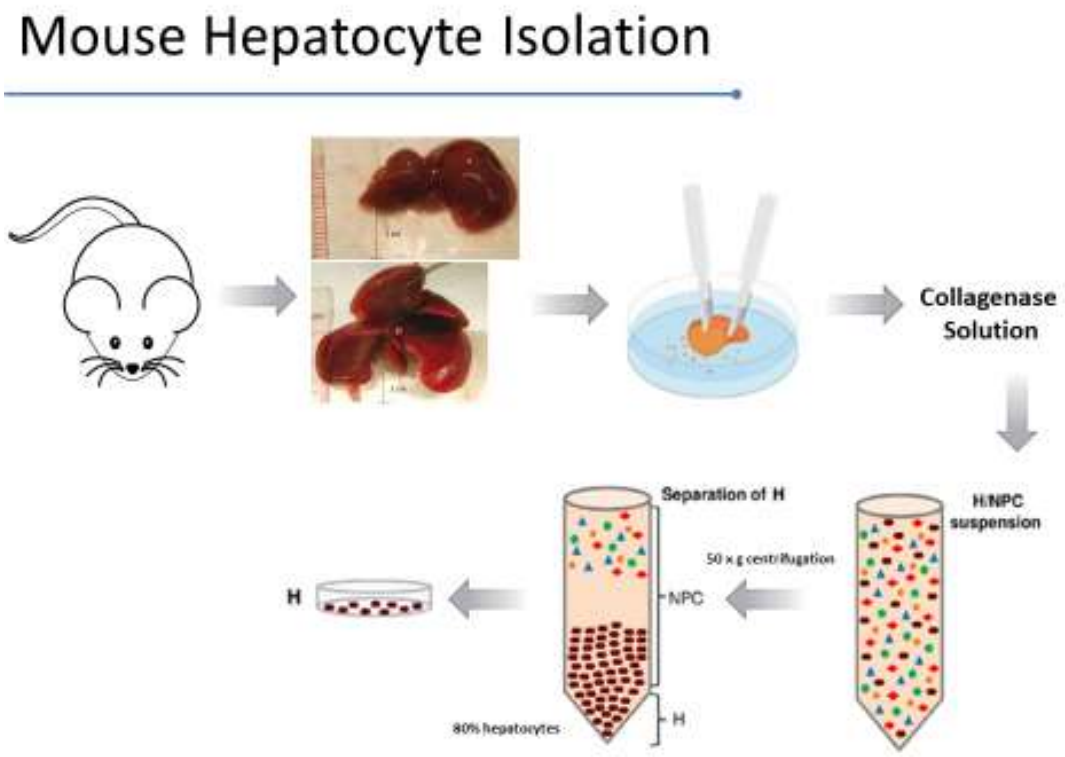

Figure 2.1. Mouse Hepatocyte Isolation. Mouse primary hepatocytes were isolated by incubation with collagenase solution followed by slow centrifugation with percoll. Percoll gradient was used to separate viable hepatocytes and trypan blue exclusion to assess cell viability.

2.2 PRIMARY MOUSE HEPATOCYTES LIVERCHIP CULTURE

After isolation, viable primary mouse hepatocytes were seeded at a density of 600k viable cells in the Liverchip platform (CN Bio Innovations Ltd., Cambridge, UK). The Liverchip platform consists of 12 individual wells in which fluid is recirculated across a collagen-coated scaffold, which enables the formation of 3D microtissues in the channels of the scaffold (Kostrzewski *et al*., 2017). Cells were seeded with flow in the downward direction through the scaffold for 24 hours at a flow rate of 1.0 µL/s. Downward flow encourages cells to seed

within the scaffold and form microtissues. Following cell attachment, the flow was changed to the upward direction and maintained at 1.0 µL/s for the remainder of the culture. The cells were maintained in WEM containing Gibco™ Primary Hepatocyte Thawing and Plating Supplements. Cells were incubated at 37°C with 5% CO_2.

2.3 BIOBANK AND LIVER RESECTION PROCEDURE

Human liver tissue was obtained from patients undergoing tumour resection surgery at University Hospitals Plymouth NHS Trust, who had consented to the use of excess liver tissue (resection surplus) for research. All participants were anonymised with a unique code and with the reference list held in a password protected file on a secure server within University Hospitals Plymouth NHS Trust with access only to the investigators. The NRES Committee London - City Road & Hampstead Research Ethics Committee (reference number 15/LO/0948) granted ethical approval for the study.

The surgeon performed the liver resection as clinically indicated; one anatomical segment of the lobe, not involved with any metastasis, as determined by the pathologist was separated for research purposes. The liver tissue was placed in ice cold DMEM and taken immediately to the laboratory for hepatocyte isolation. Liver wedges were weighed, and excess liver tissue was fresh frozen at -80°C.

2.4 PRIMARY HUMAN HEPATOCYTE ISOLATION

Primary human hepatocytes were obtained from collagenase perfusion of human liver tissue. The two-step procedure is the method of choice for the isolation of intact hepatocytes

in high yield. The key feature of this method is perfusion of the liver with a medium containing collagenase. The isolation was fully performed in a Class 2 biosafety cabinet and all solutions used were sterilized. Approximately 20 grams of human liver was placed in a petri dish and a cannula was inserted in an accessible hepatic vessel. Using a rotatory pump at 50rpm, the tissue was rinsed with pre-warmed PBS to remove residual blood and warm up the tissue. Subsequently, hydroxyethyl-piperazineethane-sulfonic acid (HEPES) buffer pH 7.2 was perfused through the liver. When the colour of the tissue became lighter, second perfusion with digestion solution containing 1mg/ml collagenase type I was performed. The end of this step was indicated by irreversible deformation of the tissue upon slight pressure. Following digestion, cannulae was removed and ice cold stop solution containing PBS with 20% faetal bovine serum (FBS) was added to prevent over digestion. Tissue was dissociated manually to release the cells (Figure 2.2). Cell suspension was filtered through a 60 µm fine mesh. Filtered suspension was transferred to 50mL tubes containing cold DMEM with 10% FBS and centrifuged at 50g for 10 minutes. Pellet was collected, added to 90% percoll solution and centrifuged at 100g for 20 minutes. Following percoll purification, cells were washed twice with 10% FBS in DMEM. After pellet resuspension in 1mL of WEM medium, cell count and viability assessment by trypan blue exclusion was performed.

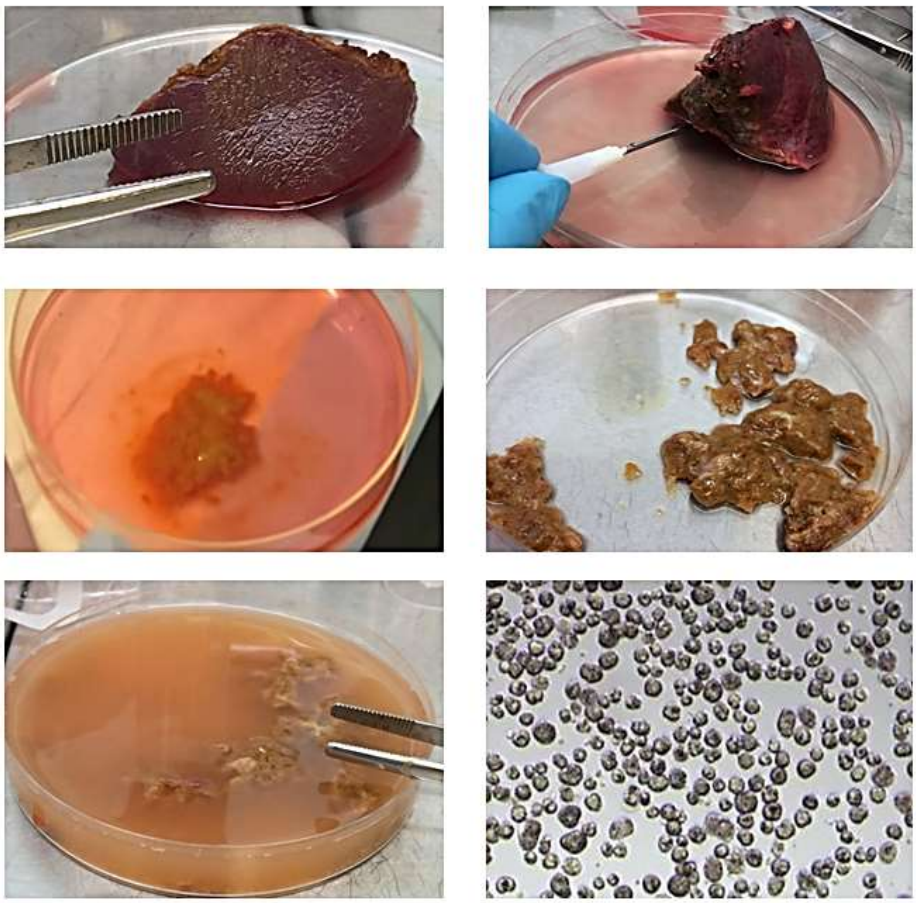

Figure 2.2. Primary human hepatocyte isolation. Isolation of human hepatocytes by two-step collagenase perfusion: human liver section was perfused with digestion solution and disrupted manually to release the cells. After percoll purification, cell yield was assessed using microscopy.

2.5 FRESH PRIMARY HUMAN HEPATOCYTE LIVERCHIP CULTURE

Following primary human hepatocyte isolation, cells were plated in the Liverchip platform. Human hepatocytes were seeded with downward flow for 8 hours at a flow rate of 1.0 µL/s. Subsequently, the flow was changed to the upward direction and maintained at 1.0 µL/s. Primary human hepatocytes were seeded at a density of 600k viable cells in 2 mL of medium per well. The cells were maintained in WEM for the first 24 hours of culture. After 24

hours, medium was replaced with WEM with Gibco™ Primary Hepatocyte Maintenance Supplements. Cells were incubated at 37°C with 5% CO_2. Scaffolds containing microtissues were removed from wells, washed with PBS and visualized by microscopy.

2.6 HEPARG 3D CELL CULTURE

Undifferentiated cryopreserved HepaRG cells passage 12 were obtained from Biopredic International (Rennes, France). Proliferative and differentiated HepaRG cells were seeded into the Liverchip platform. HepaRG cells were plated at 1 million cells per well. Downward flow was set for 8h at 1.0 µL/s flow rate prior to maintenance flow rate of 1.0 µL/s upward direction. HepaRG cells were maintained in plating medium or differentiation medium according to their phenotype. In order to induce steatosis, HepaRG cells were cultured in the Liverchip in "fat" media containing 0.6 mM of oleate and palmitate 2:1 molar ratio for 7 days prior to Oil red O staining.

2.7 OIL RED O STAINING

Oil red O solution in 0.5% isopropanol was purchased from Sigma-Aldrich (St. Louis, USA). Scaffolds containing HepaRG microtissues were removed from the Liverchip platform and placed in a 24-well flat bottom plate. Scaffolds were washed twice with PBS and fixed with 4% paraformaldehyde for 15 minutes at room temperature. After fixing, scaffolds were washed twice with 70% isopropanol for 5 minutes and stained for 1 hour with Oil red O solution. In order to remove unbound stain, scaffolds were washed three times in distilled

water and twice in 70% isopropanol. Oil red O stain images were taken with a Leica Dmi8 microscope.

2.8 SEAHORSE XF24 EXTRACELLULAR FLUX ANALYSER

The Seahorse XF24 Analyser (Agilent Technologies, Lexington, USA) was used to study mitochondrial bioenergetics. The instrument allows the measurement of important parameters of mitochondrial function: basal respiration, ATP-linked respiration, proton leak, maximal respiration, coupling efficiency, spare respiratory capacity and non-mitochondrial respiration (Figure 2.3). The instrument continuously measures oxygen concentration and proton flux in the cell supernatant over time. These measurements are converted in oxygen consumption rate (OCR) and extracellular acidification rate (ECAR) values and enable a direct quantification of mitochondrial respiration and glycolysis (Wu *et al*., 2007). Kinetic measurements are made in real-time, and the assay is completely non-invasive. The XF24 has four injection ports per well to allow up to four test compounds to be added automatically to each well at pre-designated times. Oligomycin is injected first, secondly FCCP/BAM 15 and last injection is a mixture of Rotenone and Antimycin A. Seahorse XF24 measured OCR and ECAR at intervals of approximately 4 minutes. Real-time measurements of OCR and ECAR were made by isolating a small volume (about 2 µL) of medium above a monolayer of cells within the microplate. OCR was measured by optical fluorescent biosensors fixed in the disposable cartridge that is placed into the XF24 microplate ('Seahorse XF Analyzers,' 2018). All measured mitochondrial parameters are described below.

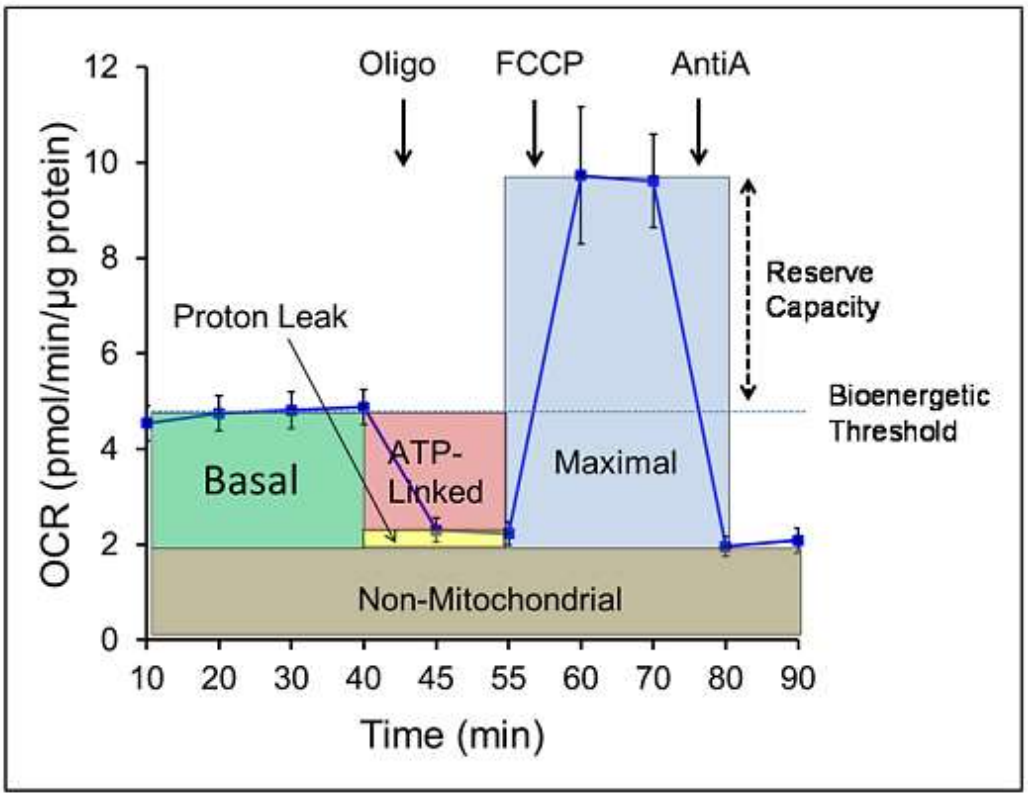

Figure 2.3. Representative image of the XF24 Mito Stress test. Seahorse was used to measure key parameters of mitochondrial function: basal respiration, ATP-linked respiration, proton leak, maximal respiration and non-mitochondrial respiration (Usmar, 2015).

2.8.1 BASAL RESPIRATION

Mitochondrial respiration is the process of energy conversion of substrates into ATP. Basal mitochondrial respiration was determined by measuring OCR in the absence of inhibitors. It represents the consumption of oxygen needed to maintain the vital cellular functions under optimal physiological conditions. Basal oxygen consumption contributes to the synthesis of ATP at complex V and proton leak. Different cell types will present highly diverse basal respiration rates due to intrinsic properties of the cells. It is also influenced by the availability of different substrates (glucose, pyruvate, and fatty acids), growth factors and

pH of the cell media. Thus, experiments were performed to find the optimal concentrations of substrates for analysis of the mitochondrial function. It is always preferable to use concentrations similar to physiological findings (Vayalil, 2019). In addition, due to inherent noise, many replicates were necessary for statistical significance of small changes. A change in basal rate in each cell type indicates some bioenergetic change in the cell. Basal OCR was calculated, by subtracting non-mitochondrial respiration from basal respiration rates. It has previously shown that hepatocytes use approximately 30% of their maximal respiratory capacity to sustain basal respiration (Marchetti *et al*., 2020). Basal respiration in the hepatoma derived cell line, HepaRG, seems to be higher in proliferative cultures compared to differentiated cell cultures (Young & Young, 2019).

2.8.2 NON-MITOCHONDRIAL RESPIRATION

Non-mitochondrial respiration represents oxygen-consuming processes that happen outside the mitochondria. While the bulk of oxygen is consumed by mitochondria in any cell, enzymatic reactions and oxygenases outside of mitochondria will also consume oxygen. Non-mitochondrial oxygen-consuming processes are not well defined but in leucocytes they are mainly attributed to enzymes associated with inflammation and are negative indicators of bioenergetic health (Vayalil, 2019). Most other cells have low, but significant, non-mitochondrial respiration, caused by desaturase and detoxification enzymes. In liver cells cytochrome P450s also play a role in non-mitochondrial OCR (Brand *et al*., 2011). Non-mitochondrial OCR is commonly increased in the presence of stressors, such as ROS, highly reactive molecules that usually target mitochondria causing harmful effects. Non-mitochondrial respiration was measured by the addition of the specific inhibitors: rotenone

and antimycin A (Chacko *et al*., 2014). The non-mitochondrial respiration rates were needed to be subtracted from all other respiratory rates.

2.8.3 ATP-LINKED RESPIRATION

ATP-linked respiration is the amount of oxygen consumed to generate ATP at complex V or ATP synthase. It was determined by measuring the OCR after the addition of oligomycin. Oligomycin is a specific inhibitor of ATP synthase which blocks its proton channel required for oxidative phosphorylation of ADP to ATP (Vayalil, 2019). ATP-linked OCR is the capacity of the cell to meet its energetic demands. When ATP-linked respiration is higher, it indicates an increased ATP demand, whereas a decrease indicates low ATP demand, the absence of substrates or great damage to oxidative phosphorylation. This prevents the flow of electrons resulting in lower OCR (Chacko *et al*., 2014). ATP linked respiration was calculated from the difference between OCR at baseline and respiration following oligomycin addition.

2.8.4 PROTON LEAK

After the addition of oligomycin, electron flow was not entirely stopped due to a process known as proton leak. Proton leak measures protons pumped during electron transport that results in oxygen consumption but not ATP production. Uncoupling protein catalyses the translocation of protons from the intermembrane space of mitochondria into the matrix. However, proton leak even occurs in cells from which uncoupling proteins are thought to be absent such as hepatocytes (Jastroch *et al*., 2010). A large increase in proton leak can mean that the mitochondria are severely damaged. Increased calcium transport can

also manifest as a change in proton leak. In addition, oxidative stress modifies the bioenergetic parameters and also increases ATP-linked oxygen consumption and proton leak (Vayalil, 2019).

2.8.5 MAXIMAL RESPIRATION

The maximum respiration rate was established after the addition of uncouplers such as FCCP or BAM15. FCCP is a potent uncoupler of mitochondrial oxidative phosphorylation. FCCP and BAM15 have a similar function, however BAM15 was shown to be more specific, less cytotoxic and stimulate a higher maximum rate of mitochondrial respiration (Kenwood *et al*., 2013).

Uncouplers are not fully specific to the mitochondrial membrane and act as protonophores across all membranes, disrupting the function of endosomes and other compartments. This effect may lead to substrate supply inhibition and results in an uncoupled rate that is lower than the real maximum respiration rate. Therefore, optimization experiments of titrated uncoupled rates were performed to obtain the amount of uncoupler necessary to achieve the maximum activity of electron transport by the cells under the assay conditions. A decrease in maximum respiratory capacity is a strong indicator of potential mitochondrial dysfunction. However, because of the nonspecificity of uncouplers, any abnormal findings might have more complex causes than expected (Vayalil, 2019).

2.8.6 SPARE RESPIRATORY CAPACITY

Spare respiratory capacity represents the ability of substrate supply and electron transport to respond to an increase in energy demand. A decreased spare respiratory capacity suggests a mitochondrial dysfunction or that mitochondrial mass is compromised. Spare respiratory capacity is an important parameter that shows how close to its bioenergetic limit a cell is operating, therefore being an important indicator of cell health. Spare respiratory capacity was obtained by subtracting basal respiration from maximal oxygen consumption after the addition of an uncoupler (Marchetti *et al*., 2020).

2.8.7 COUPLING EFFICIENCY

Coupling efficiency was determined from the change in basal respiration rate on addition of oligomycin. It is defined as the fraction of basal mitochondrial OCR used to drive ATP synthesis. It was calculated by dividing ATP production rate by basal respiration rate. Coupling efficiency is altered by ATP demand, but is typically high: approximately 70% in hepatocytes (Brand *et al*., 2011). Proliferative HepaRG cells have shown an increase in coupling efficiency compared to differentiated cells (Young & Young, 2019). As an indicator of dysfunction, coupling efficiency is advantageous as it is sensitive to changes in all bioenergetic parameters, so is likely to change in any dysfunction (Brand *et al*., 2011) (Figure 2.4).

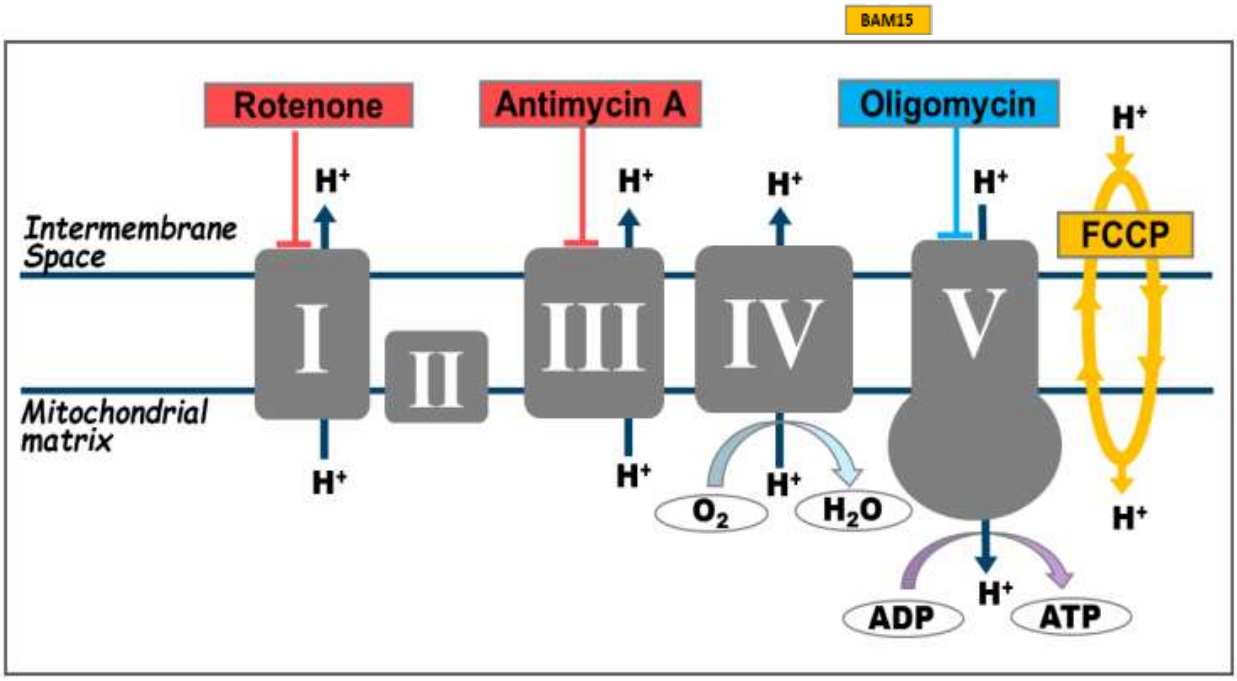

Figure 2.4. Seahorse XF Cell Mito Stress Test effectors target different parts of the electron transport chain. After basal measurements, Oligomycin is the first to be injected inhibiting ATP synthase. FCCP/BAM15 are uncoupling agents, injected after Oligomycin, that collapse the inner membrane gradient, allowing oxygen consumption by complex IV to reach maximal rates. The final injection is a mixture of rotenone (complex I inhibitor) and antimycin A (complex III inhibitor). This last injection shuts down ETC function and allows the calculation of non-mitochondrial respiration driven by processes outside the mitochondria. Adapted from (Agilent Seahorse XF Cell Mito Stress Test Kit User Guide).

2.9 MITOCHONDRIAL BIOENERGETICS IN HEPARG CELLS IN 3D CULTURE

Scaffolds with HepaRG microtissues were removed from the Liverchip platform and cut into four pieces with a sterile scalpel. Scaffold pieces were placed into the Seahorse XF24 islet capture plate and capture screens were placed to hold the scaffolds in place (Figure 2.5). Plates were then inserted in the Seahorse XF24 Analyser. Oligomycin, FCCP and rotenone/antimycin A were tested at low, medium and high concentrations (1, 3, 6 and 10 µM). Basal OCR measurement (4 cycles), injection of oligomycin port A (4 cycles), injection of FCCP port B (4 cycles), injection of rotenone/antimycin A port C (4 cycles) were performed. All cycles were set to mix for 1 minute, wait for 2 minutes and measure for 4 minutes.

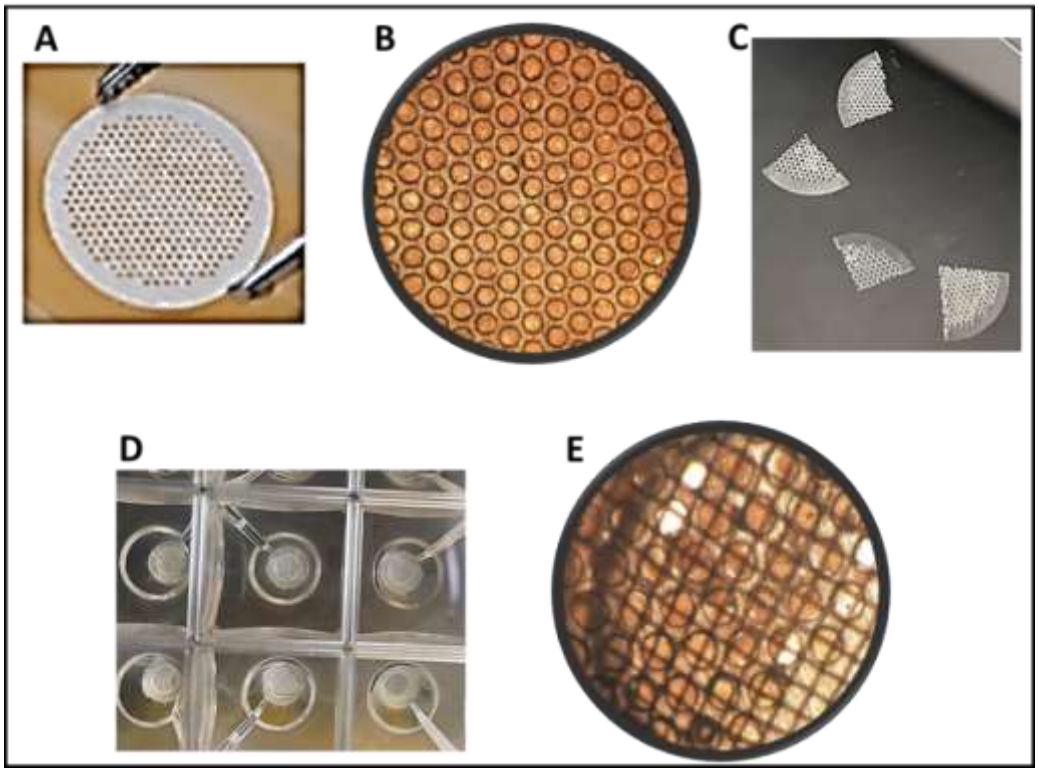

Figure 2.5. Scaffolds with HepaRG microtissues. Liverchip scaffolds containing HepaRG microtissues were cut and fitted into Seahorse XF24 Islet Capture Microplates for mitochondrial analyses. Inverted Light Microscopy images: A. Liverchip scaffold B. HepaRG microtissues formed in the scaffold C. Scaffolds cut into four pieces D. Pieces of scaffolds fitted

in the islet captures microplates E. Microscopy image of one islet capture plate well with a XF24 scaffold.

2.10 OXYGEN ELECTRODE

As an alternative method to measure oxygen consumption of microtissues formed in the Liverchip scaffolds, a Clark-type oxygen electrode was used. The electrode includes a silver chloride electrode and a platinum cathode. An oxygen-permeable Teflon membrane separates the electrode from the sample, which is housed in a chamber. The chamber is sealed from the air by a tight-fitting lid and the contents are constantly stirred. Changes in OCR are measured, and addition of effectors is manually made using needle syringes through the lid (Divakaruni *et al*., 2014). Scaffolds were removed from the Liverchip with sterile tweezers and placed in the oxygen electrode chamber containing distilled water while the electrode well contained 3M KCl potassium chloride solution. After calibration, to assess different mitochondrial features 1 µM of oligomycin was manually injected, followed by 1 µM and 2 µM of FCCP and 1 µM and 3 µM of rotenone/antimycin A.

CHAPTER 3.

RESULTS - 3D CELL CULTURE: LIVERCHIP

3.1 FRESHLY ISOLATED PRIMARY HEPATOCYTES ARE NOT SUITABLE FOR LIVERCHIP 3D CELL CULTURE

3.1.1 PRIMARY HEPATOCYTE ISOLATION FROM MOUSE LIVER

Primary hepatocyte isolation method was tested in mouse liver prior to obtaining human liver tissue. Mouse livers were specifically chosen due to the easy access to this tissue in our laboratory. Mouse livers were obtained, dissected and collagenase was added to dissociate the liver tissue into cells. Hepatocytes were separated from other cell types using slow speed centrifugation. The technique to isolate primary mouse hepatocytes presented a high yield of viable cells calculated using Trypan blue exclusion assay (Figure 3.1).

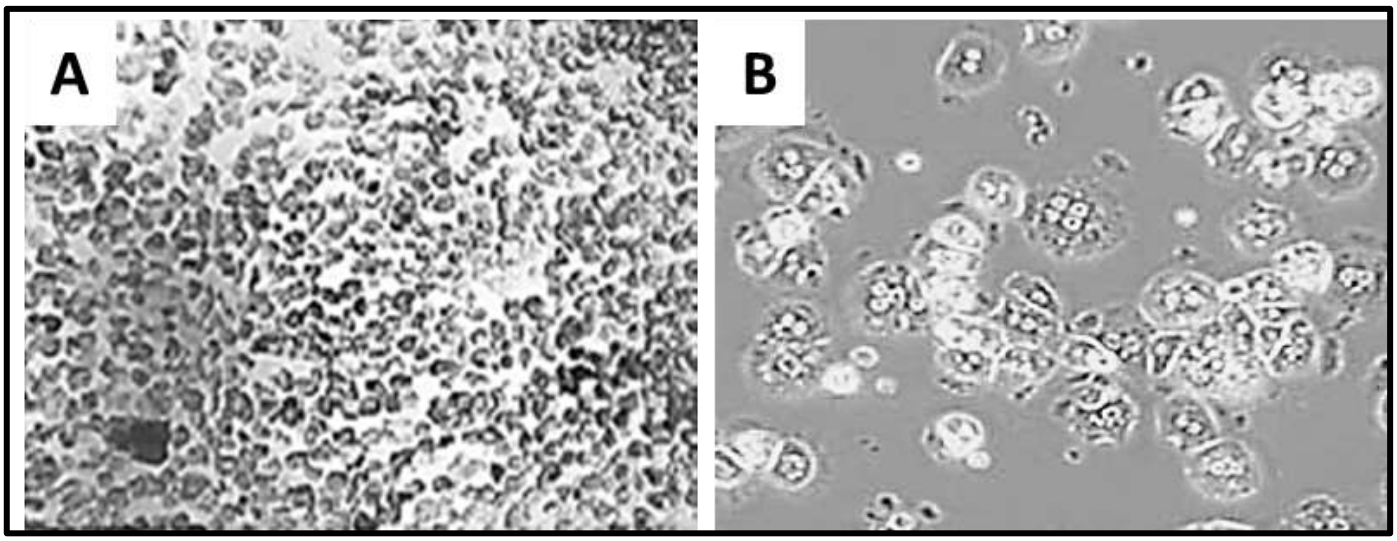

Figure 3.1. Mouse Hepatocytes in 2D. Inverted light microscopy images of isolated primary mouse hepatocytes in 2D cell culture. 10x magnification (left) and 20x magnification (right).

3.1.2 PRIMARY MOUSE HEPATOCYTE LIVERCHIP SEEDING

Freshly isolated mouse hepatocytes were seeded into the Liverchip platform (200k/well). Mouse hepatocytes are denser than human hepatocytes therefore seeding flow was kept in downward direction for 24 hours. The Liverchip has been developed for human cell use, seeding mouse hepatocytes in this 3D platform was performed solely for training purposes. Mouse hepatocyte microtissue formation within the scaffolds was highly variable showing that mouse cell adhesion was unstable (Figure 3.2).

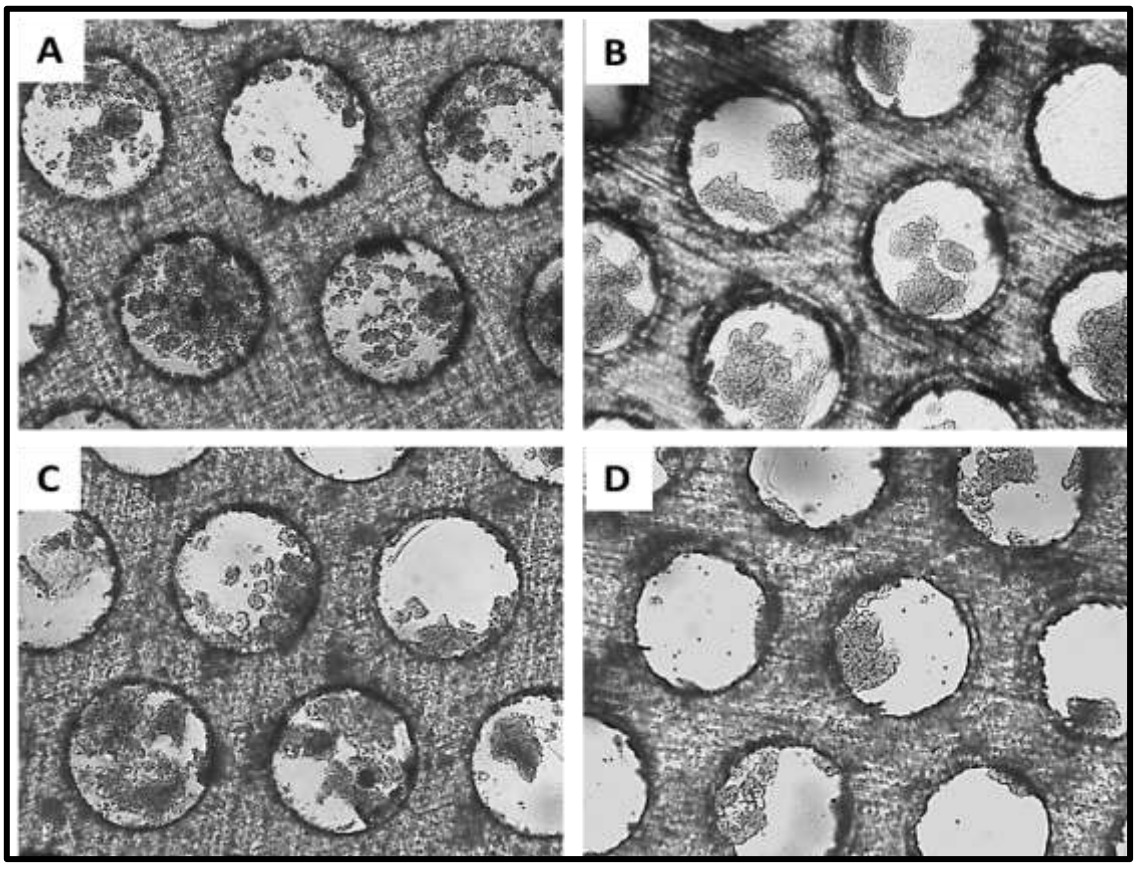

Figure 3.2. Mouse hepatocytes in 3D. Inverted light microscopy images of isolated primary mouse hepatocyte microtissues formed in the Liverchip scaffolds. Four different Liverchip scaffolds A-D. 20x magnification.

3.1.3 PRIMARY HEPATOCYTE ISOLATION FROM HUMAN LIVER RESECTIONS

Liver wedges were prepared and processed as detailed in chapter 2. 21 liver wedges were obtained from consented patients during tumour resection surgery. Tissue weight varied from 2 to 63 grams (Table 3). Hepatocyte isolation was performed using collagenase perfusion. At first, 1mg/ml of collagenase type I was used for tissue digestion of 5 liver resections. The digestion with collagenase type I resulted in very low number of cells <1million. Therefore, collagenase A at 1mg/mL was tested. Incubation for 1 hour at 37 degrees with collagenase A was performed in four samples but the yield remained low. Next step was to test a shorter incubation period, therefore from ILB21 onwards 30 minutes incubation with collagenase A was used. Shorter incubation period significantly increased the cell number obtained. However, hepatocyte yield and viability were still lower than expected. The average cell yield obtained after trypan blue assay and percoll purification was 8×10^5 per g (liver weight).

Table 3. Collected fresh liver samples

Date Collected	Sample	Tissue Weight	Number of cells
12/06/2017	ILB001	2 grams	<1million
28/06/2017	ILB003	2.4 grams	<1million
04/07/2017	ILB005	2.4 grams	<1million
14/07/2017	ILB009	7 grams	<1million
25/07/2017	ILB008	63 grams	<1million
31/07/2017	ILB007	7.5 grams	<1million
14/08/2017	ILB016	10.9 grams	<1million
21/08/2017	ILB015	38.6 grams	5×10^6
25/08/2017	ILB002	3 grams	700,000
31/08/2017	ILB018	2.68 grams	9×10^6
05/09/2017	ILB021	3.22 grams	2.8×10^6
12/09/2017	ILB022	20 grams	16×10^6
25/09/2017	ILB026	24 grams	15×10^6
26/09/2017	ILB027	20 grams	5×10^6
02/10/2017	ILB028	11 grams	3×10^6
03/10/2017	ILB024	21 grams	40×10^6
04/10/2017	ILB029	11 grams	12×10^6
11/10/2017	ILB032	17 grams	5×10^6
05/12/2018	ILB041	20 grams	9×10^6
15/01/2018	ILB044	7.2 grams	4×10^6
17/01/2018	ILB045	2.3 grams	<1million

3.1.4 FRESHLY ISOLATED PRIMARY HUMAN HEPATOCYTES ARE GENERALLY POOR FOR FORMING MICROTISSUES IN LIVERCHIP SCAFFOLDS

Since the first seven samples resulted in less than a million hepatocytes, they were not cultured in 3D. ILB015 was the first sample tested, 200k cells were seeded per well at a flow rate of 1.0 µL/s but no cells attached. The same protocol was tested in three more samples but no tissue formation in the Liverchip was observed. ILB022 resulted in a higher cell number, therefore cell density was increased. 600k cells were seeded per well but no attachment to the scaffold was seen. Previously, the downward flow was kept for 1 hour before switching to the upward direction. A longer downward flow was then tested, cells were seeded in the wells and media flow was kept in the downward direction for 8 hours before switching to upward direction. Following these optimization steps, hepatocytes isolated from ILB026

attached and formed 3D microtissues in the Liverchip scaffolds after 12 days in culture. Microtissue formation and adhesion from ILB026 was unstable and high variability was observed (Figure 3.3). Hepatocytes from ILB027 and 028 did not adhere, therefore a second collagen coating to the scaffold was tested. Liverchip scaffolds were immersed in rat tail collagen coating solution for 15 minutes to assess whether attachment would improve. After coating, scaffolds were then transferred into the Liverchip and hepatocytes from ILB024 and 029 were tested, no viable microtissues were formed. For ILB032-045 downward flow rate was increased since it is known that hepatocytes are dense and heavy cells, 2.0 µL/s flow rate was tested, in addition density was increased to 1 million cells per well but again no tissue formation was observed. After several optimisation steps, primary human hepatocytes did not attach and form proper microtissues in the Liverchip scaffolds. For this reason, HepaRG cells were then used for further experiments.

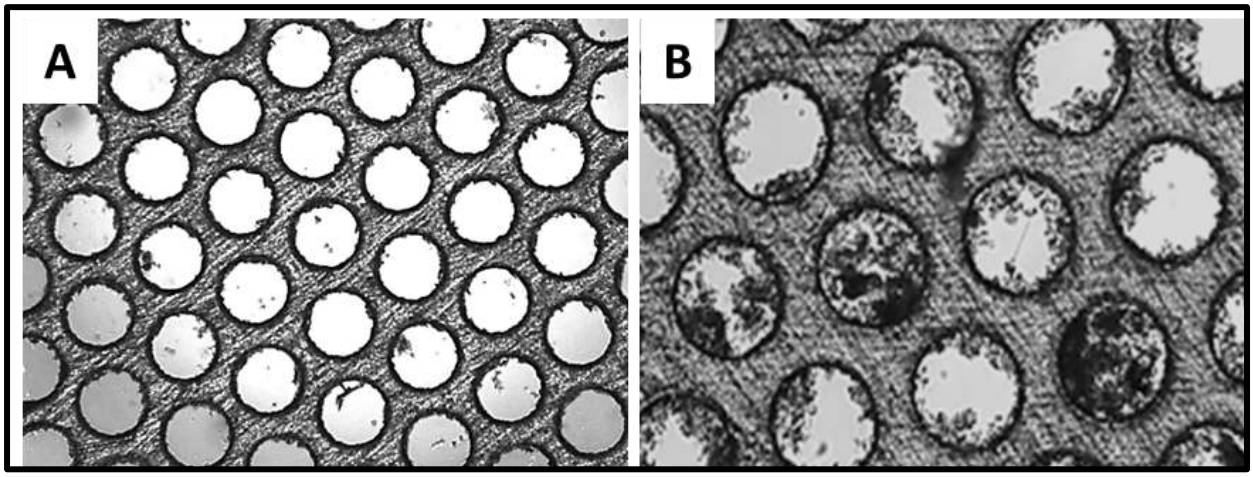

Figure 3.3. Primary human hepatocytes in 3D. Inverted light microscopy images of primary human hepatocytes in the Liverchip scaffolds. Hepatocytes from 13 samples did not attach to the scaffold (left); hepatocytes from sample ILB026 formed hepatic microtissue in the Liverchip (right). A. 10x magnification B. 20x magnification.

3.1.5 PROLIFERATIVE HEPARG CELLS ARE CAPABLE OF FORMING MICROTISSUES IN 3D CELL CULTURE

Due to the low viability and lack of adherence to the scaffolds from primary hepatocytes in the Liverchip, the next step was to test whether a hepatocyte-like cell line would form viable microtissues in 3D cell culture. Proliferative HepaRG cells were seeded in the Liverchip platform (1 million/well). HepaRG cells successfully attached to the collagen-coated scaffold. Cells were sustained in 3D for three weeks and presented consistent microtissue formation (Figure 3.4).

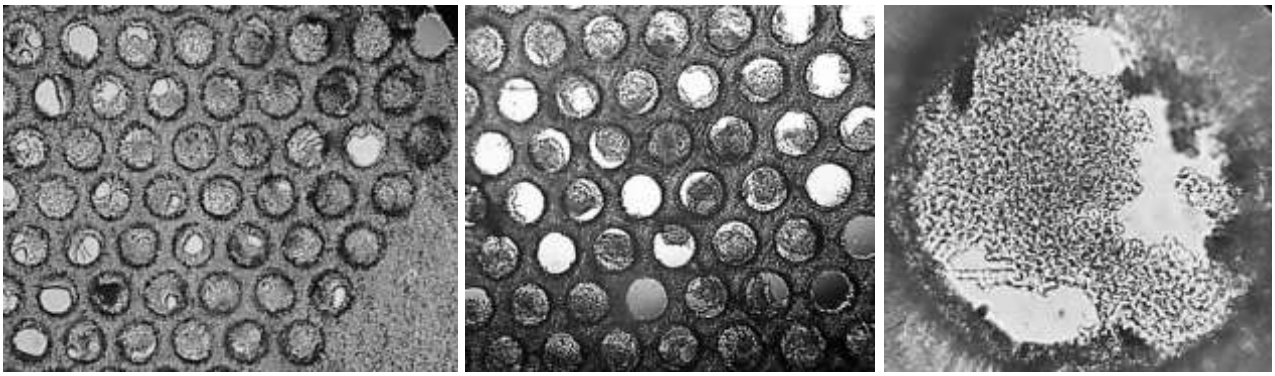

Figure 3.4. HepaRG cells in 3D culture. Inverted light microscopy images of HepaRG microtissues within the channels of the Liverchip scaffolds. 10x magnification (left) and 40x magnification (right).

3.1.6 PROLIFERATIVE HEPARG CELLS DO NOT BECOME STEATOTIC AFTER EXPOSURE TO OLEATE AND PALMITATE IN 3D CELL CULTURE

In order to establish whether HepaRG 3D microtissues were a suitable model to mimic fatty liver disease, proliferative cells were cultured in the Liverchip in fat media containing 0.6mM of oleate and palmitate. After 7 days, scaffolds containing microtissues were removed

and stained with Oil Red O for one hour. Oil Red O was chosen as its use has been described in Liverchip scaffolds (Kostrzewski *et al.*, 2017). Unfortunately, microscopy images showed that Oil Red O was not taken up by any of the cells cultured in 3D (Figure 3.5).

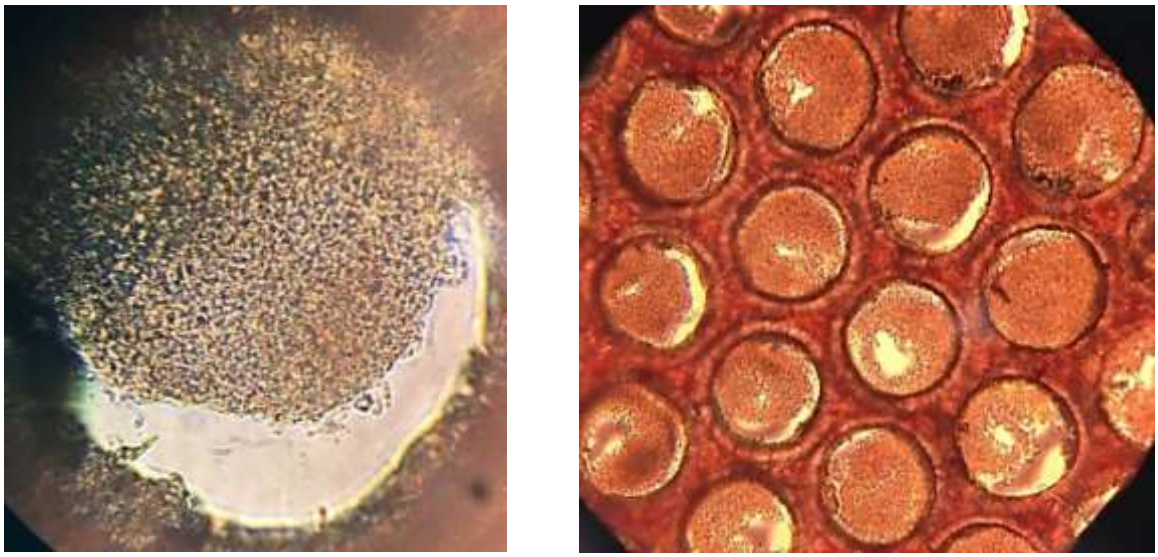

Figure 3.5. Oil Red O Staining Inverted light microscopy images of HepaRG microtissues in the Liverchip scaffolds after Oil Red O staining. 40x magnification (left) and 20x magnification (right).

3.1.7 SEAHORSE XF24 ANALYSER IS INCAPABLE OF MEASURING MITOCHONDRIAL OXYGEN CONSUMPTION IN 3D SCAFFOLD CELL CULTURE OF HEPARG CELLS

Following microtissue formation of HepaRG cells in the Liverchip scaffolds, the scaffolds were removed, cut in four pieces and placed in the Seahorse XF24 analyser. Eight tests were performed with Liverchip scaffolds, however the scaffolds presented low OCR and no appropriate response to the injected effectors (Figure 3.6). To eliminate the step of cutting the scaffolds, CN Bio provided a prototype of a Liverchip containing 24 wells. Scaffolds from

the Liverchip-24 are smaller and fit entirely in the SeaHorse XF24 plates. 400k HepaRG were seeded per well, scaffolds were removed and placed in the XF24 plates. Again, extremely low OCR and no effector response was observed. These results indicate that Liverchip scaffolds are not suitable to interrogate mitochondrial function using the XF24 analyser.

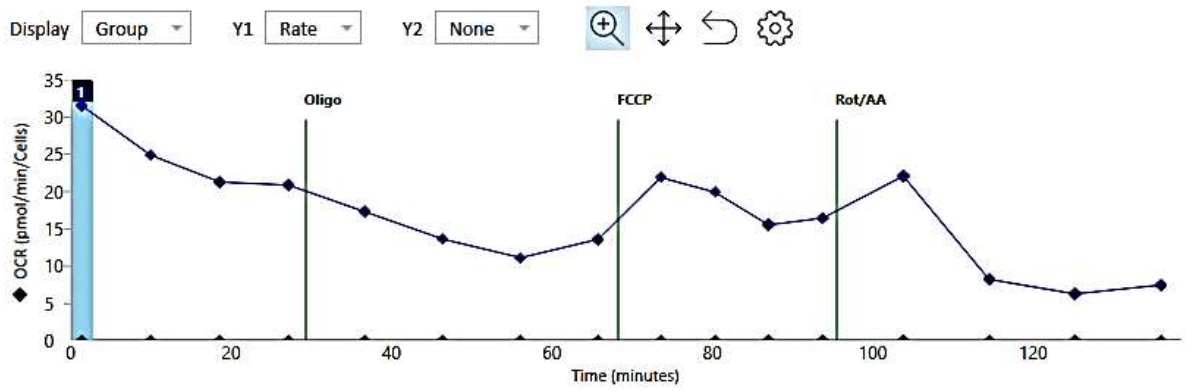

Figure 3.6. Mito stress test performed in Liverchip scaffolds. Basal OCR rates (4 cycles), injection of oligomycin port A (4 cycles), injection of FCCP port B (4 cycles), injection of rotenone/antimycin A port C (4 cycles). Data are presented as mean ± SD, n = 3

In addition to testing Liverchip scaffolds in the Seahorse system, mitochondrial oxygen consumption was also assessed using an oxygen electrode. The oxygen electrode was chosen as it enables testing various concentrations of effectors in real time and altering settings during the experiment. One scaffold containing HepaRG microtissue was inserted in the oxygen electrode and 1 µM of oligomycin, 1-2 µM of FCCP and 1-3 µM of rotenone/antimycin were manually injected. HepaRG cells grown in the Liverchip scaffolds presented extremely low oxygen consumption not suitable for the oxygen electrode assay. Therefore we concluded that the structure of the microtissues do not allow access to the effectors (Figure 3.7).

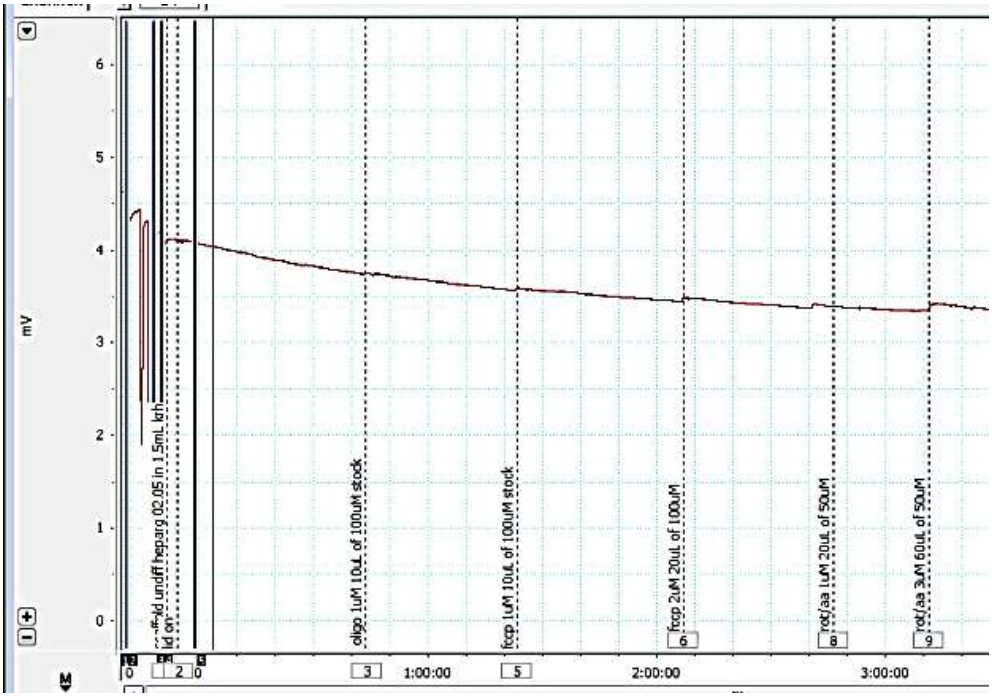

Figure 3.7. Liverchip scaffold in the oxygen electrode. Mitochondrial respiration inhibitors were manually injected: one injection of oligomycin followed by two injections of FCCP and two injections of rotenone/antimycin A.

CHAPTER 4.

MATERIAL AND METHODS - 2D CELL CULTURE & WHOLE LIVER TISSUE

This chapter describes the methods used for the data presented in Results Chapter 5 – 2D cell culture & whole liver tissue

4.1 FRESHLY ISOLATED PRIMARY HUMAN HEPATOCYTE 2D CULTURE

In order to culture freshly isolated human hepatocytes, XF24 culture plates were coated with 250µL of Rat Tail Collagen Coating Solution (Sigma-Aldrich, St. Louis, USA) for two hours. Coating solution was then removed, and plates were washed twice with PBS. Cell suspension was seeded onto plates at a density of 500k viable cells per well. Cells were maintained in WEM with Gibco™ Primary Hepatocyte Thawing and Plating Supplements in a humidified cell culture incubator at 37°C with 5% CO_2 for further bioenergetics analyses.

4.2 MITOCHONDRIAL BIOENERGETICS OF FRESH PRIMARY HUMAN HEPATOCYTES

After 4 days in culture, mitochondrial bioenergetics of freshly isolated human hepatocytes was measured with the XF24 Seahorse analyser. Mito stress kit was performed with final concentrations of effectors of 1 µM oligomycin, 1 µM FCCP and 1 µM rotenone/antimycin A.

4.3 WHOLE LIVER TISSUE PREPARATION AND BIOENERGETICS

As an alternative for freshly isolated primary human hepatocytes, whole liver tissue was also assessed in the XF24 Seahorse instrument. In a category 2 safety cabinet, fresh liver wedges were washed with warm PBS to remove excess of blood. Using an Integra™ Miltex™

Standard Biopsy Punch, 3mm sections of fresh tissue were cut and placed in XF24 islet capture plates in XF base medium. Forceps were used to fit and secure the capture screen on top of the liver tissue section.

Whole tissue requires higher concentrations of effectors in comparison to cell suspensions, therefore oligomycin, FCCP and rotenone/antimycin A were used at 10 µM and 50 µM. Basal OCR was measured for 4 cycles, oligomycin for 5 cycles, FCCP for 4 cycles and rotenone/antimycin A for 4 cycles. All cycles were set to mix for 1 minute, wait for 2 minutes and measure for 4 minutes.

4.4 HOMOGENISE LIVER TISSUE PREPARATION AND BIOENERGETICS

In addition to whole liver tissue, mitochondrial bioenergetics of homogenised liver tissue was also tested. 3-5 grams of liver tissue was placed in a Cole-Parmer Tissue Grinder and liver tissue was macerated using manual force. Liver homogenise was resuspended in XF base medium and transferred to XF24 islet capture plates. Seahorse bioenergetics analysis was then carried on following same protocol as for whole liver tissue.

4.5 HEPARG 2D CELL CULTURE

HepaRG cells were seeded in 24-well SeaHorse plates at 200k cells per well. The cells were cultured in Williams E medium (WEM) containing Gibco™ Primary Hepatocyte Thawing and Plating Supplements for 14 days before differentiation (proliferative phenotype). Medium was renewed every 3 days. After 14 days in culture when HepaRG were highly confluent, plating medium was replaced with WEM containing HepaRG Differentiation

Medium Supplement with antibiotics. After 14 days, cell differentiation was verified by visualization of two cell types: hepatocyte colonies and primitive biliary cells.

4.6 OLEATE AND PALMITATE EXPOSURE

To induce steatosis, Oleate and palmitate were purchased from Sigma-Aldrich (St. Louis, USA) and prepared at a 2:1 molar ratio. Fatty acids present poor solubility in the cell culture media and *in vivo* free fatty acids travel in the bloodstream bound to albumin. Thus, to allow solubilisation in the media and mimic physiological conditions, oleate and palmitate were conjugated to BSA as previously described by Kown *et al*., 2014. Oleate and palmitate were used at 100 µM, 250 µM, 500 µM and 1000 µM concentrations. BSA vehicle solution was used for all control conditions. BSA vehicle was prepared at the highest concentration of 1000 µM. Cells were treated with oleate and palmitate or BSA vehicle control for 24 or 48 hours, cells were then washed five times with phosphate-buffered saline (PBS) prior to intracellular lipid staining.

4.7 BODIPY™ STAINING AND STEATOSIS QUANTIFICATION

After oleate and palmitate exposure, HepaRG cells were stained in the 24-well SeaHorse plate. HepaRG cells were first fixed with 4% paraformaldehyde for 30 minutes at room temperature and washed three times with PBS.

BODIPY™ staining was then performed to visualise lipid droplets and measure hepatocellular fat content semi-quantitatively. BODIPY™ 505/515 (Invitrogen, California, USA) was prepared in DMSO to give a stock solution of 5mM and stored in a dark bottle

protected from light. BODIPY™ 505/515 is a lipophilic green fluorescent probe that identifies intracellular lipid droplets. On the day of the assay, 2 µM BODIPY™ staining solution was prepared by diluting stock solution in PBS. 2 µM BODIPY™ was added to fixed cells for 15 minutes at room temperature. After staining, cells were washed with PBS and imaged. HepaRG cells were imaged under a Leica DMi8 fluorescence microscope using 505nm excitation and 515nm emission filters. Images were recorded and lipid droplets were quantified using CellProfiler software. Percentage of steatotic cells was calculated by the average of three wells scanned by the software.

4.8 TMAO AND PAA EXPOSURE

Trimethylamine N-oxide and phenylacetic acid were purchased from Sigma-Aldrich (St. Louis, USA). 1mg/mL TMAO and PAA stock solution were prepared in ethanol and stored at –20°C. On the day of the experiment, TMAO was diluted in plating medium at different concentrations 20 µM, 50 µM, 100 µM and 200 µM and PAA at 100 µM and 200 µM. HepaRG cells were treated with TMAO or PAA for 24 and 48 hours. After treatment, cells were washed with PBS and mitochondrial bioenergetics or BODIPY™ staining were performed.

4.9 BIOENERGETIC ANALYSIS OF HEPARG CELLS

Seahorse XF24 cell culture plates, XF24 islet capture plates, sensor cartridges with utility plates, XF base medium and XF calibrant solution were obtained from Agilent Technologies (Lexington, USA). Oligomycin, BAM15, FCCP, rotenone and antimycin A were purchased from Sigma-Aldrich (St. Louis, USA). The final concentrations of effectors were:

0.25 µM oligomycin, 1 µM BAM15 and 1 µM rotenone/antimycin A. 60µL of each effector were loaded into the injection ports.

Sensor cartridges were hydrated overnight with 1mL of XF calibrant solution at a non-CO_2 incubator. Plating medium was replaced with XF base medium and HepaRG cells were equilibrated at 37°C in a non-CO_2 incubator for 1h. After complete calibration, cell plate was loaded into the Seahorse Analyser. Mito Stress protocol consisted of equilibration, basal OCR/ECAR rates (3-4 cycles), injection of oligomycin port A (3-5 cycles), injection of BAM15 port B (3-4 cycles), and injection of rotenone/antimycin A port C (3-4 cycles). All cycles were set to mix for 3 minutes, wait for 2 minutes and measure for 3 minutes.

4.10 SEAHORSE CELL NUMBER NORMALISATION

DAPI (4',6-diamidino-2-phenylindole) a bright blue nuclear counterstain was used to determine the number of nuclei present in each well. DAPI (Invitrogen, California, USA) was prepared in deionized water to give a stock solution of 5mg/mL in a dark bottle protected from light. An intermediate solution of 300 µM was prepared in PBS and stored at -20°C. On the day of the assay, 300 nM DAPI staining solution was prepared by diluting intermediate solution in PBS. DAPI was then added to the final reagent of the Seahorse assay before injection. The cells in the well were stained during the final step of the assay. Once the cells were stained, the plate was removed from the Seahorse and placed in the Fluostar® Omega (BMG Labtech, Ortenberg, Germany). DAPI fluorescence was measured using 350 nm excitation and 470 nm emission filter settings.

4.11 RNA ISOLATION

RNA isolation was performed by using Trizol® (Life Technologies, California, USA) and Direct-zol™ RNA Miniprep Kit (Zymo Research, Irvine, USA). RNA isolation was conducted according to the manufacturers' protocol. In brief, Trizol® was added directly to the culture plate to lyse cells and equal part of ethanol was added. Mixture was transfer to Zymo-Spin™ IICR Column, washed three times and eluted in 50µL of Rnase-free water. NanoDrop™ 2000 spectrophotometer (Thermo Fisher Scientific, San Jose, USA) was used to assess RNA purity and quantity.

4.12 REAL-TIME PCR

Transcription of RNA into cDNA was conducted with the High-Capacity cDNA Reverse Transcription Kit (Applied Biosystems, California, USA) according to the manufacturer's protocol. cDNA reactions were loaded into the G-Storm GS0004M Thermal Cycler (Gene Technologies Ltd., Somerset, UK) and stored at 4°C for further real-time PCR.

The real-time PCR was carried out with the PowerUp™ SYBR® Green Master Mix (Thermo Fisher Scientific, San Jose, USA) on a LightCycler® 480 instrument (Roche Life Science, Penzberg, Germany). The thermal cycling procedure started with an initial denaturation at 95°C for 15 minutes. This was followed by 40 cycles of denaturation for 15s at 95°C, primer binding for 1 minute at 60°C and elongation for 1 minute at 60°C. The procedure ended with a final elongation at 60°C for 15 minutes and the addition of a dissociation curve step. Primers were purchased from Invitrogen (California, USA). The primer pairs' sequences used for the real-time PCR are shown on table 4.

Table 4. Primer Sequences

Gene	Forward 5’	Reverse 3’-5’
HPRT1 (housekeeping)	CCCTGGCGTCGTGATTAGTG	TCGAGCAAGACGTTCAGTCC
Albumin	GGAATTGCTGCCATGGAGATCTGC	CCTTCAGTTTACTGGAGATCG
CPT-1a	AGATTTTGCTGTCGGTCTTGGA	CACCAGTCGCTCACGTAATTTG
CYP3A4	CATTCCTCATCCCAATTCTTGAAGT	CCACTCGGTGCTTTTGTGTATCT
FXR	TGGGGAACTGAAAATGACTC	ACAGGCAAAGTGTTGAGGAT
HNF4a	TGTACTCCTGCAGATTTAGCC	CTGTCCTCATAGCTTGACCT
MRP2	CAAACTCTATCTTGCTAAGCAGG	TGAGTACAAGGGCCAGCTCTA
MDR1/Pglycoprotein	CTAATGCCGAACACATTGGA	CAGTCGCTTTATTTCTTTGCC

4.13 STATISTICAL ANALYSES

All data presented are mean values ± standard deviations (SDs). Statistical significance of parametric data was assessed by one-way analysis of variance (ANOVA). Pearson’s correlation test was used for correlation analyses. All statistical analyses were performed using GraphPad Prism 5.0 (GraphPad Software Inc., USA). P-values less than 0.05 were considered statistically significant.

CHAPTER 5.
RESULTS - 2D CELL CULTURE & WHOLE LIVER TISSUE

5.1 PRIMARY HUMAN HEPATOCYTES AND WHOLE TISSUE BIOENERGETICS

5.1.1 FRESHLY ISOLATED PRIMARY HUMAN HEPATOCYTES FROM LIVER RESECTIONS RAPIDLY LOSE THEIR PHENOTYPE IN 2D CULTURE

Since primary human hepatocytes isolated from resection tissue did not reliably attach to the Liverchip scaffolds, Human hepatocytes were then cultured and maintained in monolayer 2D culture to enable exploration of the primary hypothesis of TMAO and PAA effects on mitochondrial bioenergetics. In 2D, isolated primary human hepatocytes were cultured for 4 to 5 days before losing their morphological features (Figure 5.1).

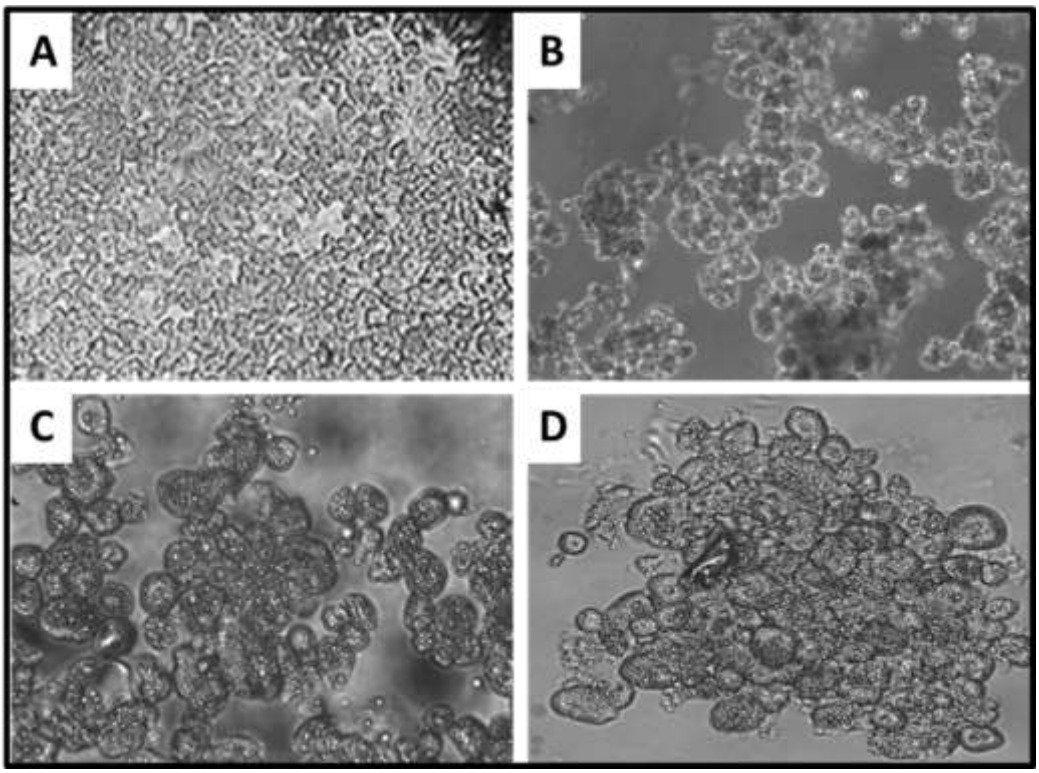

Figure 5.1. Primary human hepatocytes in 2D. Inverted light microscopy images of freshly isolated primary human hepatocytes in 2D cell culture. A. Hepatocytes cultured for 2 days

maintain their hexagonal shape and double nuclei in a flat cell monolayer (10x magnification) B. Hepatocytes aggregate and preserve their typical hexagonal shape after cultured for 5 days (20x magnification) C. After 6 days in culture, hepatocytes lose their morphological features presenting round shapes (20x magnification) D. After 8 days in culture, hepatocytes show a complete loss in morphology with spherical shapes and multi nuclei (20x magnification).

5.1.2 FRESHLY ISOLATED PRIMARY HUMAN HEPATOCYTES FROM LIVER WEDGES OBTAINED FROM TUMOUR RESECTION SURGERY ARE NOT VIABLE FOR MITOCHONDRIAL ANALYSES

Isolation of primary human hepatocytes is extremely challenging, and it relies on the quality of the liver tissue obtained. To analyse whether the freshly isolated primary human hepatocytes were viable and consuming oxygen, 500k cells per well were analysed using the Seahorse XF24. Oligomycin, FCCP and rotenone/antimycin were used to interrogate mitochondrial bioenergetics. Freshly isolated hepatocytes did not respond to any of the effectors injected and did not consume oxygen (Figure 5.2). This finding suggests that the primary human hepatocytes obtained were not viable for mitochondrial analyses due to the ischemic condition of the liver wedges used for these experiments.

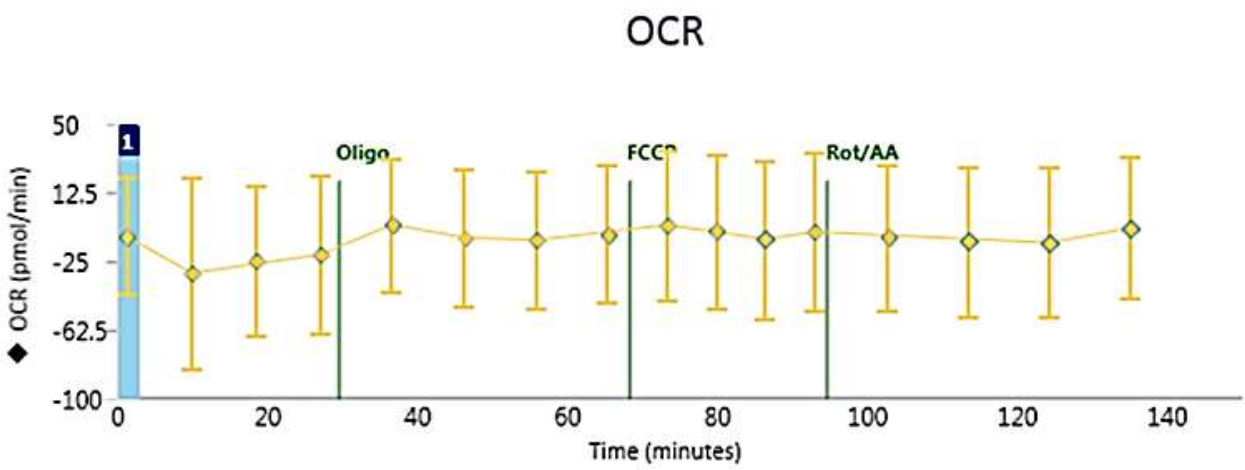

Figure 5.2. Mito stress test performed in freshly isolated primary human hepatocytes. Mitochondrial respiration reflected by OCR levels was not detected in freshly isolated primary human hepatocytes. Basal OCR rates (4 cycles), injection of oligomycin port A (4 cycles), injection of FCCP port B (4 cycles), and injection of rotenone/antimycin A port C (4 cycles). Data are presented as mean ± SD, n = 3.

5.1.3 WHOLE LIVER TISSUE SLICES AND HOMOGENISED LIVER TISSUE ARE NOT VIABLE FOR MITOCHONDRIAL ANALYSES USING THE XF24 ANALYSER

Mitochondrial bioenergetics of freshly isolated primary human hepatocytes indicated that these cells were not consuming oxygen. Final attempts to measure mitochondrial respiration from the liver wedges were performed. Whole tissue slices and macerated liver tissue were tested with oligomycin, FCCP and rotenone/antimycin injected at 10 µM and 50 µM concentrations. Whole and homogenised liver tissue presented oxygen consumption; however, they did not respond to any of the tested effectors (Figure 5.3).

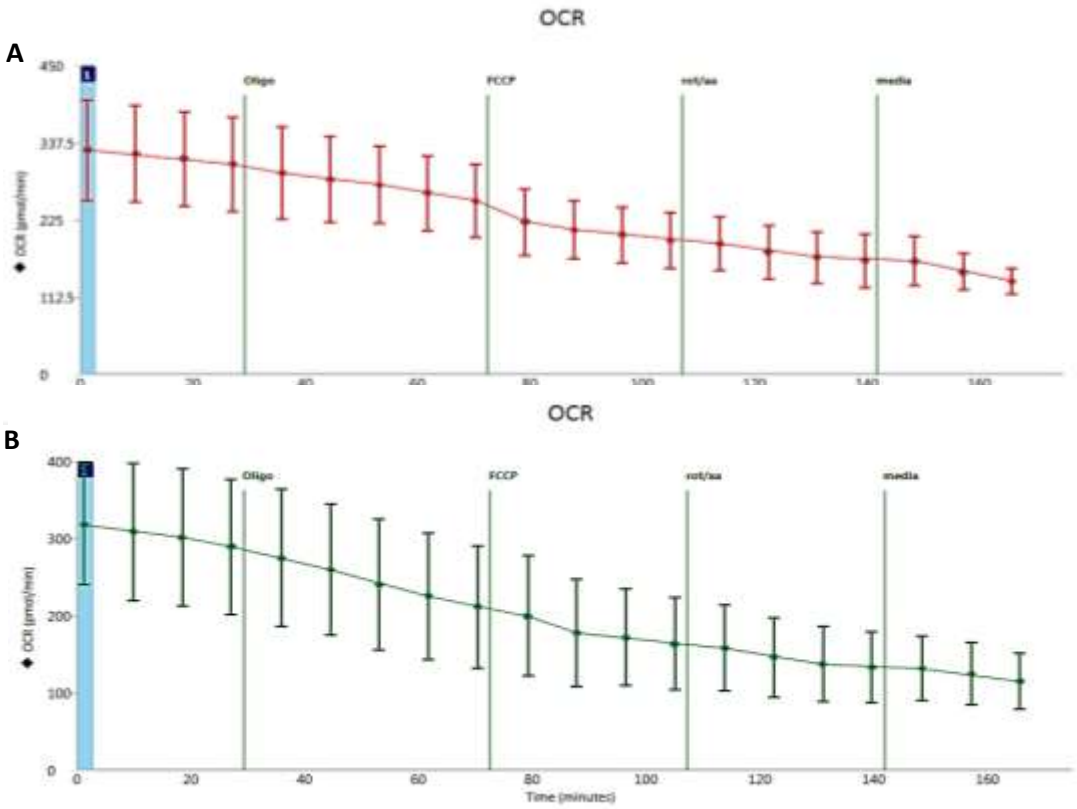

Figure 5.3. Mito stress test performed in whole liver tissue (A) and liver homogenise (B). Basal OCR rates (4 cycles), injection of oligomycin port A (5 cycles), injection of FCCP port B (4 cycles), injection of rotenone/antimycin A port C (4 cycles), injection of media port D (3 cycles). Data are presented as mean ± SD, n = 3.

5.2 INDUCTION OF STEATOSIS IN 2D CULTURE OF HEPARG CELLS

5.2.1 HEPARG CELLS PRESENT HEPATIC FEATURES WHEN EXPOSED TO DMSO

Due to the challenges involved in obtaining reliable and robust mitochondrial measurements in ex vivo liver material, we shifted focus to work on HepaRG cells to test our hypothesis that TMAO and PAA have effects on steatosis and mitochondrial bioenergetics. HepaRG cells in proliferative and differentiated states were analysed to mimic different cell

phenotypes that are found in diseased livers. Proliferative HepaRG present low CYP450 activity therefore they are similar to hepatocytes in progenitor states or aged cells. Differentiated HepaRG cells are resistant to DMSO and present high CYP450 expression, these cells are more representative to healthy young hepatocytes found in healthy livers. HepaRG cells started proliferation presenting the typical fibroblastic morphology of proliferating cells (day 3). At around day 7, HepaRG reached tight confluency and initiated the differentiation program. Cells remained in growth medium for an additional 7 days. During that time cells started to re arrange themselves, forming islands in which the cells adopted a hepatocyte morphology, at that point (day 14) the medium was switched to the differentiation medium containing 1.7% DMSO. After 14 days in the differentiation medium HepaRG cells were fully differentiated. HepaRG cells morphologically resembled two different populations of hepatocyte and biliary-like cells (Figure 5.4).

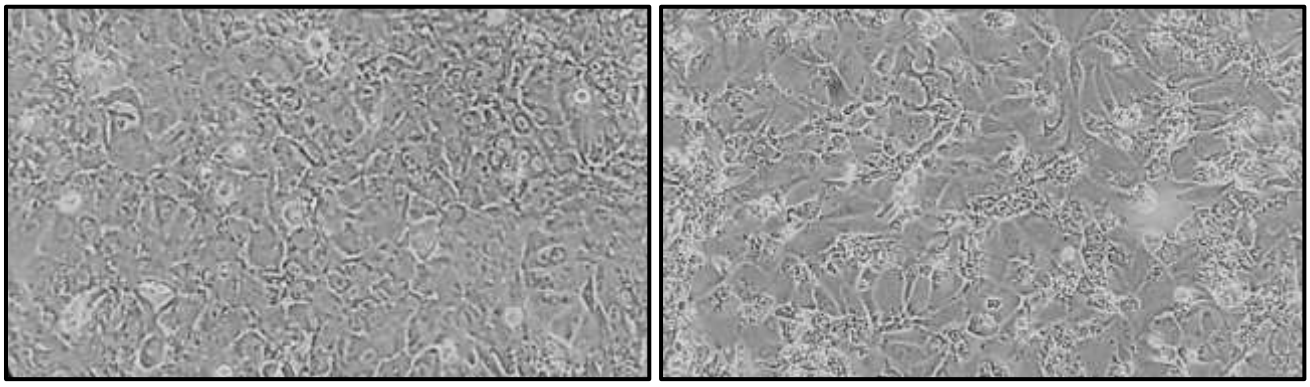

Figure 5.4. Inverted Light Microscopy images of HepaRG 2D cultures. Proliferative HepaRG cells 14 days after seeding preserve epithelial-like morphology (left). At day 15, growth medium was changed to differentiation medium and cells were cultured for 14 more days. Differentiated HepaRG cells morphologically resemble two distinct populations of hepatocyte-like and biliary-like cells (right). 20x magnification.

5.2.2 OLEATE AND PALMITATE INDUCE STEATOSIS IN PROLIFERATIVE HEPARG CELLS

Steatosis was successfully induced in proliferative HepaRG cells exposed to oleate and palmitate for 48 hours. BODIPY™ imaging and respective quantification are depicted below (Figure 5.5). Negative control and BSA vehicle control did not present fatty acid accumulation (Figure 5.5A and 5.5B). 100 µM of oleate and palmitate caused lipid accumulation in 10% of HepaRG cells (Figure 5.5C), while 250 µM of oleate and palmitate promoted steatosis in 31% of the cells (Figure 5.5D). When exposed to 500 µM of oleate and palmitate 45% of proliferative HepaRG showed intracellular lipids (Figure 5.5E), the highest concentration of 1000 µM of oleate and palmitate induced steatosis in 73% of proliferative HepaRG cells (Figure 5.5F). The accumulation of intracellular lipids after Oleate and palmitate exposure was statistically significant when compared to BSA vehicle control. These results suggest that HepaRG cells are a suitable model to study liver steatosis as lipid accumulation was consistent and occurred in a dose dependent manner.

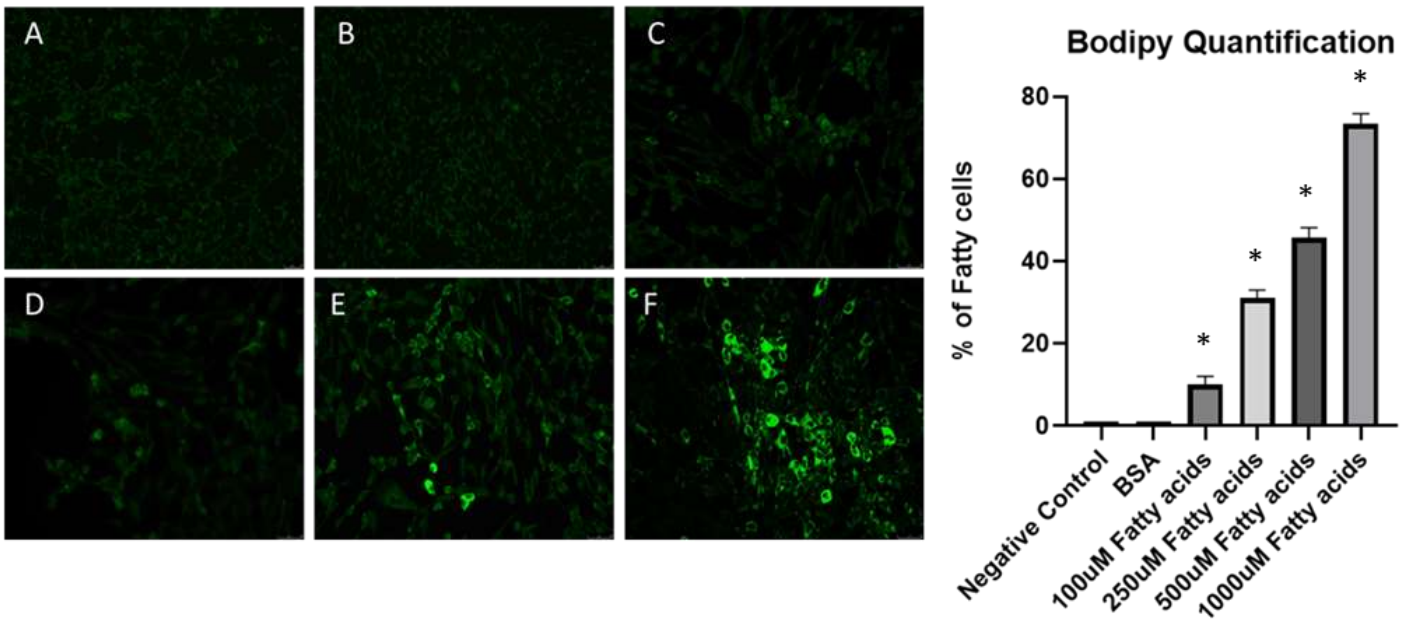

Figure 5.5. Proliferative HepaRG cells exposed to fatty acids. BODIPY™ staining of intracellular lipid droplets in proliferative HepaRG cells (left). Quantification of BODIPY™ staining using the CellProfiler software (right). A. Negative Control B. BSA vehicle control C. Proliferative HepaRG cells exposed to 100 µM Oleate and Palmitate. D. Proliferative HepaRG cells exposed to 250 µM Oleate and Palmitate. E. Proliferative HepaRG cells exposed to 500 µM Oleate and Palmitate. F. Proliferative HepaRG cells exposed to 1000 µM Oleate and Palmitate. *Indicates that the values are significantly different from negative control, $p < 0.05$.

5.2.3 TMAO EXARCEBATES STEATOSIS IN PROLIFERATIVE HEPARG CELLS

To elucidate whether TMAO exacerbates intracellular lipid accumulation in proliferative HepaRG cells, oleate and palmitate combined with TMAO were added to the culture medium for 48 hours. No lipid droplets were observed in culture medium, BSA and TMAO controls (Figure 5.6A, 5.6B, 5.6C). 250 µM of oleate and palmitate combined with 20 µM of TMAO caused fat accumulation in 38% of cells (Figure 5.6E), while 45% was steatotic with fatty acids combined with 50 µM of TMAO (Figure 5.6F), 77% of HepaRG cells were steatotic with 1000 µM of TMAO (Figure 5.6G) in comparison to only 35% with 250 µM of

oleate and palmitate alone (Figure 5.6D). These findings indicated that TMAO combined with fatty acids significantly elevated intracellular lipid content in proliferative HepaRG cells.

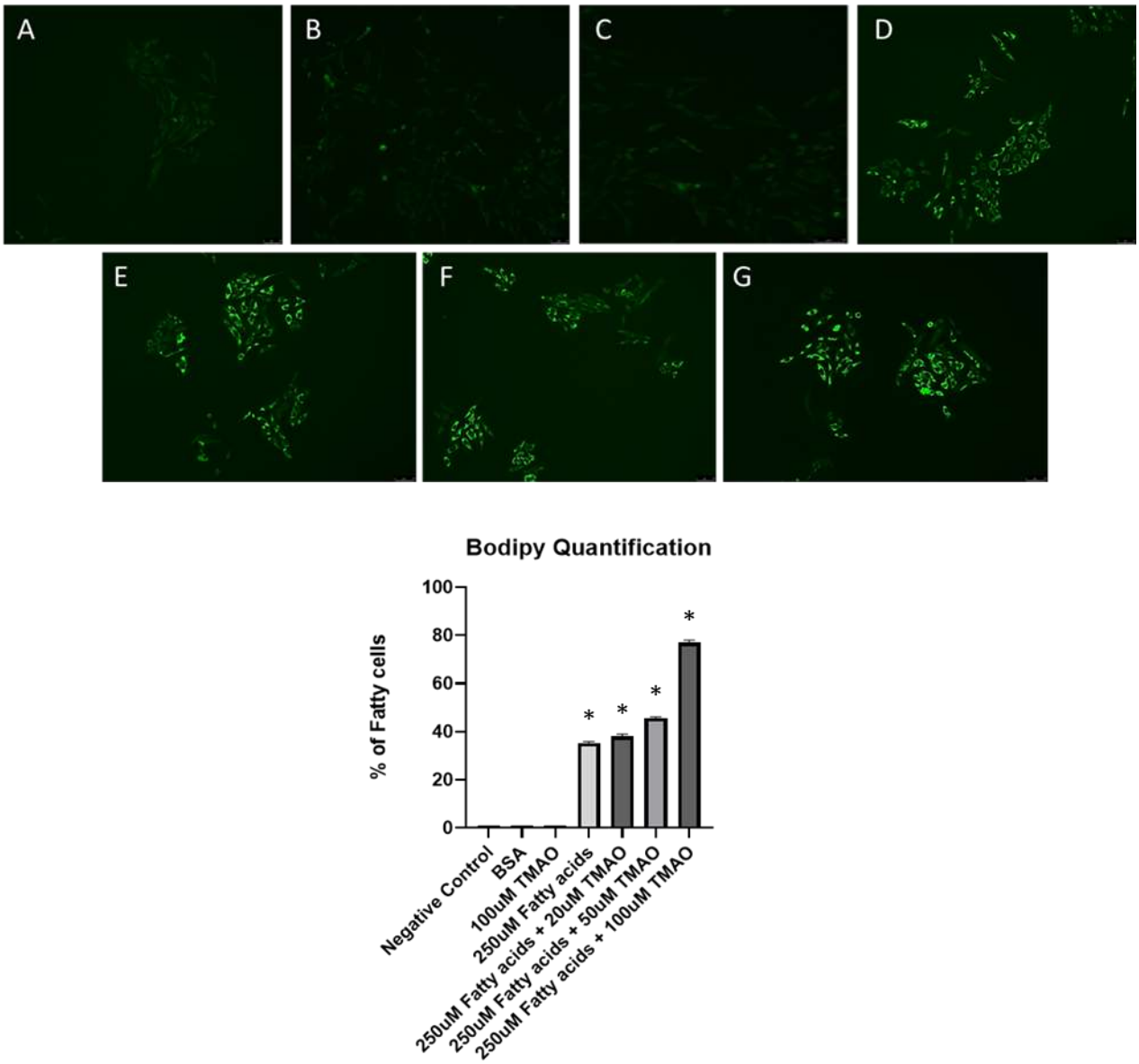

Figure 5.6. Proliferative HepaRG cells exposed to fatty acids combined with TMAO. BODIPY™ staining of intracellular lipid droplets in proliferative HepaRG cells (top). Quantification of BODIPY™ staining using the CellProfiler software (bottom). A. Negative Control B. BSA vehicle control C. Proliferative HepaRG cells exposed to 100 µM of TMAO. D. Proliferative HepaRG

cells exposed to 250 µM Oleate and Palmitate E. Proliferative HepaRG cells exposed to 250 µM Oleate and Palmitate combined with 20 µM of TMAO. F. Proliferative HepaRG cells exposed to 250 µM Oleate and Palmitate combined with 50 µM of TMAO. G. Proliferative HepaRG cells exposed to 250 µM Oleate and Palmitate combined with 100 µM of TMAO. *Indicates that the values are significantly different from negative control, $p < 0.05$.

5.2.4 PAA EXARCEBATES STEATOSIS IN PROLIFERATIVE HEPARG CELLS

The same determinations of BODIPY quantification of steatosis were performed in the presence of increasing concentrations of PAA combined with 250 µM oleate and palmitate for 48 hours. PAA exposure promoted higher lipid accumulation than TMAO. Oleate and palmitate combined with 50 µM of PAA induced lipid droplets in 56% of HepaRG cells (Figure 5.7E), 68% of cells were steatotic with 100 µM of PAA (Figure 5.7F) and 89% of cells with 200 µM of PAA plus oleate and palmitate (Figure 5.7G). PAA alone without oleate and palmitate did not lead to lipid accumulation (Figure 5.7C), showing that the presence of fatty acids are necessary for the steatosis aggravation caused by PAA.

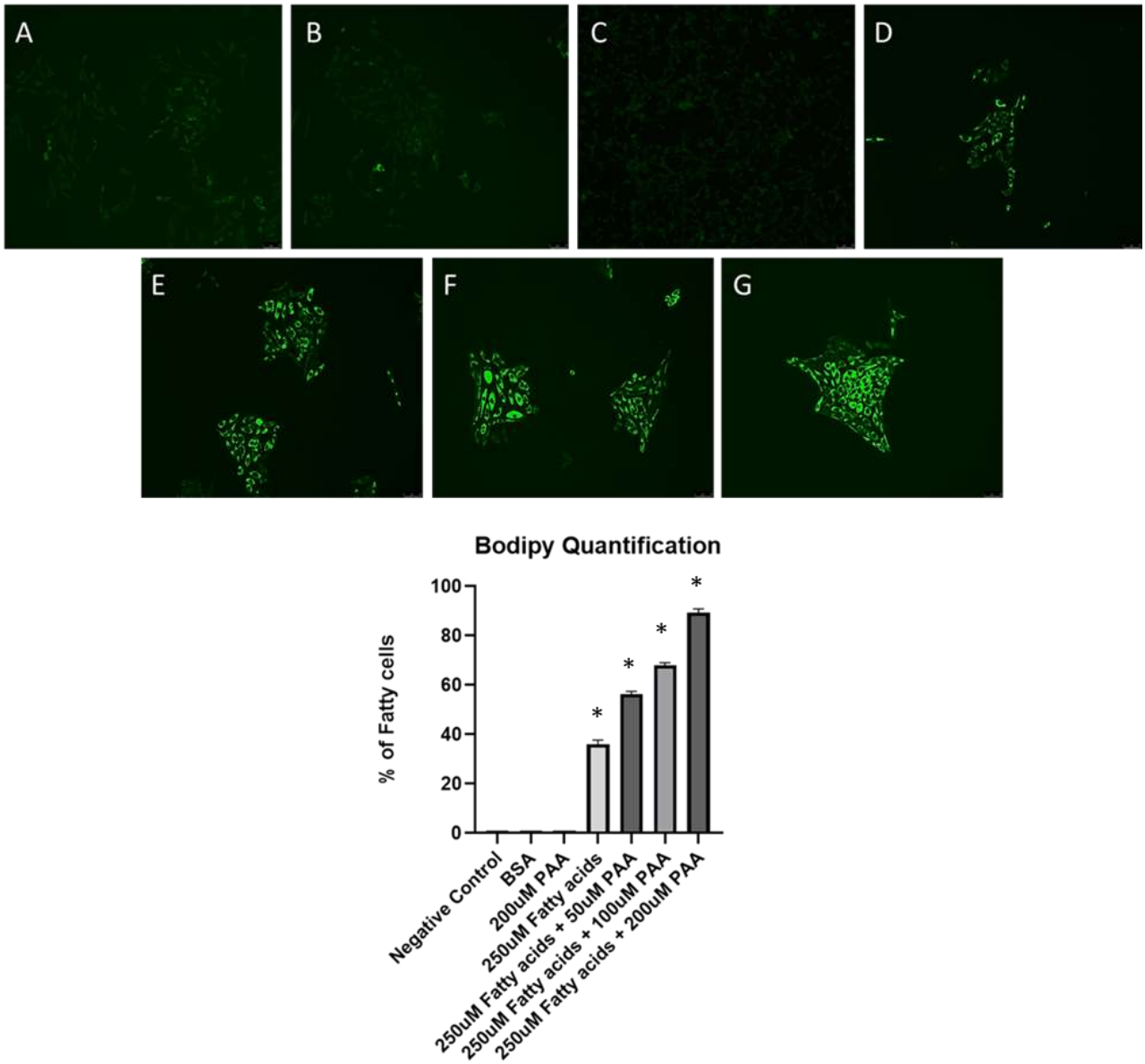

Figure 5.7. Proliferative HepaRG cells exposed to fatty acids combined with PAA. BODIPY™ staining of intracellular lipid droplets in proliferative HepaRG cells (top). Quantification of BODIPY™ staining using the CellProfiler software (bottom). A. Negative Control B. BSA vehicle control C. Proliferative HepaRG cells exposed to 200 µM of PAA. D. Proliferative HepaRG cells exposed to 250 µM Oleate and Palmitate E. Proliferative HepaRG cells exposed to 250 µM Oleate and Palmitate combined with 50 µM of PAA. F. Proliferative HepaRG cells exposed to 250 µM Oleate and Palmitate combined with 100 µM of PAA. G. Proliferative HepaRG cells exposed to 250 µM Oleate and Palmitate combined with 200 µM of PAA. *Indicates that the values are significantly different from negative control, $p < 0.05$.

5.2.5 DIFFERENTIATED HEPARG CELLS ARE MORE RESISTANT TO OLEATE AND PALMITATE INDUCED STEATOSIS THAN PROLIFERATIVE HEPARG CELLS

Differentiated HepaRG cells maintain key hepatic functions including drug transporters such as OCT1 and MRP3 and xenobiotic-metabolizing CYP450 enzymes (Marion *et al*., 2010). To gain insight whether differentiated HepaRG cells would respond in a different way than proliferative cultures, oleate and palmitate were added to differentiation medium for 48 hours. Negative control, BSA vehicle control and 100 µM of oleate and palmitate did not present intracellular lipid droplets (Figure 5.8A, 5.8B, 5.8C). 250 µM of oleate and palmitate caused lipid accumulation in 1.6% of HepaRG cells (Figure 5.8D), while 500 µM of oleate and palmitate promoted steatosis in 2.6% of the cells (Figure 5.8E). When exposed to 1000 µM of oleate and palmitate 3.6% of differentiated HepaRG showed intracellular lipids (Figure 5.8F). These results indicate that when HepaRG cells are fully differentiated they become more resistant to steatosis than proliferative cells.

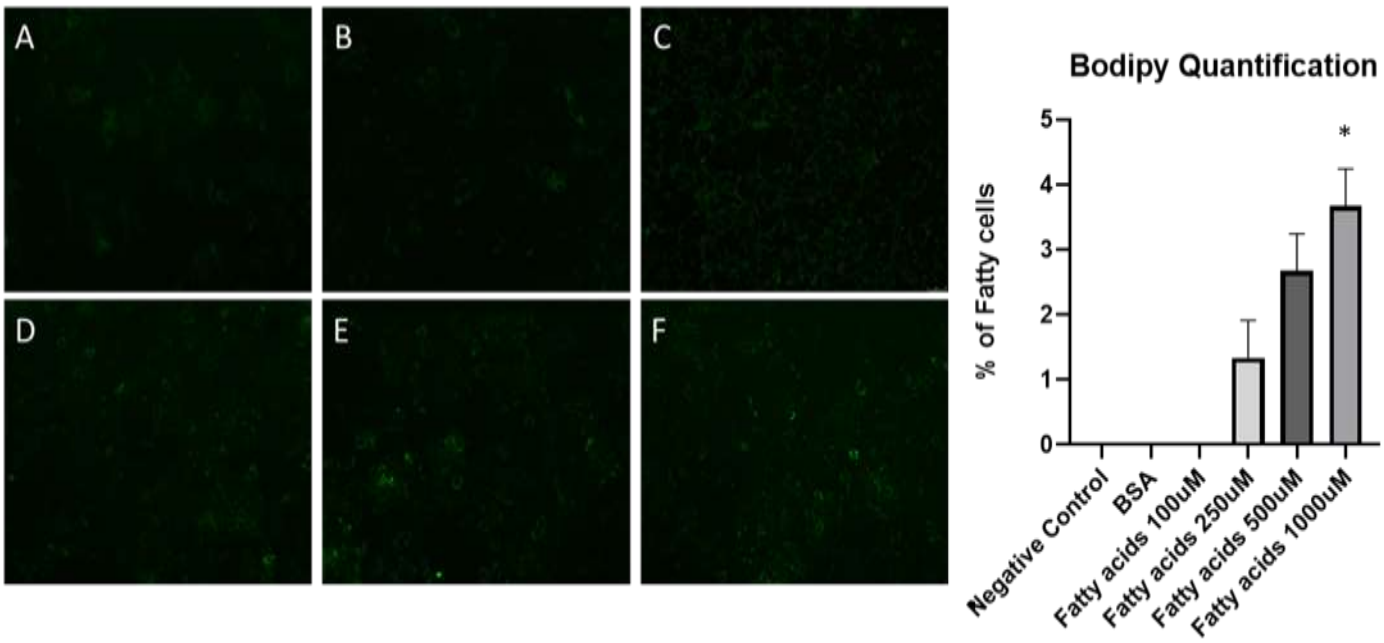

Figure 5.8. Differentiated HepaRG cells exposed to fatty acids. BODIPY™ staining of intracellular lipid droplets in differentiated HepaRG cells (left). Quantification of BODIPY™ staining using the CellProfiler software (right). A. Negative Control B. BSA vehicle control C. Differentiated HepaRG cells exposed to 100 µM Oleate and Palmitate. D. Differentiated HepaRG cells exposed to 250 µM Oleate and Palmitate. E. Differentiated HepaRG cells exposed to 500 µM Oleate and Palmitate. F. Differentiated HepaRG cells exposed to 1000 µM Oleate and Palmitate. *Indicates that the values are significantly different from negative control, $p < 0.05$.

5.2.6 TMAO SLIGHTLY INCREASES STEATOSIS IN DIFFERENTIATED HEPARG CELLS

TMAO was added to differentiated HepaRG cells in combination with oleate and palmitate for 48 hours. No lipid accumulation was observed in culture medium, BSA and TMAO controls (Figure 5.9A, 5.9B, 5.9C). 250 µM of oleate and palmitate combined with 20 µM of TMAO caused fat accumulation in 1.6% of cells (Figure 5.9E), while 2.3% was steatotic with fatty acids combined with 50 µM of TMAO (Figure 5.9F), 3.7% of HepaRG cells were

steatotic with 100 µM of TMAO (Figure 5.9G) in comparison to only 1.3% with 250 µM of oleate and palmitate alone (Figure 5.9D). These findings indicate that TMAO combined with fatty acids slightly elevated intracellular lipid content in differentiated cells, but these results were not statistically significant.

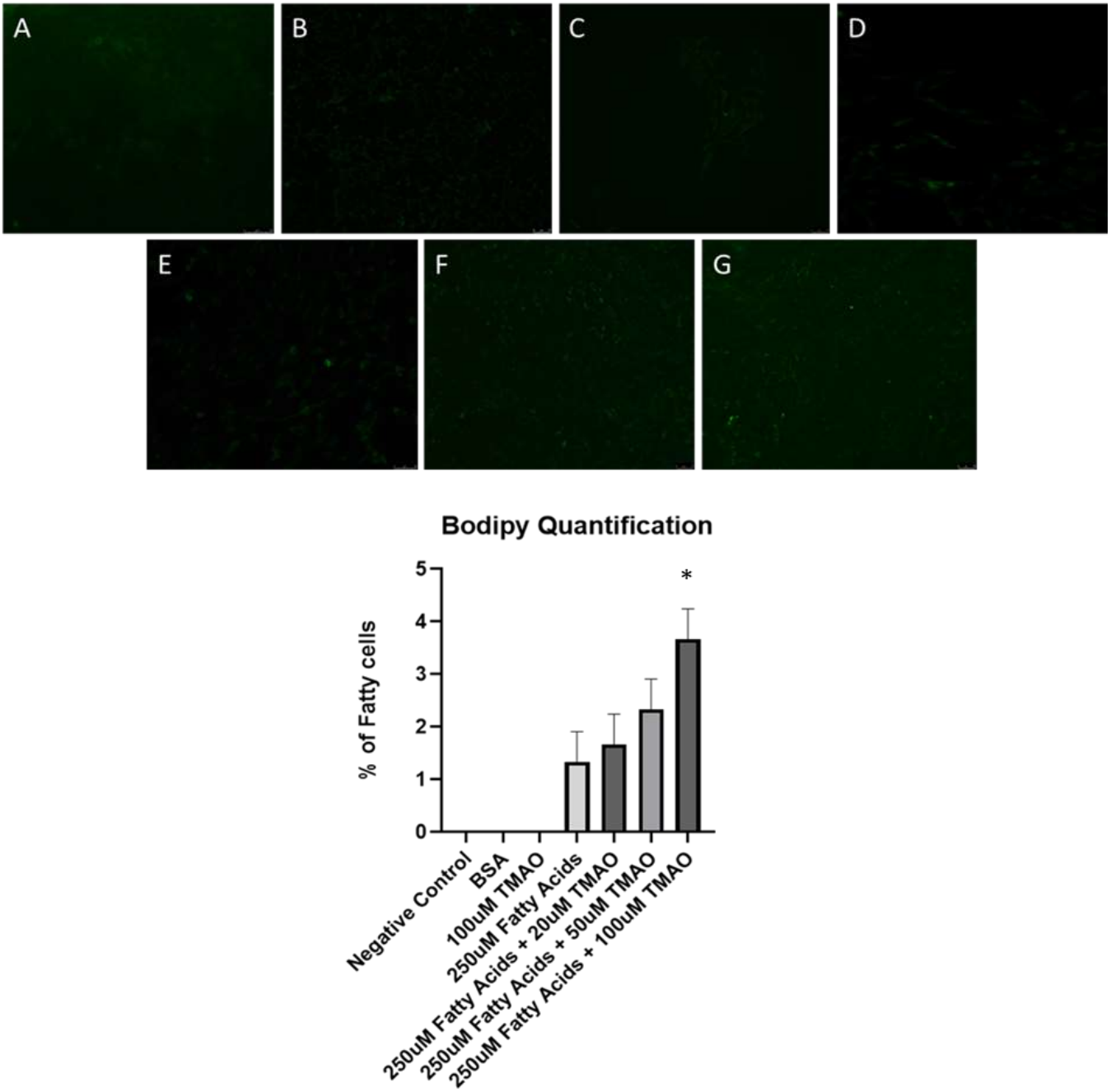

Figure 5.9. Differentiated HepaRG cells exposed to fatty acids combined with TMAO. BODIPY™ staining of intracellular lipid droplets in differentiated HepaRG cells (top). Quantification of BODIPY™ staining using the CellProfiler software (bottom). A. Negative Control B. BSA vehicle

control C. Differentiated HepaRG cells exposed to 100 µM of TMAO. D. Differentiated HepaRG cells exposed to 250 µM Oleate and Palmitate E. Differentiated HepaRG cells exposed to 250 µM Oleate and Palmitate combined with 20 µM of TMAO. F. Differentiated HepaRG cells exposed to 250 µM Oleate and Palmitate combined with 50 µM of TMAO. G. Differentiated HepaRG cells exposed to 250 µM Oleate and Palmitate combined with 100 µM of TMAO. *Indicates that the values are significantly different from negative control, $p < 0.05$.

5.2.7 PAA SLIGHTLY EXARCEBATES STEATOSIS IN DIFFERENTIATED HEPARG CELLS

BODIPY™ staining was quantified in differentiated HepaRG cells exposed to PAA combined with oleate and palmitate for 48 hours. Oleate and palmitate combined with 50 µM of PAA induced lipid droplets in 1.6% of HepaRG cells (Figure 5.10E), 5.3% of cells were steatotic with 100 µM of PAA (Figure 5.10F) and 12% of cells with 200 µM of PAA combined with oleate and palmitate (Figure 5.10G). High concentrations of PAA combined with fatty acids caused a 10% increase in lipid accumulation in differentiated HepaRG cells when compared to fatty acids alone (Table 5).

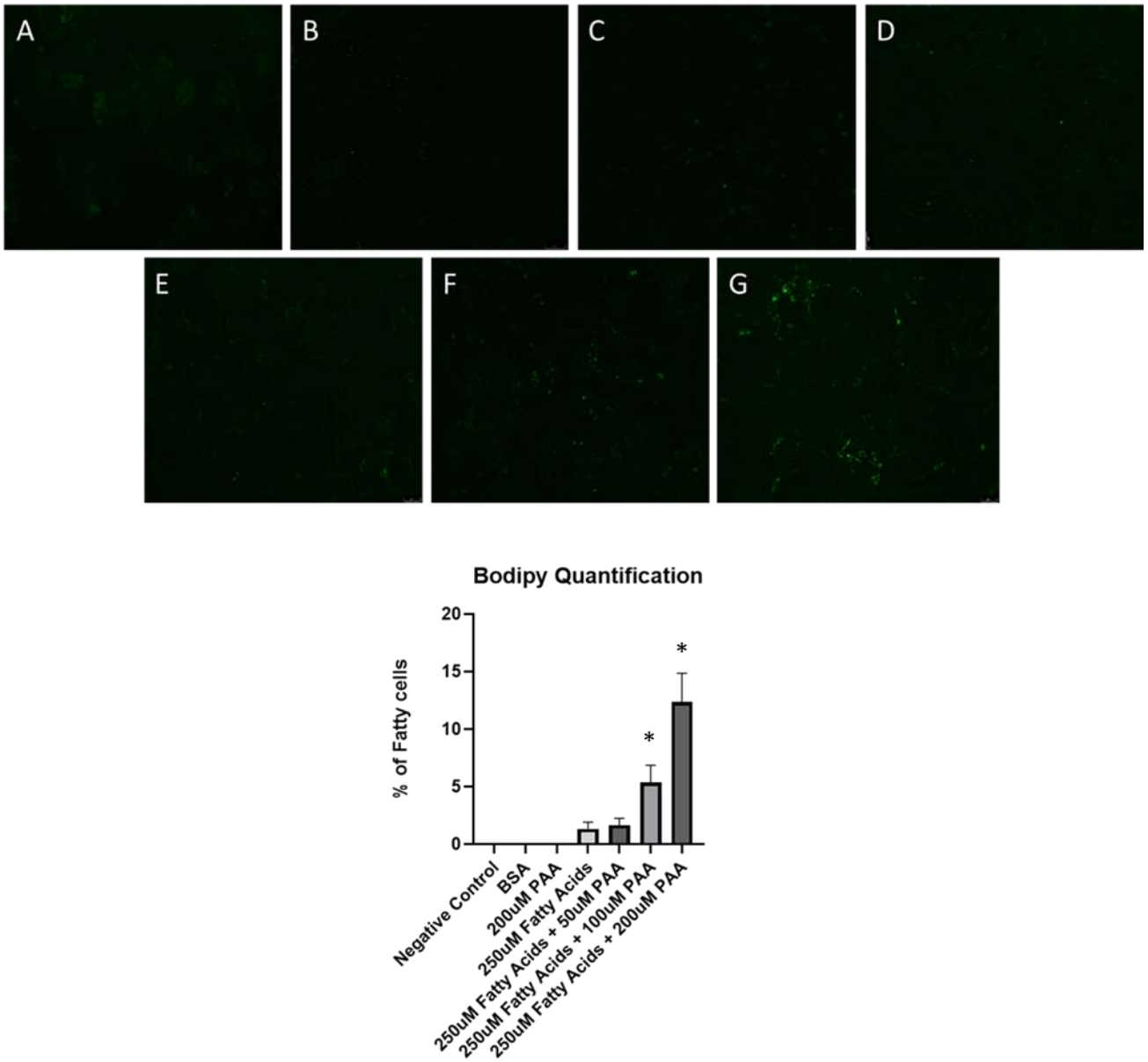

Figure 510. Differentiated HepaRG cells exposed to fatty acids combined with PAA. BODIPY™ staining of intracellular lipid droplets in differentiated HepaRG cells (top). Quantification of BODIPY™ staining using the CellProfiler software (bottom). A. Negative Control B. BSA vehicle control C. Differentiated HepaRG cells exposed to 200 µM of PAA. D. Differentiated HepaRG cells exposed to 250 µM Oleate and Palmitate E. Differentiated HepaRG cells exposed to 250 µM Oleate and Palmitate combined with 50 µM of PAA. F. Differentiated HepaRG cells exposed to 250 µM Oleate and Palmitate combined with 100 µM of PAA. G. Differentiated

HepaRG cells exposed to 250 µM Oleate and Palmitate combined with 200 µM of PAA. *Indicates that the values are significantly different from negative control, $p < 0.05$.

Table 5. Bodipy Quantification of Fatty Cells in Proliferative vs. Differentiated HepaRG

48h Exposure	Proliferative HepaRG	Differentiated HepaRG
	Percentage of Fatty Cells	
250µM Fatty Acids	31%	1.3%
250µM Fatty Acids + 20µM TMAO	38%	1.6%
250µM Fatty Acids + 50µM TMAO	45%	2.3%
250µM Fatty Acids + 100µM TMAO	77%	3.7%
250µM Fatty Acids + 50µM PAA	56%	1.6%
250µM Fatty Acids + 100µM PAA	68%	5.3%
250µM Fatty Acids + 200µM PAA	89%	12%

5.3 MITOCHONDRIAL BIOENERGETICS IN 2D CULTURE OF HEPARG CELLS

The Seahorse XF24 analyser was used to interrogate fundamental parameters of mitochondrial function: Basal respiration, ATP-linked respiration, Proton Leak, Maximal Respiration, Spare Respiratory Capacity, Coupling efficiency and Non-mitochondrial respiration as previously detailed in chapter 2 (Figure 5.11).

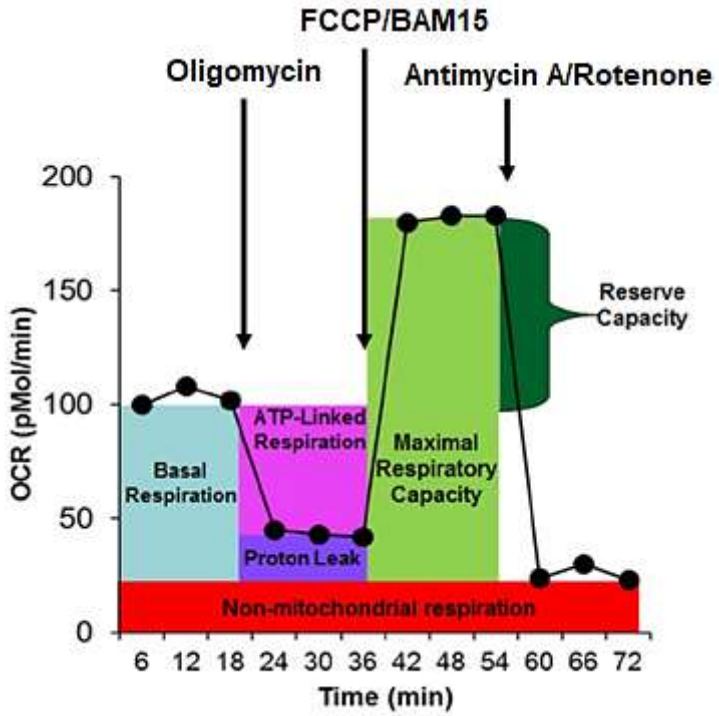

Figure 5.11. XF24 Mito Stress Test. OCR is measured before and after the addition of respiration inhibitors: Oligomycin, FCCP/BAM15 and Antimycin A/Rotenone to derive several parameters of mitochondrial respiration. Adapted from (Nicholas *et al.*, 2017).

5.3.1 PROLIFERATIVE HEPARG CELLS ARE SENSITIVE TO BIOENERGETIC INHIBITORS

Proliferative HepaRG cells were harvested for bioenergetics studies. 200k HepaRG cells at passage 16 were seeded in the XF24 microplate and exposed to oligomycin, BAM15 and antimycin/rotenone. OCR was normalized to number of cells using DAPI nuclear staining. Cells responded robustly to bioenergetic effectors with low intra-assay variability. Proliferative HepaRG cells typically present high values of basal respiration. In the absence of effectors, basal respiration varied from 250 to 350 pmol/min. Calculated proton leak was fairly low with an average of 20 pmol/min, signifying intact mitochondrial metabolism. After the addition of BAM 15 maximum respiration rate was greatly achieved, proliferative cells demonstrated around 1000 pmol/min maximal OCR. Spare respiratory capacity was

calculated by subtracting basal rates from maximal respiration. HepaRG cells in proliferative state expressed appropriate cell health with high spare capacity of 800 pmol/min. Non-mitochondrial respiration measured approximately 140 pmol/min and was used to correct OCR calculations. HepaRG cells are a hepatoma cell line known to produce maximal ATP synthesis through OXPHOS (Seyfried *et al*.,2020), ATP production varied from 200 to 350 pmol/min. As mentioned previously, proliferative cells present higher coupling efficiency when compared to fully differentiated cells. Proliferative HepaRG demonstrated coupling efficiency close to 100%, reflecting previous observations where hepatocytes present high coupling efficiency (Brand *et al*., 2011) (Figure 5.12).

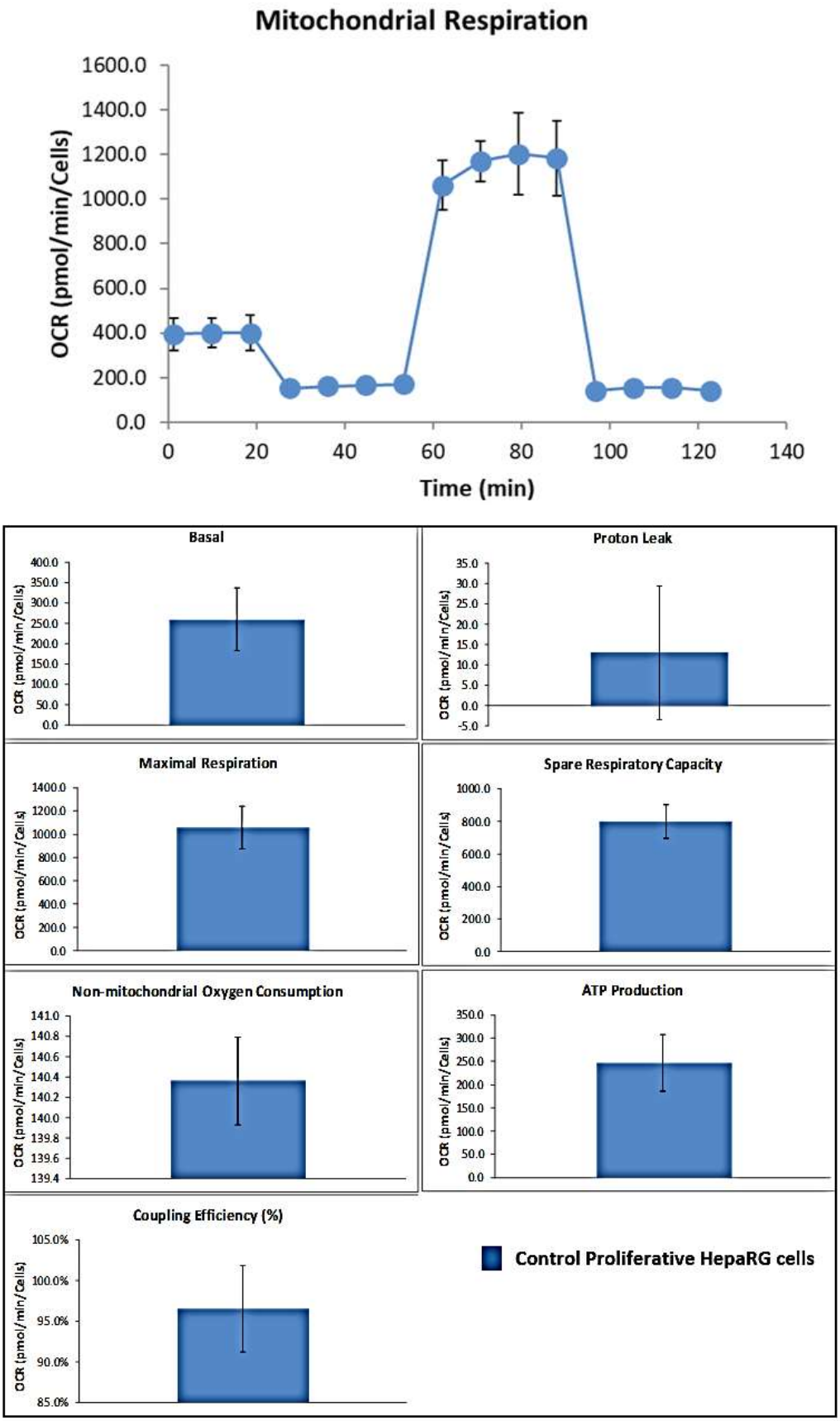

Figure 5.12. Results from a representative Mito Stress test in proliferative HepaRG cells. Depiction of mitochondrial bioenergetic parameters: basal respiration, ATP-linked

respiration, maximal respiration, spare respiratory capacity, proton leak, and non-mitochondrial respiration. Basal OCR rates (3 cycles), injection of oligomycin port A (4 cycles), injection of BAM15 port B (4 cycles), and injection of rotenone/antimycin A port C (4 cycles). Data are presented as mean ± SD, n = 3.

5.3.2 EXPOSURE TO OLEATE AND PALMITATE ALTERS MITOCHONDRIAL BIOENERGETICS IN PROLIFERATIVE HEPARG CELLS

As previously described, proliferative HepaRG cells became steatotic when exposed to oleate and palmitate for 48 hours. To elucidate whether different concentrations of oleate and palmitate would also affect mitochondrial function, HepaRG cells were exposed to the same high fat conditions and analysed with the Seahorse XF24 analyser.

Basal respiration was decreased when cells were exposed to oleate and palmitate. The lowest concentration of 100 µM of fatty acids did not cause any changes when compared to controls, however 250 µM, 500 µM and 1000 µM concentrations significantly reduced basal respiration rates. Proton leak was considerably low and oleate and palmitate caused a further reduction. Maximal respiration was significantly minimized in a dose dependent manner, the higher the concentration of oleate and palmitate, the lower the maximum rates. Maximal respiration of control cells was around 400 pmol/min while cells exposed to 1000 µM of oleate and palmitate presented maximal OCR of no more than 50 pmol/min. Additionally, high fat conditions caused a major reduction in spare respiratory capacity, non-mitochondrial respiration and ATP production with stronger effects observed at 250 µM, 500 µM and 1000 µM concentrations. Exposure to fatty acids for 48 hours did not cause any significant changes in coupling efficiency. Taken together these findings suggest that exposure to oleate and palmitate decrease important features of the mitochondrial respiration in proliferative

HepaRG cells (Figure 5.13).

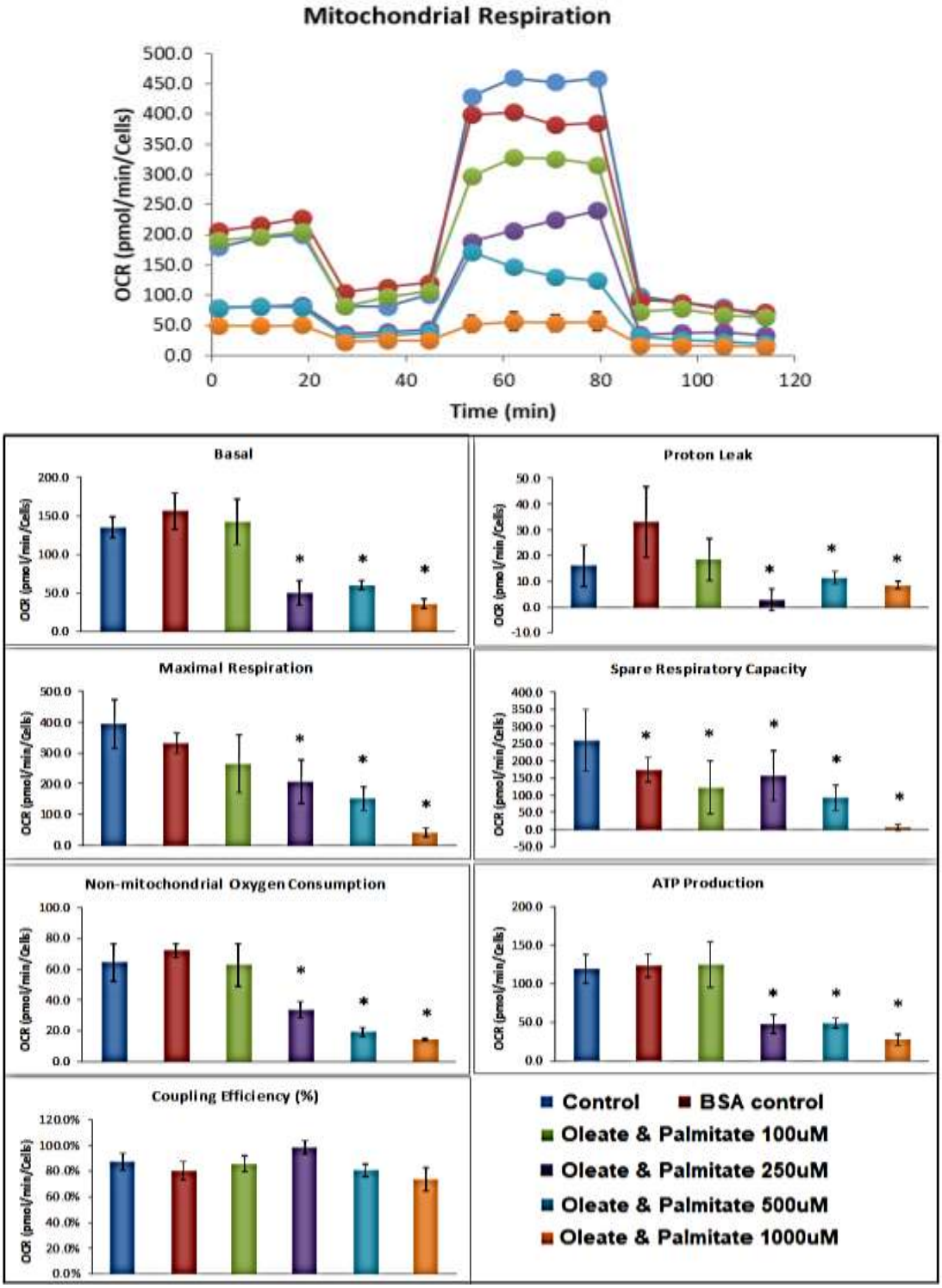

Figure 5.13. Results from a representative Mito Stress test in lipid loaded proliferative HepaRG cells. Cells were exposed to different concentrations of Oleate and Palmitate for 48 hours prior to bioenergetic analyses. Depiction of mitochondrial bioenergetic parameters: basal

respiration, ATP-linked respiration, maximal respiration, spare respiratory capacity, proton leak, and non-mitochondrial respiration. Basal OCR measurement (3 cycles), injection of oligomycin port A (3 cycles), injection of BAM15 port B (4 cycles), and injection of rotenone/antimycin A port C (4 cycles). Data are presented as mean ± SD, n = 3.

5.3.3 EXPOSURE TO GUT METABOLITES TMAO AND PAA CHANGES KEY MITOCHONDRIAL PARAMETERS IN PROLIFERATIVE HEPARG CELLS

Having demonstrated that TMAO and PAA increase steatosis in a concentration dependent manner, next the effects of TMAO and PAA on mitochondrial function were assessed in proliferative HepaRG cells. Cells were exposed to 20 µM and 50 µM of TMAO or 100 µM and 200 µM of PAA for 48 hours and OCR was measured with the Mito Stress test kit. All tested concentrations of TMAO and PAA triggered a 3-fold decrease in basal respiration. Proton leak rates were very low and for this reason high variability was expected. Maximum OCR rates were decreased dose-dependently by both metabolites, PAA having a greater stronger effect than TMAO at the concentrations being tested. Likewise, spare respiratory capacity was also reduced by PAA. PAA considerably lowered capacity rates while TMAO changes were not statistically significant when compared to control. No significant changes were seen in non-mitochondrial respiration, whereas ATP production declined approximately 50% with the addition of TMAO and PAA. Coupling efficiency could not be calculated since basal and ATP production rates were identical (Figure 5.14).

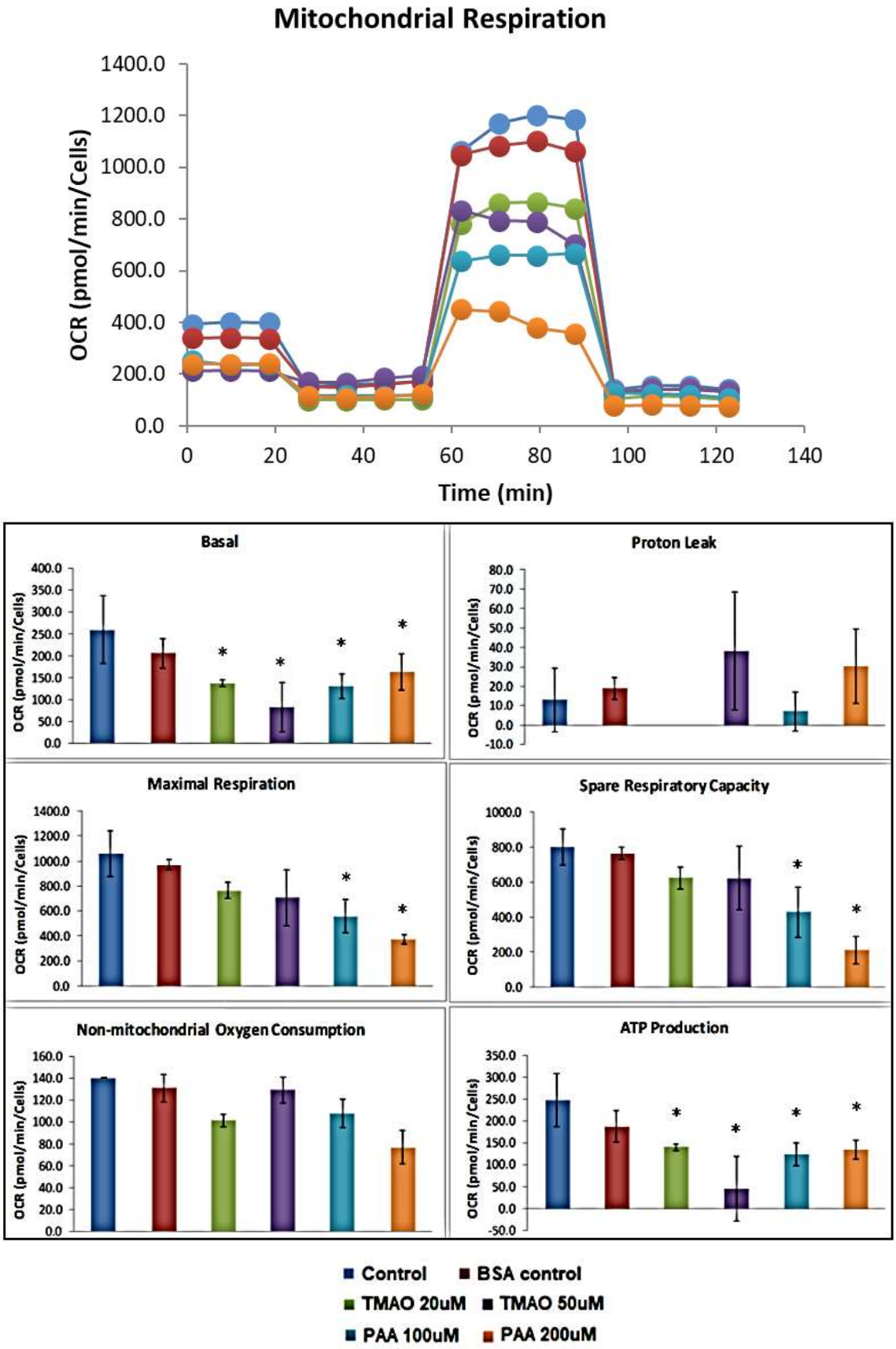

Figure 5.14. Results from a representative Mito Stress test in proliferative HepaRG cells exposed to TMAO and PAA. Cells were exposed to different concentrations of TMAO and PAA

for 48 hours prior to bioenergetic analyses. Depiction of mitochondrial bioenergetic parameters: basal respiration, proton leak, maximal respiration, spare respiratory capacity, non-mitochondrial respiration and ATP production. Basal OCR measurement (3 cycles), injection of oligomycin port A (4 cycles), injection of BAM15 port B (4 cycles), and injection of rotenone/antimycin A port C (4 cycles). Data are presented as mean ± SD, n = 3.

5.3.4 ADDITION OF TMAO AND PAA COMBINED WITH 250 μM OLEATE AND PALMITATE ALTERS MITOCHONDRIAL BIOENERGETICS IN PROLIFERATIVE HEPARG CELLS

Combination of fatty acids with TMAO and PAA aggravated lipid accumulation as depicted above. In order to elucidate whether steatosis exacerbation was associated with mitochondrial dysfunction, proliferative cells were exposed to microbiome metabolites TMAO and PAA combined with 250 μM of fatty acids and mitochondrial OCR was measured. In conditions of combining fatty acids with TMAO or PAA, proliferative HepaRG cells appeared to be highly stressed since overall OCR was significantly reduced. No significant changes in basal respiration and proton leak were detected. Maximal respiration and spare respiratory capacity decreased by TMAO and further reduced with PAA exposure. PAA lowered non-mitochondrial rates and ATP production, while TMAO did not show any significant effect to these parameters. No significant change in coupling efficiency was observed. These results indicate that the major effect of TMAO and PAA is a reduction in spare respiratory capacity which corresponds and is associated with steatosis observed with BODIPY™ staining (Figure 5.15).

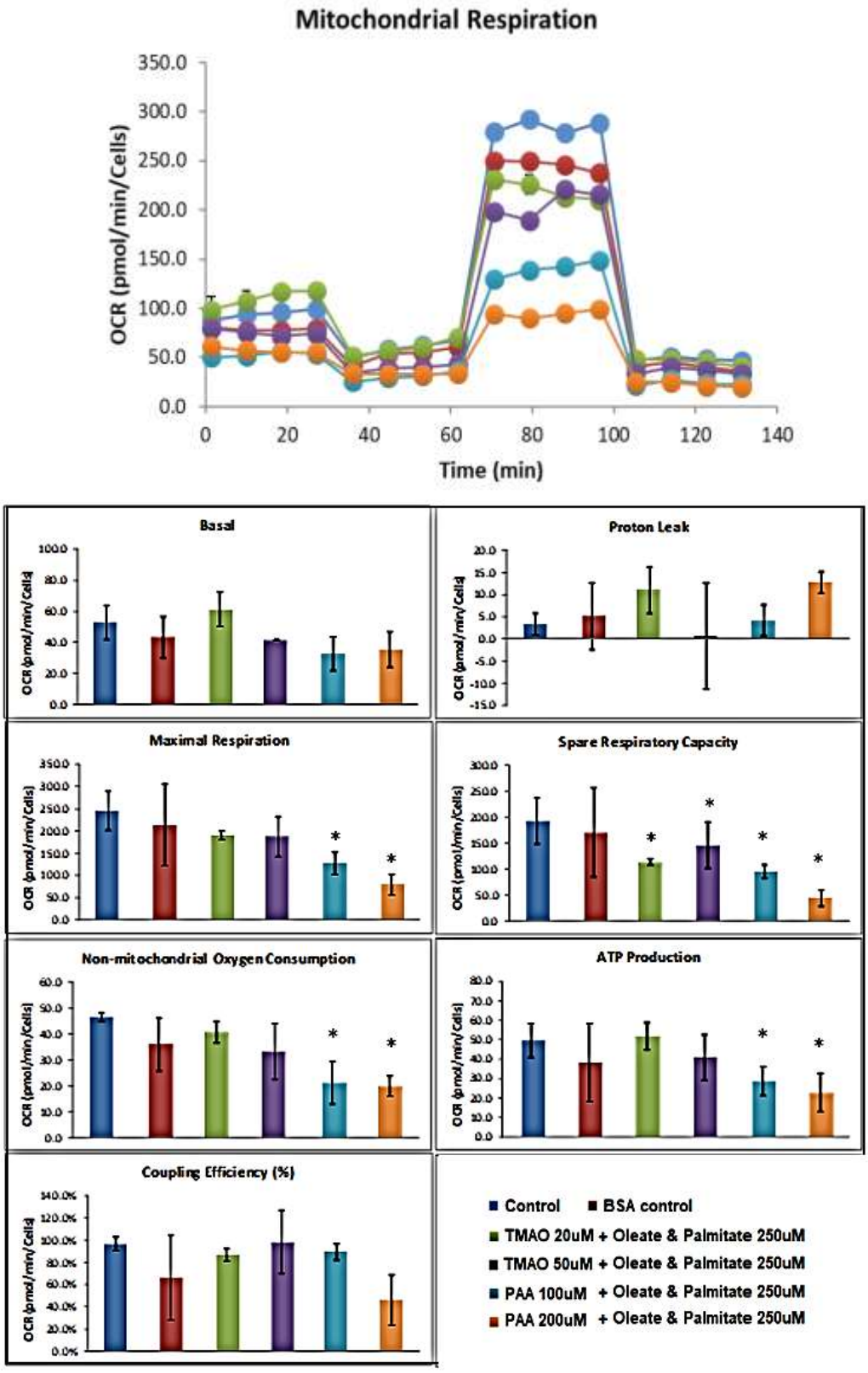

Figure 5.15. Mito Stress test in proliferative HepaRG cells exposed to fatty acids and TMAO and PAA. Cells were exposed to different concentrations of Oleate and Palmitate combined

with TMAO or PAA for 48 hours prior to bioenergetic analyses. Depiction of mitochondrial bioenergetic parameters: basal respiration, ATP-linked respiration, maximal respiration, spare respiratory capacity, proton leak, and non-mitochondrial respiration. Basal OCR measurement (4 cycles), injection of oligomycin port A (4 cycles), injection of BAM15 port B (4 cycles), and injection of rotenone/antimycin A port C (4 cycles). Data are presented as mean ± SD, n = 3.

5.3.5 DIFFERENTIATED HEPARG CELLS RESPOND TO BIOENERGETIC EFFECTORS

Differentiated HepaRG cells present two different cell populations of hepatocyte-like and biliary-like cells. To assess whether differentiation would impact mitochondrial respiration, differentiated HepaRG cells were prepared and analysed identically to proliferative HepaRG cells. The overall oxygen rates from differentiated cells were significantly lower than proliferative. Differentiated HepaRG Cells responded appropriately to oligomycin, BAM15 and antimycin/rotenone injections.

Differentiated HepaRG presented low basal oxygen consumption rates varying from 40 to 60 pmol/min. Proton leak remained extremely low averaging 2 pmol/min. Maximal respiration rates reached 200 pmol/min after exposure to BAM15. Calculated spare respiratory capacity from differentiated cells was 150 pmol/min. Non-mitochondrial oxygen consumption of around 23 pmol/min was used to correct rate calculations. Differentiated HepaRG cells presented ATP production rates of 50pmol/min and coupling efficiency averaging 95% (Figure 5.16).

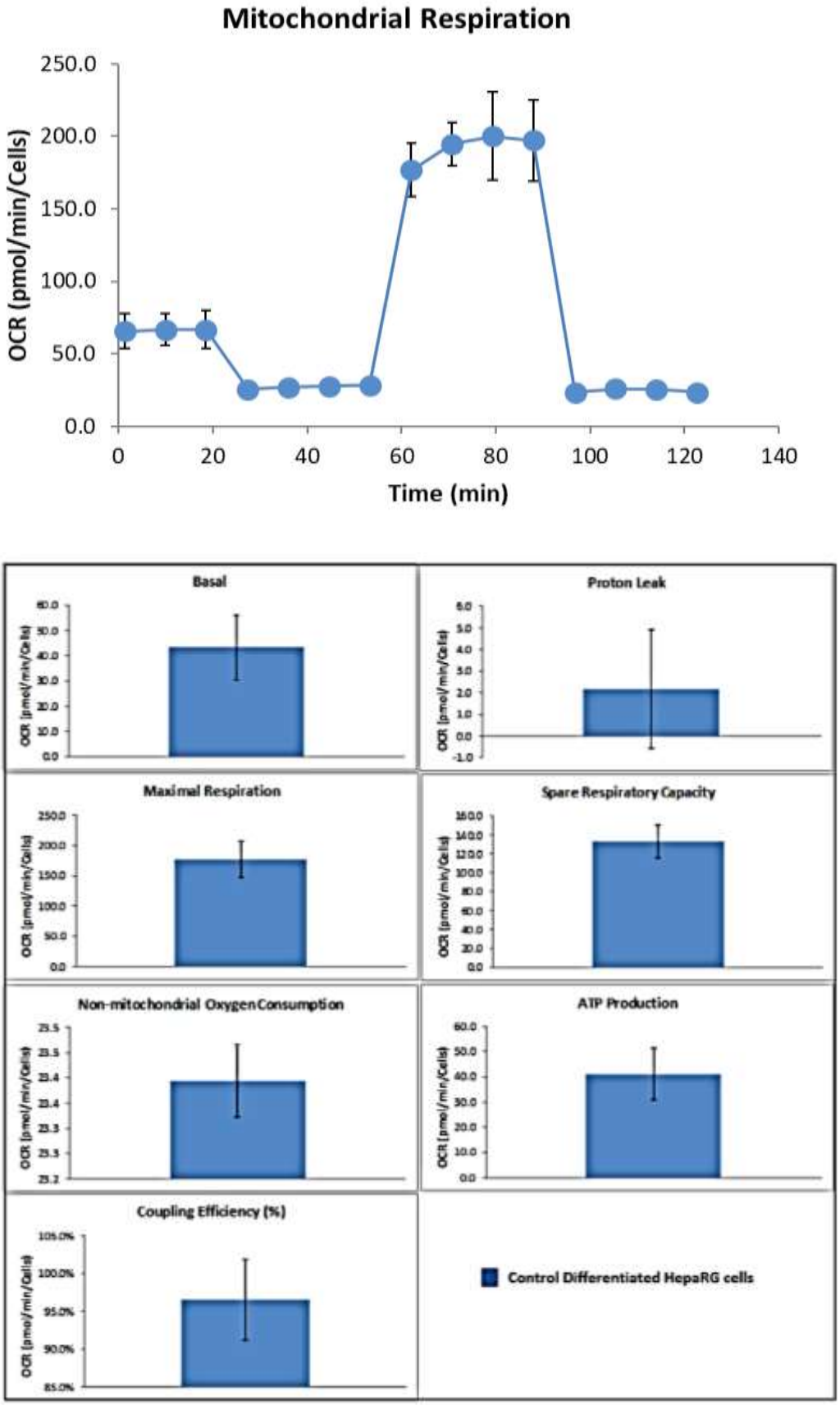

Figure 5.16. XF24 Mito Stress test in control differentiated HepaRG cells. Depiction of mitochondrial bioenergetic parameters: basal respiration, ATP-linked respiration, maximal respiration, spare respiratory capacity, proton leak, and non-mitochondrial respiration. Basal

OCR measurement (3 cycles), injection of oligomycin port A (4 cycles), injection of BAM15 port B (4 cycles), and injection of rotenone/antimycin A port C (4 cycles). Data are presented as mean ± SD, n = 3.

5.3.6 EXPOSURE TO OLEATE AND PALMITATE DOES NOT TRIGGER ANY SIGNIFICANT MITOCHONDRIAL CHANGES EXCEPT FOR SPARE RESPIRATORY CAPACITY IN DIFFERENTIATED HEPARG CELLS

Exposure to oleate and palmitate for 48 hours suggested that differentiated HepaRG cells are fairly resistant to steatosis. To that end, the same concentrations of fatty acids were added to the cells to interrogate whether oleate and palmitate would cause any changes in mitochondrial bioenergetics. Exposure to 100 µM, 250 µM, 500 µM and 1000 µM of oleate and palmitate did not affect basal, maximal and non-mitochondrial respiration in a significant way. ATP production and coupling efficiency also remained unchanged. The only statistically significant reduction caused by high fat conditions was in spare respiratory capacity where a decrease of 50% was observed. These findings are consistent with BODIPY™ quantification showing that when HepaRG cells are fully differentiated they are barely affected by fatty acids (Figure 5.17).

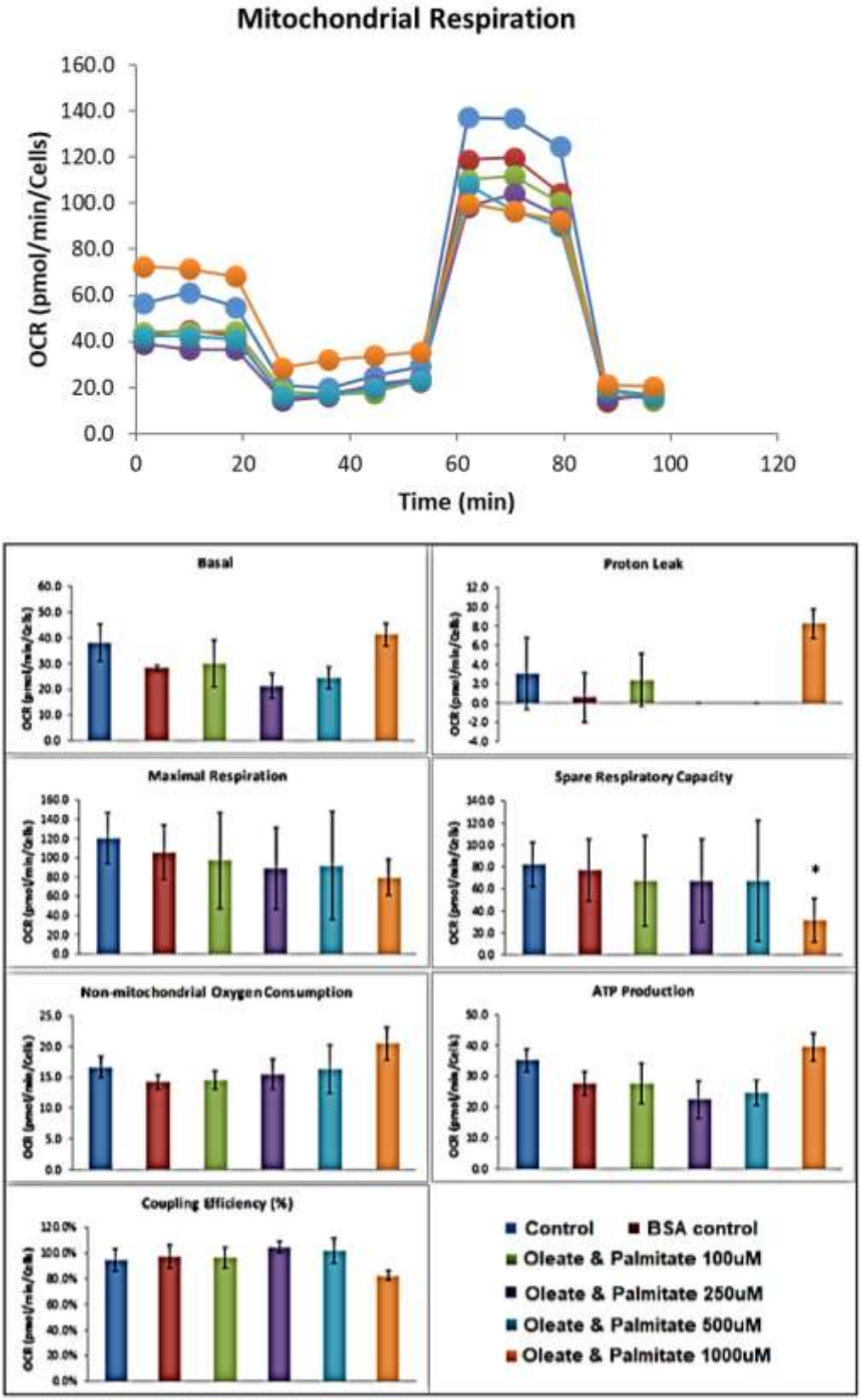

Figure 5.17. XF24 Mito Stress test in lipid loaded differentiated HepaRG cells. Cells were exposed to different concentrations of Oleate and Palmitate for 48 hours prior to bioenergetic analyses. Depiction of mitochondrial bioenergetic parameters: basal respiration, ATP-linked

respiration, maximal respiration, spare respiratory capacity, proton leak, and non-mitochondrial respiration. Basal OCR measurement (3 cycles), injection of oligomycin port A (4 cycles), injection of BAM15 port B (4 cycles), and injection of rotenone/antimycin A port C (4 cycles). Data are presented as mean ± SD, n = 3.

5.3.7 ADDITION OF TMAO AND PAA SLIGHTLY ALTERS MITOCHONDRIAL BIOENERGETICS IN DIFFERENTIATED HEPARG CELLS

Since fully differentiated HepaRG were more resistant to becoming steatotic than proliferative HepaRG, the effect of microbial metabolites in these differentiated cells (without fatty acids) was analysed. 20 µM and 50 µM of TMAO or 100 µM and 200 µM of PAA were added to the cells for 48 hours prior to the bioenergetics assay. Basal respiration was reduced significantly by exposure to PAA. Proton leak was highly variable and low, no significant changes were observed. Maximal respiration was considerably lowered by 50 µM of TMAO and both concentrations 100 µM and 200 µM of PAA. Likewise, same effect was seen in spare respiratory capacity. 50 µM of TMAO and 100 µM of PAA caused a 40% reduction whereas 200 µM of PAA decreased capacity by 75%. When compared to control, no significant changes were seen in non-mitochondrial respiration and ATP production. Coupling efficiency was slightly decreased but this change was not statistically significant (Figure 5.18).

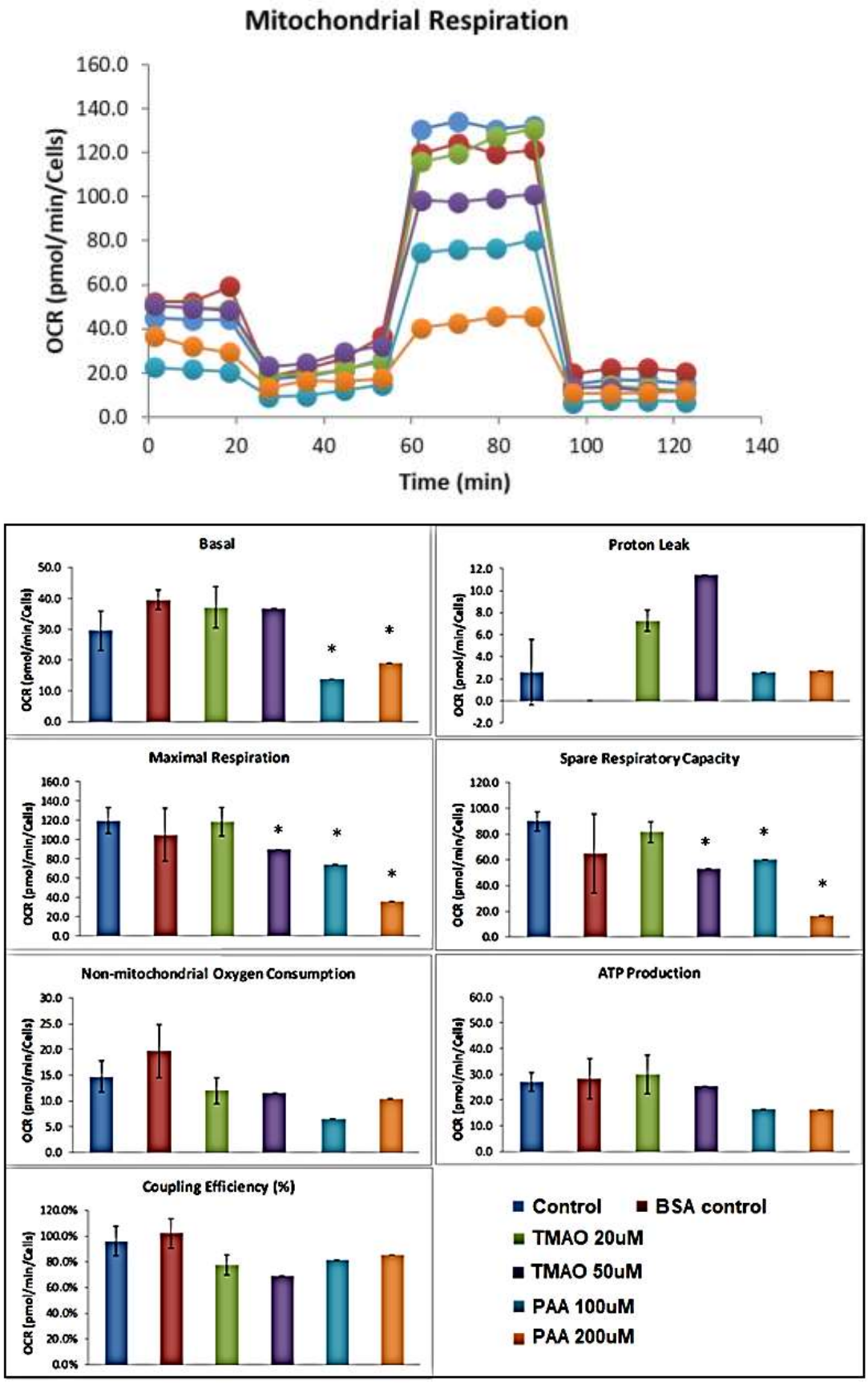

Figure 5.18. Mito Stress test in differentiated HepaRG cells exposed to TMAO and PAA. Cells were exposed to different concentrations of TMAO and PAA for 48 hours prior to bioenergetic

analyses. Depiction of mitochondrial bioenergetic parameters: basal respiration, ATP-linked respiration, maximal respiration, spare respiratory capacity, proton leak, and non-mitochondrial respiration. Basal OCR measurement (3 cycles), injection of oligomycin port A (4 cycles), injection of BAM15 port B (4 cycles), and injection of rotenone/antimycin A port C (4 cycles). Data are presented as mean ± SD, n = 3.

5.3.8 TMAO AND PAA COMBINED WITH 250 µM OLEATE AND PALMITATE SIGNIFICANTLY REDUCED KEY PARAMETERS OF MITOCHONDRIAL BIOENERGETICS IN DIFFERENTIATED HEPARG CELLS

BODIPY™ demonstrated that lipid accumulation was slightly increased by TMAO and PAA in differentiated HepaRG cells exposed to fatty acids. To further understand the mechanisms behind the increase in steatosis, TMAO and PAA were combined with 250 µM of oleate palmitate and added to the cells for 48 hours. Mito stress was performed with oligomycin, BAM15 and antimycin/rotenone using the XF24 analyser. Basal respiration was slightly reduced by TMAO and significantly reduced by PAA. Same effect was observed in ATP production and non-mitochondrial respiration. Proton leak and coupling efficiency remained unchanged. Maximal respiration and spare respiratory capacity were significantly lowered in a dose-dependent manner (Figure 5.19) (Table 6).

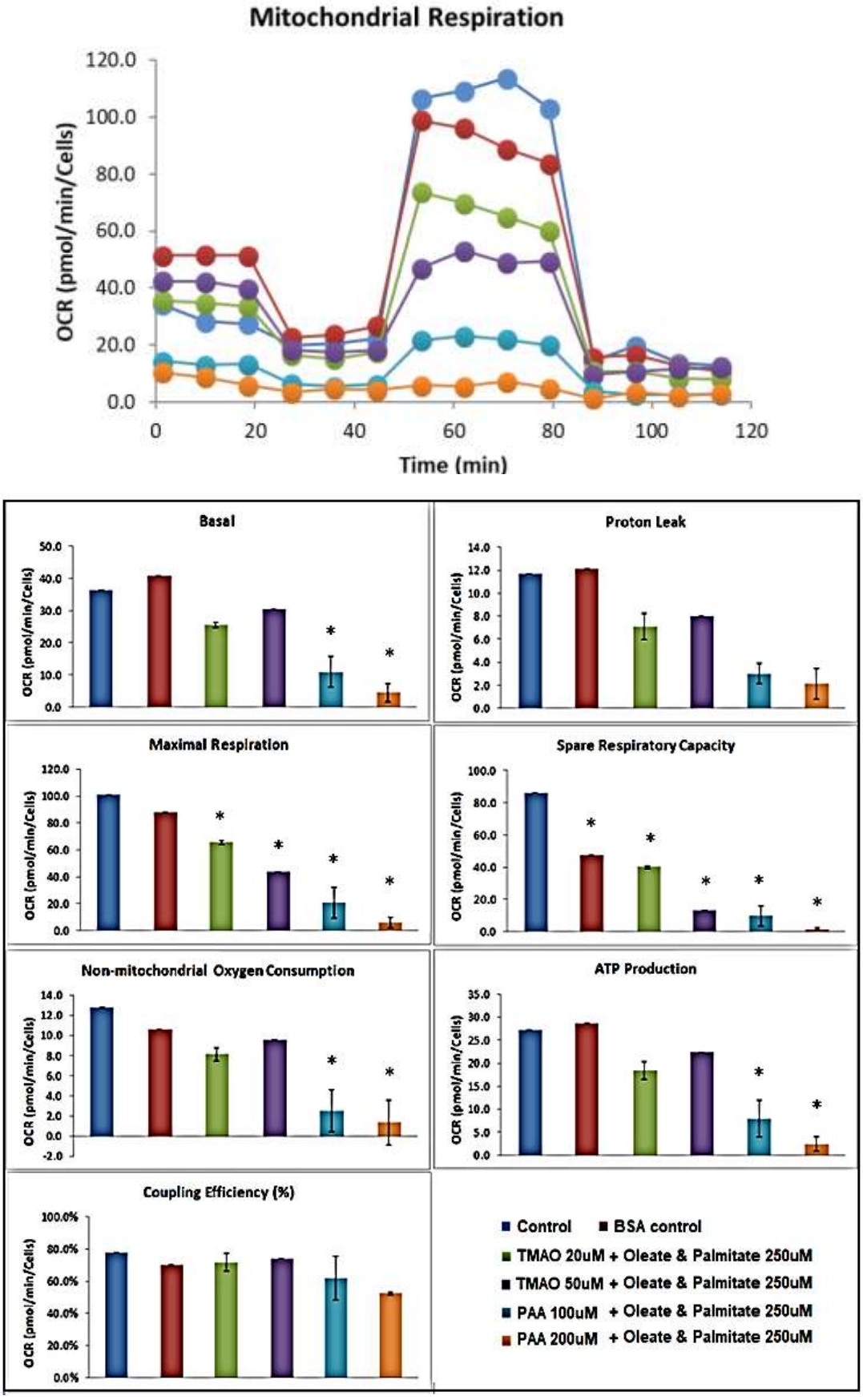

Figure 5.19. Mito Stress test in differentiated HepaRG cells exposed to fatty acids and TMAO and PAA. Cells were exposed to different concentrations of Oleate and Palmitate combined

with TMAO or PAA for 48 hours prior to bioenergetic analyses. Depiction of mitochondrial bioenergetic parameters: basal respiration, ATP-linked respiration, maximal respiration, spare respiratory capacity, proton leak, and non-mitochondrial respiration. Basal OCR measurement (3 cycles), injection of oligomycin port A (3 cycles), injection of BAM15 port B (4 cycles), and injection of rotenone/antimycin A port C (4 cycles). Data are presented as mean ± SD, n = 3.

Table 6. Comparison of Spare Respiratory Capacity in Proliferative vs. Differentiated HepaRG

48h Exposure	Proliferative HepaRG	Differentiated HepaRG
	Spare Respiratory Capacity (pmol/min/cells)	
BSA control	171.0	78.0
250µM Fatty Acids	163.0	64.0
250µM Fatty Acids + 20µM TMAO	108.0	39.0
250µM Fatty Acids + 50µM TMAO	147.0	11.0
250µM Fatty Acids + 100µM PAA	96.0	8.0
250µM Fatty Acids + 200µM PAA	49	0.1

5.4 MITOCHONDRIAL DYSFUNCTION PRECEDES LIPID ACCUMULATION IN PROLIFERATIVE AND DIFFERENTIATED HEPARG CELLS

5.4.1 PROLIFERATIVE HEPARG CELLS DO NOT BECOME STEATOTIC AFTER EXPOSURE TO OLEATE AND PALMITATE FOR 24 HOURS

Numerous insults are involved in NAFLD development including steatosis and mitochondrial dysfunction; however, the sequence of events remain poorly understood (Buzzetti *et al*., 2016). To elucidate whether steatosis would establish prior to changes in mitochondrial respiration, proliferative HepaRG cells were exposed to oleate and palmitate for 24 hours. In contrast to 48 hours exposure where steatosis was observed, 24 hours exposure with oleate and palmitate alone or combined with TMAO and PAA did not cause lipid accumulation. BODIPY™ staining demonstrated that longer than 24 hours exposure is needed for proliferative HepaRG cells to become steatotic (Figure 5.20).

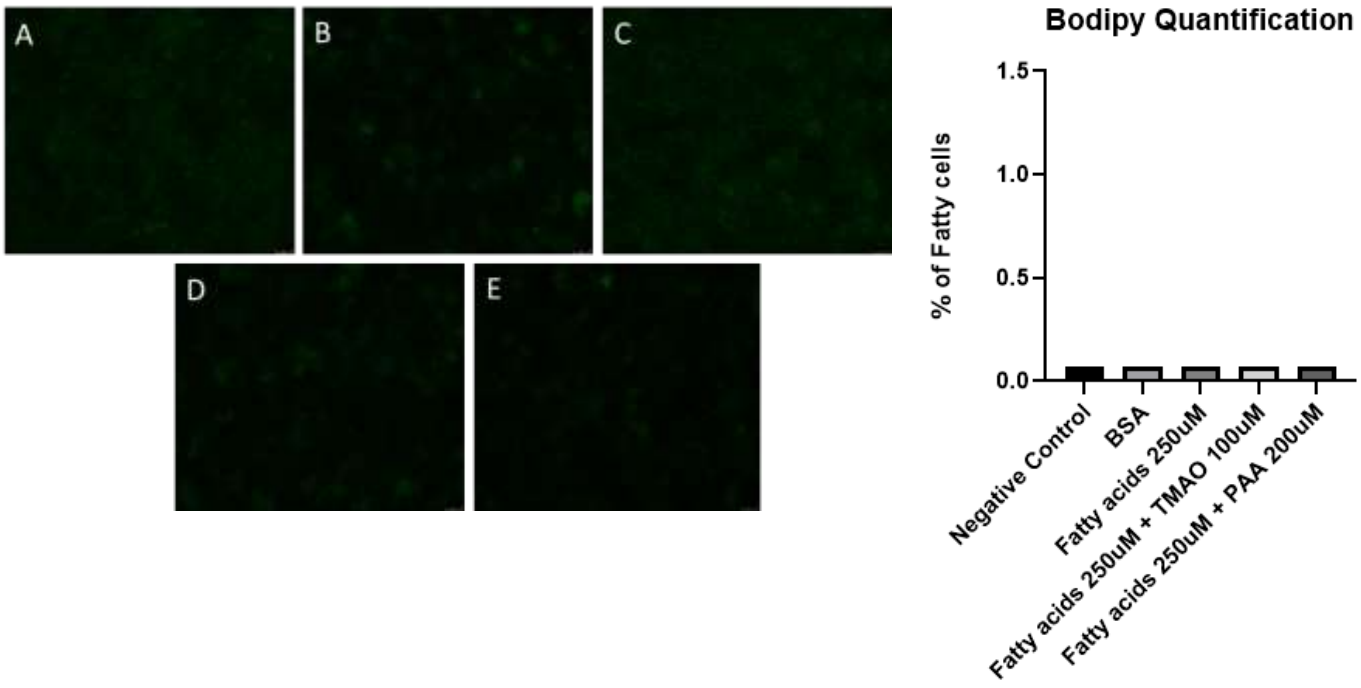

Figure 5.20. Proliferative HepaRG cells exposed to fatty acids for 24 hours. BODIPY™ staining of intracellular lipid droplets in proliferative HepaRG cells (left). Quantification of BODIPY™

staining using the CellProfiler software (right). A. Negative Control B. BSA vehicle control C. Proliferative HepaRG cells exposed to 250 µM Oleate and Palmitate. D. Proliferative HepaRG cells exposed to 250 µM Oleate and Palmitate combined with TMAO 100 µM. E. Proliferative HepaRG cells exposed to 250 µM Oleate and Palmitate combined with PAA 200 µM.

5.4.2 CHANGES IN MITOCHONDRIAL BIOENERGETICS OCCUR PRIOR TO LIPID ACCUMULATION IN PROLIFERATIVE HEPARG CELLS

Given that no significant differences were found in intracellular lipid accumulation after exposing proliferative HepaRG to oleate and palmitate combined with TMAO and PAA for 24 hours. The effects of the two highest concentrations of TMAO and PAA in mitochondrial function were additionally assessed after 24 hours exposure to determine whether the mitochondrial bioenergetics was affected at an earlier time point than steatosis.

Shorter exposure of 24 hours of 250 µM of oleate and palmitate with TMAO and PAA did not cause any significant differences in basal respiration, proton leak, non-mitochondrial oxygen consumption, ATP production and coupling efficiency. However, proliferative HepaRG maximal respiration and spare respiratory capacity were significantly lowered. These findings suggest that reductions in mitochondrial function occur first, before steatosis, and lipid accumulation develops subsequently as a consequence (Figure 5.21).

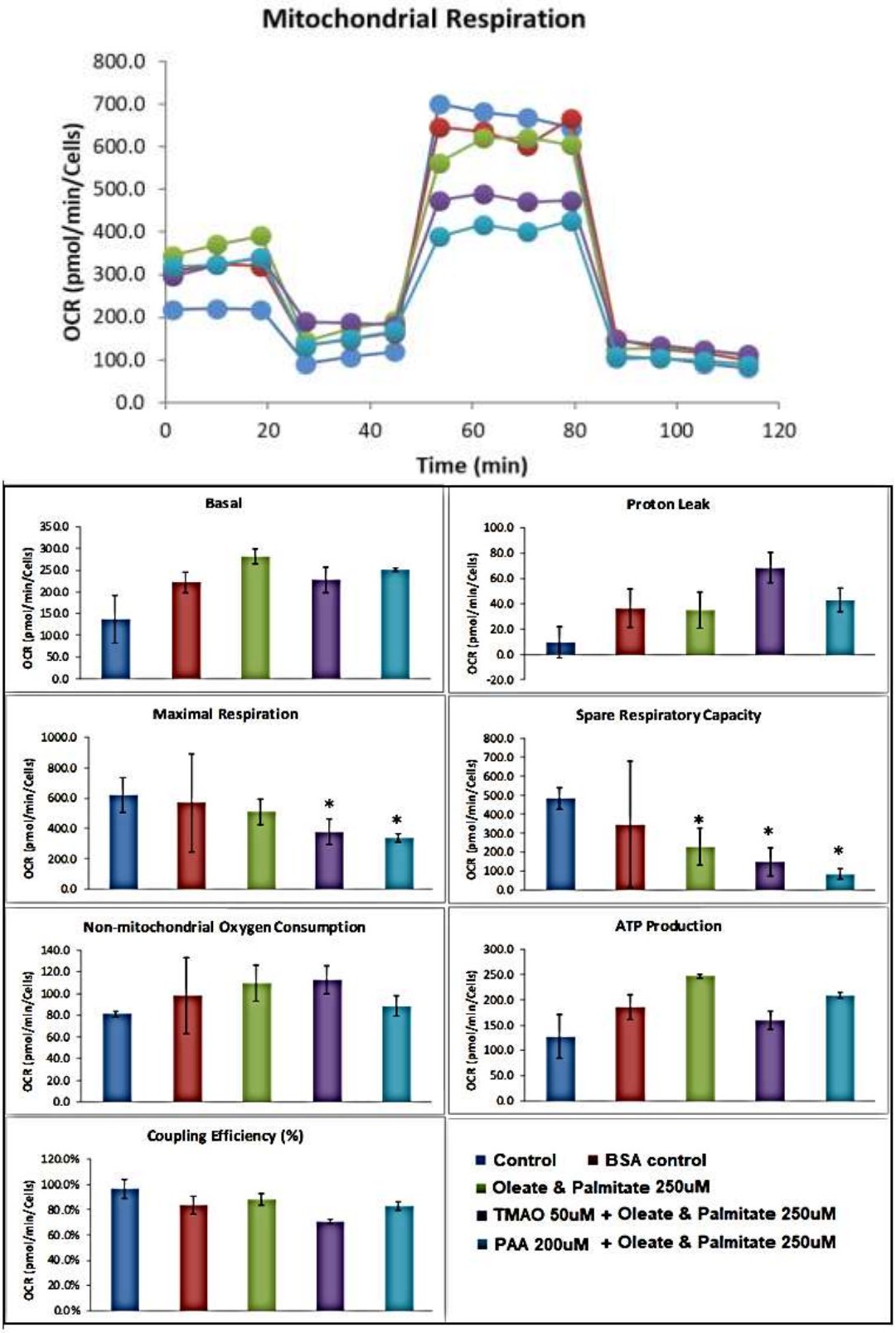

Figure 5.21. XF24 Mito Stress test in proliferative HepaRG cells after 24 hours. Cells were exposed to different concentrations of Oleate and Palmitate combined with TMAO or PAA for 24 hours prior to bioenergetic analyses. Depiction of mitochondrial bioenergetic parameters:

basal respiration, ATP-linked respiration, maximal respiration, spare respiratory capacity, proton leak, and non-mitochondrial respiration. Basal OCR measurement (3 cycles), injection of oligomycin port A (3 cycles), injection of BAM15 port B (4 cycles), and injection of rotenone/antimycin A port C (4 cycles). Data are presented as mean ± SD, n = 3.

5.4.3 DIFFERENTIATED HEPARG CELLS DO NOT BECOME STEATOTIC AFTER EXPOSURE TO OLEATE AND PALMITATE FOR 24 HOURS

The same time course experiment was repeated in differentiated HepaRG cells. Differentiated HepaRG cells exposed to oleate and palmitate presented small amounts of intracellular lipids after 48 hours. When cells were exposed to oleate and palmitate combined with TMAO and PAA for 24 hours no intracellular lipid droplets were detected (Figure 5.22).

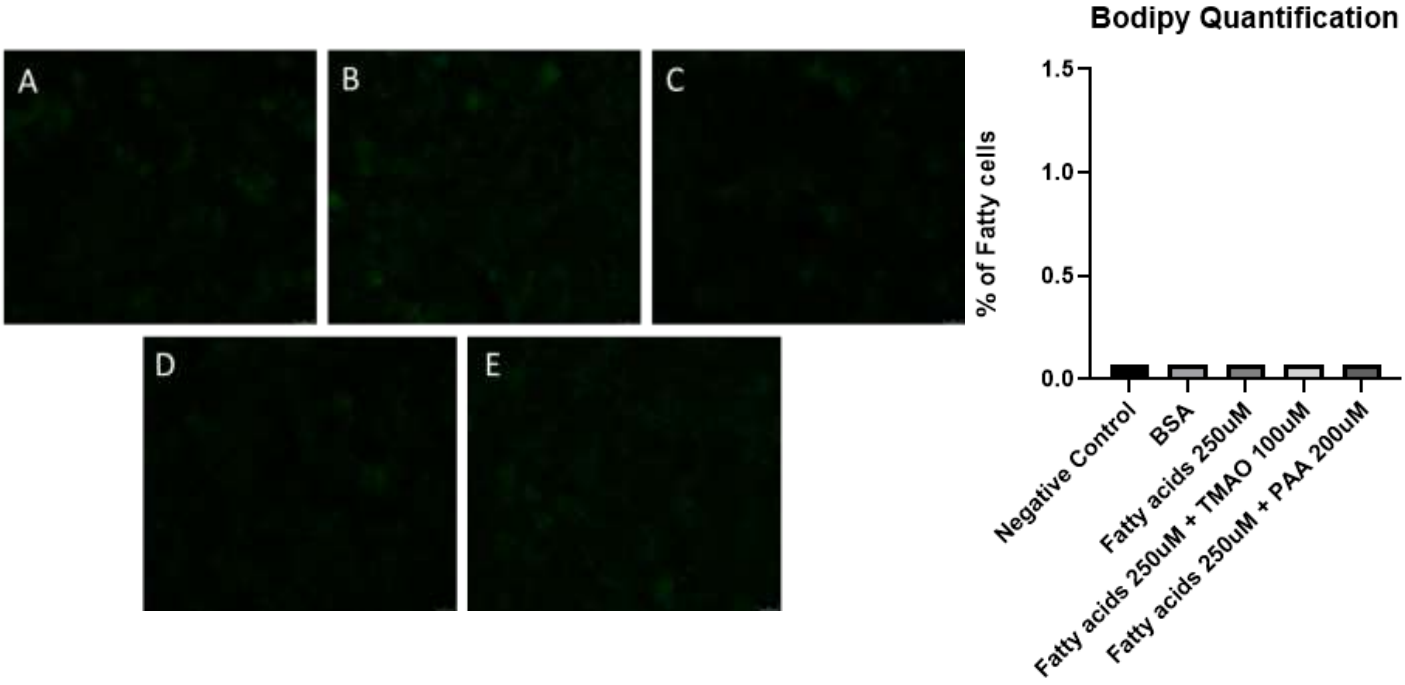

Figure 5.22. Differentiated HepaRG cells exposed to fatty acids for 24 hours. BODIPY™ staining of intracellular lipid droplets in differentiated HepaRG cells (left). Quantification of BODIPY™ staining using the CellProfiler software (right). A. Negative Control B. BSA vehicle control C. Differentiated HepaRG cells exposed to 250 µM Oleate and Palmitate. D. Differentiated

HepaRG cells exposed to 250 µM Oleate and Palmitate combined with 100 µM of TMAO. E. Differentiated HepaRG cells exposed to 250 µM Oleate and Palmitate with 200 µM of PAA.

5.4.4 ADDITION OF OLEATE AND PALMITATE SIGNIFICANTLY REDUCES BASAL RESPIRATION IN DIFFERENTIATED HEPARG CELLS AFTER 24 HOURS

To further understand whether mitochondrial dysfunction or lipid build-up occurs first, differentiated HepaRG were exposed to fatty acids combined with PAA and TMAO for 24 hours and mitochondrial bioenergetics was assessed using the mito stress kit. HepaRG cells responded to all injected effectors. Mitochondrial features were calculated after injection with oligomycin, BAM 15 and rotenone/antimycin. No differences in proton leak, maximal respiration, spare respiratory capacity, non-mitochondrial oxygen consumption, ATP production and coupling efficiency were observed. Basal respiration was significantly reduced by oleate and palmitate, TMAO and PAA. These results indicate that prior to lipid droplets accumulating in differentiated HepaRG cells, basal respiration already begins to decrease. (Figure 5.23).

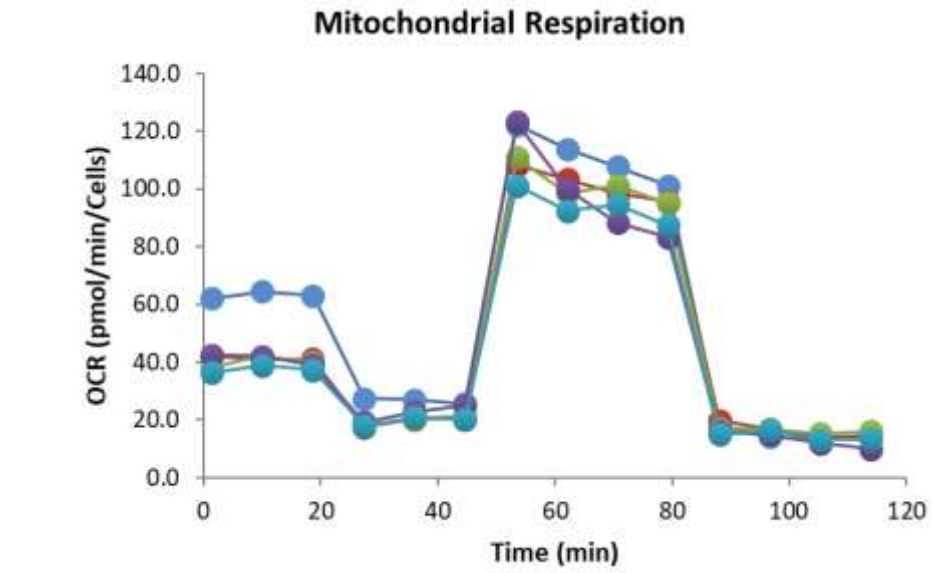

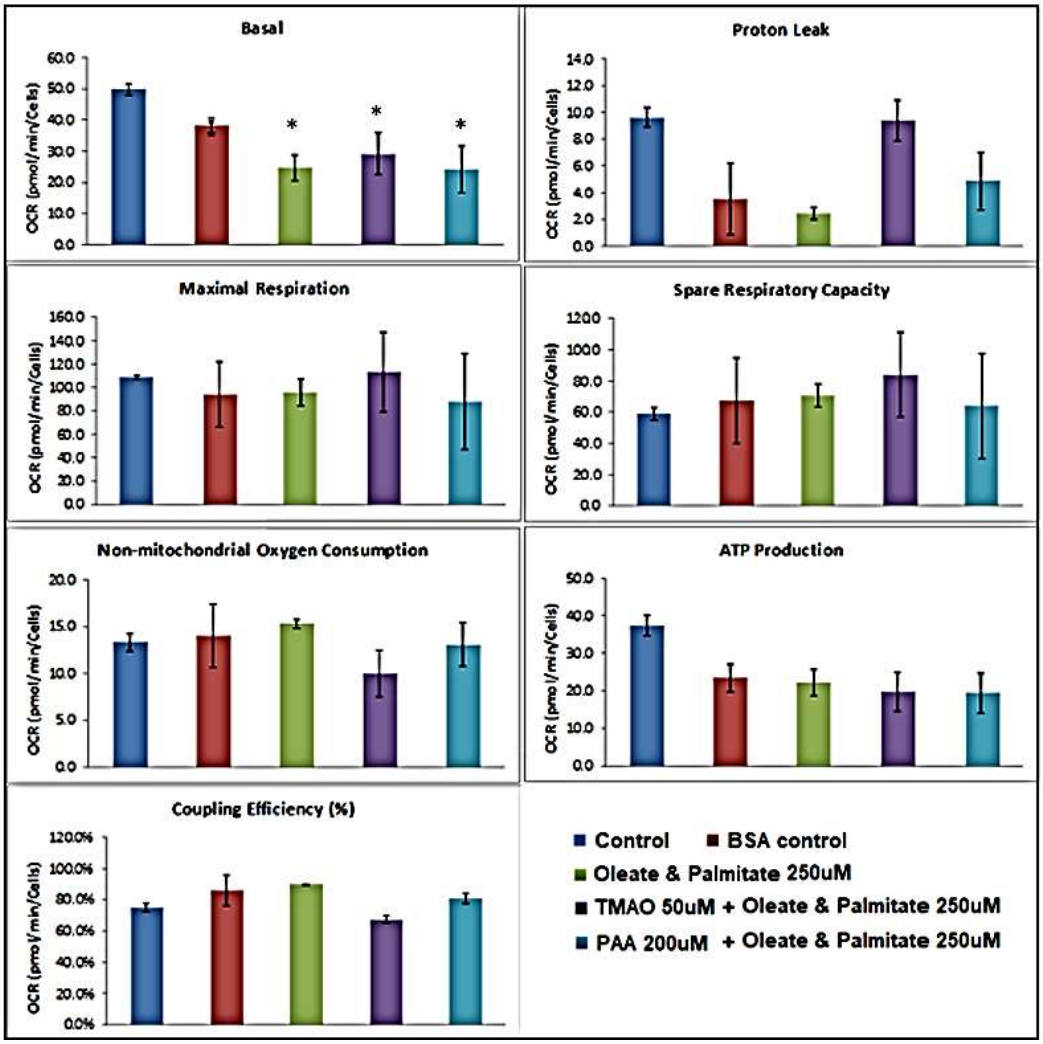

Figure 5.23. XF24 Mito Stress test in differentiated HepaRG cells after 24 hours. Cells were exposed to different concentrations of Oleate and Palmitate combined with TMAO or PAA for

24 hours prior to bioenergetic analyses. Depiction of mitochondrial bioenergetic parameters: basal respiration, ATP-linked respiration, maximal respiration, spare respiratory capacity, proton leak, and non-mitochondrial respiration. Basal OCR measurement (3 cycles), injection of oligomycin port A (3 cycles), injection of BAM15 port B (4 cycles), and injection of rotenone/antimycin A port C (4 cycles). Data are presented as mean ± SD, n = 3.

5.5 LIPID ACCUMULATION IS REVERSIBLE IN PROLIFERATIVE HEPARG CELLS

To elucidate whether intracellular lipid build up can be reversed, proliferative HepaRG were first exposed to oleate and palmitate combined to TMAO and PAA for 48 hours, then following exposure components were removed and cells were maintained in culture medium for additional 48 hours to recover. 39% of cells became steatotic after being exposed to 250 µM oleate palmitate and 20 µM of TMAO, the percentage of fatty cells reduced to 35% after fatty acids and TMAO were removed from the media. When exposed to 250 µM oleate palmitate combined with 100 µM of PAA 78% of proliferative cells presented lipid droplets, steatosis was significantly reduced to 65% after removal of these components (Figure 5.24).

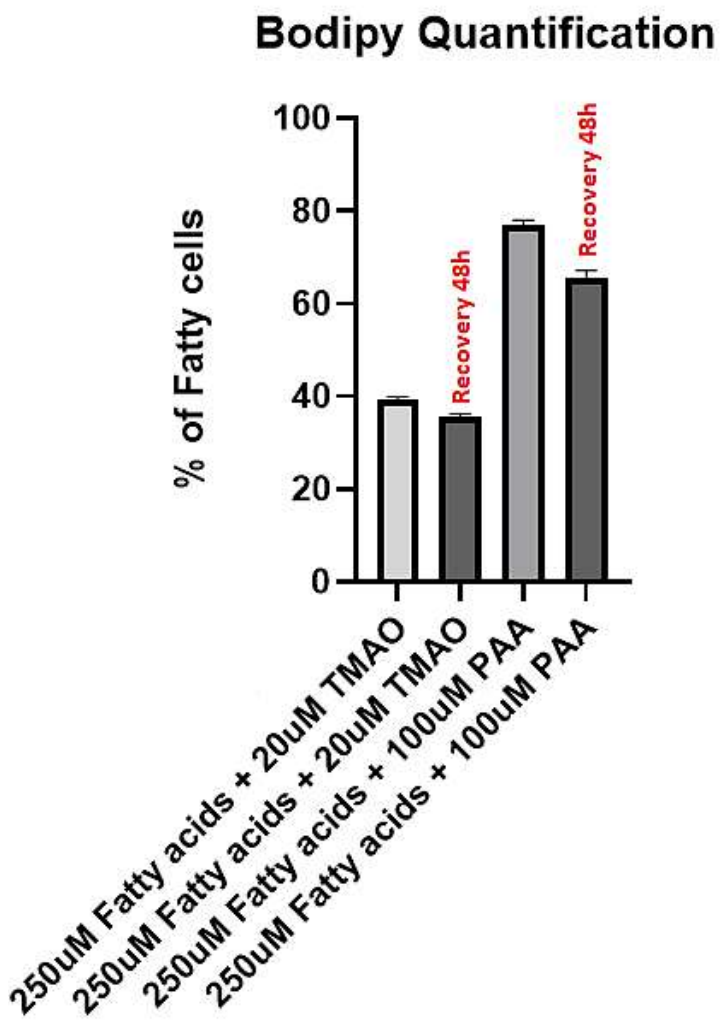

Figure 5.24. Comparison of 24h vs 48h recovery. BODIPY™ quantification after recovery experiments using the CellProfiler software. Proliferative HepaRG cells were exposed to fatty acids combined with TMAO or PAA for 48 h and components were removed for 24h or 48h.

5.6 DIFFERENTIATED HEPARG CELLS PRESENT GREATER EXPRESSION OF LIVER SPECIFIC GENES

5.6.1 GENE EXPRESSION OF DIFFERENTIATED VS PROLIFERATIVE HEPARG CELLS

RT-qPCR was performed to confirm the expected gene expression profile of differentiated HepaRG compared to proliferative HepaRG cells, which may be relevant to how differentiated HepaRG cells were more resistant to the effects of fatty acids and gut metabolites than proliferative cells. HPRT1 was used as housekeeping gene and relevant liver specific genes were analysed. Expression of the albumin gene which encodes a major protein produced in the liver was increased in differentiated cells. CPT-1a gene was increased, showing that fatty acid oxidation is higher in differentiated cells. Differentiated cells showed an 8-fold increase in CYP3A4 gene expression. CYP3A4 belongs to the cytochrome P450 family, and it plays an important role in xenobiotics oxidation facilitating the removal of these toxins from hepatocytes and subsequent excretion from the body in urine or bile.

A 4-fold increase was found in FXR gene expression, this suggests that fatty acid oxidation is significantly enhanced in differentiated HepaRG. HFN4a regulates genes involved in normal liver function and it was slightly elevated in cells that underwent differentiation. MRP2 acts as a major efflux transporter of xenobiotics via bile acids conjugation in the liver. MRP2 gene expression was decreased in differentiated cells. Taken together these results indicate that differentiated HepaRG cells present enhanced hepatic phenotype when compared to proliferative cells as expected. In addition, differentiation increases expression of a number of genes responsible for oxidizing fatty acids and eliminating toxins from the liver (Figure 5.25).

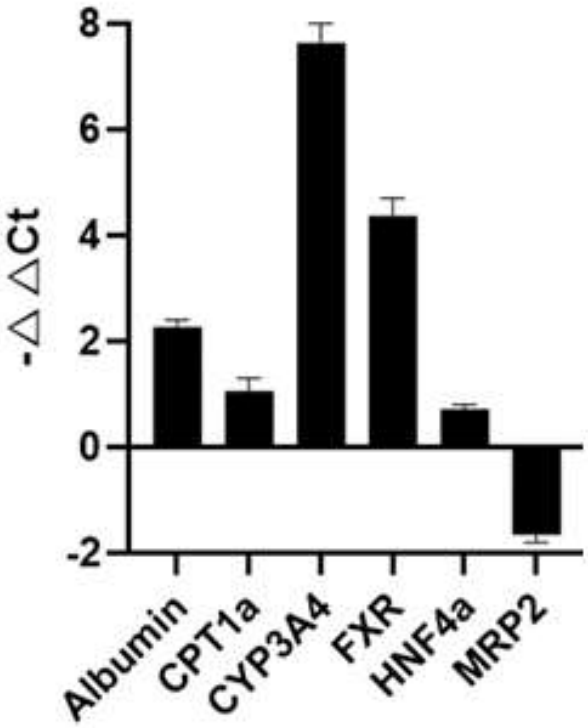

Figure 5.25. Delta delta Ct of differentiated HepaRG cells in comparison to proliferative HepaRG cells. qPCR graph showing relative up or down fold change in differentiated mRNA levels over levels of proliferative cells. qPCR data bars indicate mean relative fold change values ± SEM of three independent sets. Error bars: ± SD, n = 3.

5.7 CORRELATIONS BETWEEN STEATOSIS AND MITOCHONDRIAL PARAMETERS

5.7.1 PERCENTAGE OF LIPID LOADED CELLS IS NEGATIVELY CORRELATED WITH SPARE RESPIRATORY CAPACITY IN HEPARG CELLS

The analysis of the mitochondrial parameters in HepaRG cells revealed several strong associations between key bioenergetic parameters and the amount of steatotic cells. Strong negative correlation was found between lipid accumulation and spare respiratory capacity in proliferative HepaRG cells (r= -0.999) but was less marked in differentiated HepaRG cells (r= -0.774). The negative correlations suggested that as spare respiratory capacity decreased, cells became more steatotic. In proliferative cells, spare respiratory capacity was approximately 50 pmol/min when cells were 90% steatotic, and 350 pmol/min in control cells. All mitochondrial rates were significantly lower in differentiated cells; spare respiratory capacity measured was around 8 pmol/min when 15% of the cells were steatotic, while capacity was 86 pmol/min in non-steatotic cells. These findings suggest that hepatocyte-like cells are not able to cope with the energy demand in a high fat environment (Figure 5.26).

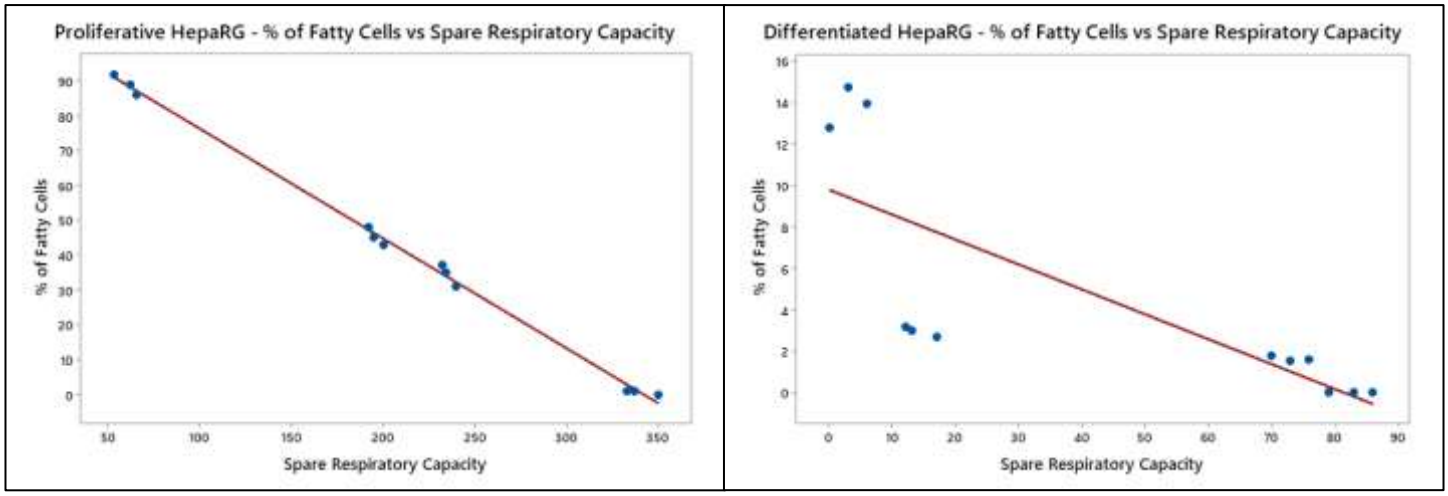

Figure 5.26. Correlation between spare respiratory capacity and % steatotic of HepaRG cells. Each dot represents the mean of 3 replicates and the line represents the regression. Correlation was calculated using Pearson's correlation test.

5.7.2 PERCENTAGE OF STEATOTIC CELLS IS NEGATIVELY CORRELATED WITH BASAL RESPIRATION IN HEPARG CELLS

Strong inverse correlations between lipid accumulation and basal oxygen consumption was found in differentiated HepaRG cells (r= -0.966) and in proliferative HepaRG cells (r= -0.856). Analysis suggested that the lower the basal respiration the higher the lipid deposition. In differentiated HepaRG cells basal respiration was around 4 pmol/min when 15% of the cells presented intracellular lipid droplets, while basal was approximately 40 pmol/min when no steatosis was detected. Proliferative HepaRG cells demonstrated basal rates of 43 pmol/min when 90% of cells were steatotic and 155 pmol/min without lipid deposition (Figure 5.27).

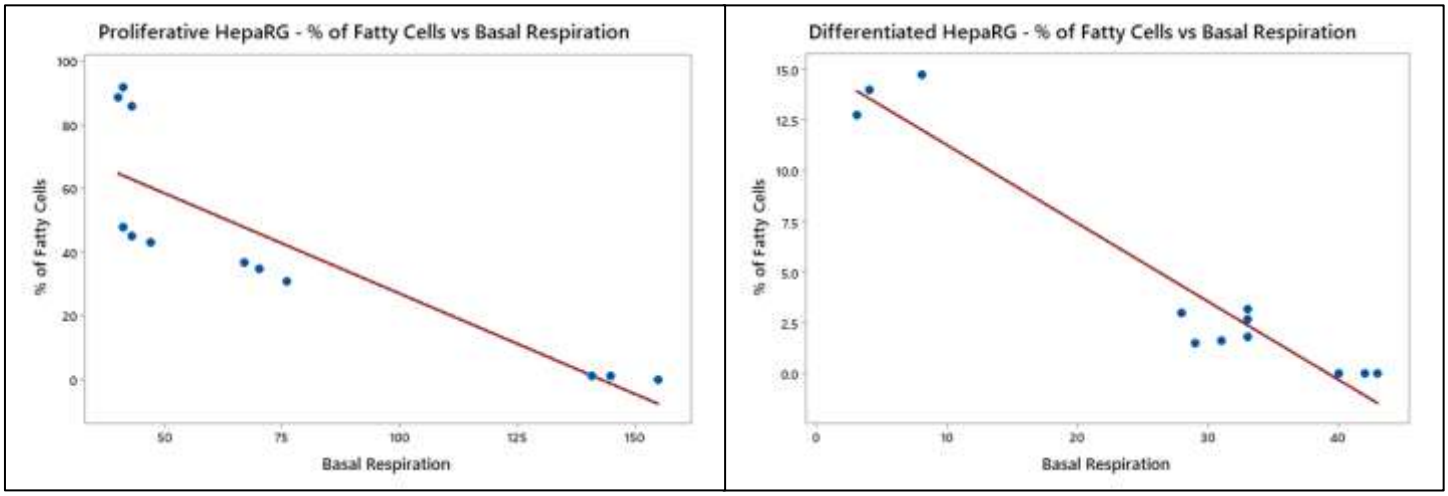

Figure 5.27. Correlation between basal respiration and % steatotic of HepaRG cells. Each dot represents the mean of 3 replicates and the line represents the regression. Correlation was calculated using Pearson's correlation test.

5.7.3 ATP PRODUCTION IS STRONGLY NEGATIVE CORRELATED WITH LIPID BUILD-UP IN HEPARG CELLS

Interestingly, the strongest correlation between steatosis and mitochondrial bioenergetics was found in ATP production. Both proliferative (r= -0.909) and differentiated HepaRG cells (r= -0.955) presented negative correlations between steatosis and ATP production. As ATP production declined, lipid build-up increased. Control proliferative HepaRG cells exhibited ATP production of 130 pmol/min whilst ATP production was around 40 pmol/min in 90% of steatotic cells. Control differentiated cells presented ATP rates of 40 pmol/min, contrastingly when 90% of cells were steatotic ATP production was approximately 6 pmol/min (Figure 5.28). These findings suggest that intracellular lipid accumulation is associated with extensive damage to oxidative phosphorylation and the production of ATP.

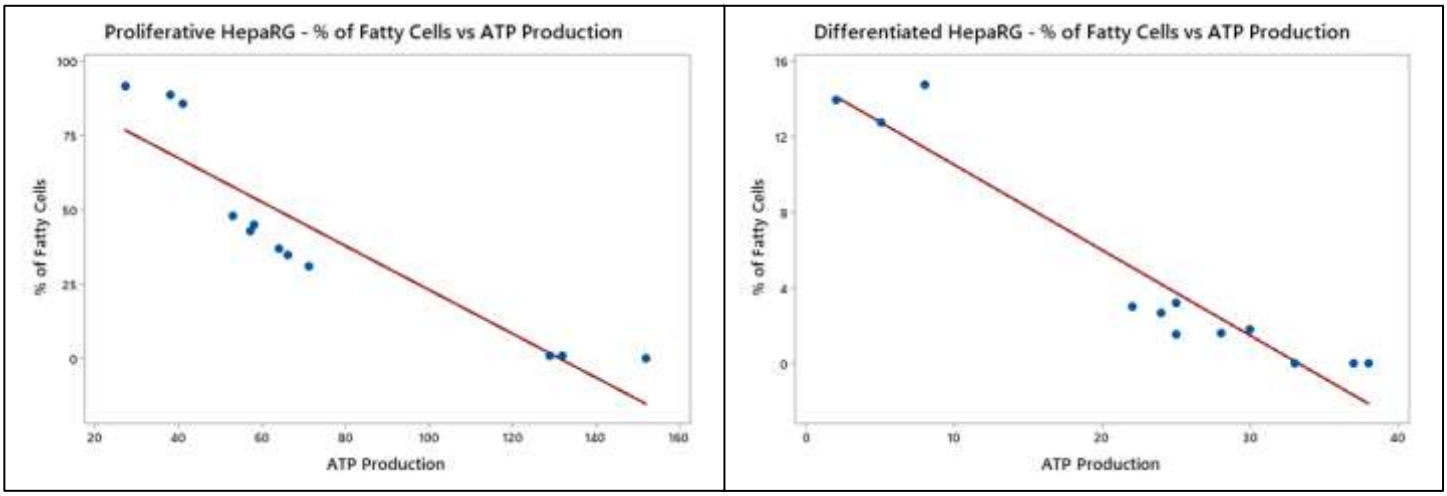

Figure 5.28. Correlation between ATP production and % steatotic of HepaRG cells. Each dot represents the mean of 3 replicates and the line represents the regression. Correlation was calculated using Pearson's correlation test.

CHAPTER 6.

DISCUSSION AND CONCLUSIONS

This is the first study describing the effects of TMAO and PAA in mitochondrial bioenergetics and lipid accumulation in a hepatocyte-derived cell culture model. We were able to establish that TMAO and PAA induces steatosis and causes mitochondrial dysfunction in proliferative HepaRG, a progenitor like hepatocyte model. When HepaRG are fully differentiated expressing high CYP450 activity, these cells become resistant to the harmful effects of TMAO and PAA. This may reflect the susceptibility of regenerating liver concurrent with liver disease to further damage from microbiome metabolites, while mature and healthy liver are less susceptible to damage. We aimed to develop and utilise more physiologically relevant models including a 3D cell culture model using freshly isolated human hepatocytes, but the challenges in reproducing a liver ex vivo remain too challenging apart from using specialised proven hepatocyte lots. We aimed to couple cutting-edge models with advances in technology of observing mitochondrial metabolism, but the challenges of ex vivo hepatocyte culture in the Liverchip platform were unsurmountable.

6.1 QUALITY OF LIVER TISSUE IS CRUCIAL FOR THE USE OF PHH IN 3D CELL CULTURE

As described in chapter 2, in this study primary human hepatocytes were isolated from liver wedges. The obtained human liver tissue was retrieved from patients undergoing tumour resection surgery. The viability of fresh isolated primary human hepatocytes was extremely low in the present study. It is important to notice that most of the patients undergoing tumour surgery were given chemotherapy prior to the procedure leading to extensive cell senescence. In addition, the use of vascular inflow occlusion during liver surgery to prevent

severe blood loss induces to hepatic ischemia. Hepatic ischemia is a condition in which the liver does not receive enough oxygen leading to acute damage to liver cells.

The Liverchip 3D platform requires extremely healthy hepatocytes and we learned that only specific batches of commercial cryopreserved PHH seem to attach to the Liverchip scaffolds. Unfortunately, the primary hepatocytes isolated from patients presented extremely low viability and reproducibility and did not perform efficiently in the 3D cell culture model and did therefore not present a viable model system to further interrogate the effects of TMAO and PAA on mitochondrial bioenergetics.

6.2 HEPARG CELL LINE EXPOSED TO OLEATE AND PALMITATE CAN BE UTILISED AS A NAFLD MODEL

Different immortalized cells lines have been used as an alternative to PHH culture (Duval *et al*., 2017). PHH isolation is challenging from surgical resection liver tissue, and commercially available PHH are batch dependent and extremely expensive to purchase from a commercial supplier. In addition, PHH viability as a 2D monolayer culture time is short since they lose their morphology in around 5 days (Kozyra *et al.*, 2018). We chose to use a more physiologically-relevant cell line, HepaRG, than previously used hepatoma cell lines. The proliferative cell line HepG2 cells have been used extensively as a NAFLD model *in vitro.* HepG2 is a human liver cancer cell line that was derived from a hepatocellular carcinoma. Despite its common use HepG2 has more limitations than HepaRG cells for metabolic mechanistic studies (Gerets *et al.,* 2012). HepaRG cells were chosen for this study for better resembling the liver and exhibiting a significantly higher level of CYP450 enzyme activities when compared to other hepatic cell lines. HepaRG cells are remarkably stable, convenient

and long living, however the full differentiation programme takes 30 days (Marion *et al*., 2010). The long process of obtaining cells after a month certainly influenced and slowed down the experiments here described. For this reason, proliferative HepaRG cells were also investigated. Proliferative HepaRG cells are a good model to investigate hepatocytes that present lower CYP450 activity such as hepatocytes from NASH patients. HepaRG cells have been previously shown to be an appropriate cell line for steatosis induction in vitro (Di Cocco et al., 2019). In addition, Yuan *et al*. demonstrated that HepG2 have the I148M homozygous PNPLA3 variant that induces steatosis, whereas HepaRG cells do not present this variant (Yuan *et al.* 2020).

Anthérieu *et al*. detected formation of lipid droplets when exposing HepaRG cells to 500 µM oleic acid for 24 hours (Anthérieu *et al.*, 2012). Likewise, Di Cocco *et al*. treated differentiated HepaRG to 500 µM oleate and palmitate 2:1 for 48 hours prior to Oil Red O staining. Lipid droplets were easily identified after fatty acid exposure (Di Cocco *et al.*, 2019). However, both studies did not quantify the lipid droplets observed. Pant *et al*. treated HepaRG cells with 0.33, 0.66, or 1mM oleate palmitate and quantification of the staining revealed steatosis increased in a dose dependent manner, consistent to the findings in this study (Pant *et al.*, 2019). Nunn *et al.* used 250 µM oleate for 5 days to induce steatosis in HepaRG cells, BODIPY™ staining showed bright green fluorescent lipid droplets demonstrating that oleate on its own also causes steatosis (Nunn *et al.*, 2016).

Oleate and palmitate are physiologically relevant as they are the most abundant fatty acids in western diets. Both fatty acids are widely applied to induce lipid accumulation in various cell types (Di Cocco *et al*., 2019). Palmitate is a saturated fatty acid toxic to cells causing mitochondrial dysfunction, insulin resistance and inflammation, however as

described by Kwon *et al.* the addition of oleate, an unsaturated fatty acid, protects cells from these harmful effects. (Kwon *et al.*, 2014) Similarly, Yuzefovych *et al*. found that oleate ameliorates palmitate-induced mitochondrial dysfunction and apoptosis (Yuzefovych *et al*., 2010)

6.3 TMAO AND PAA AGGRAVATE STEATOSIS

The effects of TMAO in the liver remain poorly investigated. In this study, the addition of TMAO significantly increased cellular lipid content. High concentrations of TMAO caused an increase of 42% of lipid droplets in proliferative cells and 1.6% increase in differentiated HepaRG cells. Similar findings were indicated by Tan *et al*. liver histology of 10 mice being fed a high-fat diet with TMAO showed aggravated liver steatosis scores (Tan *et al*., 2019). León-Mimila *et al*. analysed TMAO serum levels and liver biopsies from 357 obese Mexican patients. TMAO levels were positively correlated with grade of steatosis, hepatocyte ballooning, NAS score and lobular inflammation (León-Mimila *et al.*, 2021). Taken together, these results demonstrate a significant effect of TMAO in increasing intracellular lipid droplet accumulation.

Data from the described experiments demonstrated that the effects of PAA in lipid build-up were stronger than those observed with TMAO. PAA raised lipid droplets by 54% in proliferative HepaRG and by 10% in fully differentiated cells. Consistently, Hoyles *et al.* treated primary human hepatocytes with 10mM of PAA combined with 200 µM of palmitate for 24 hours. Oil Red O staining demonstrated that PAA significantly induced steatosis. Furthermore, seven mice fed a standard diet supplemented with 0.8% of PAA for two weeks displayed raised hepatic triglyceride content. The same author also analysed liver biopsies of

105 morbidly obese women obtained during bariatric surgery. Plasma samples and liver histology indicated that high PAA concentrations were associated with severe liver steatosis (Hoyles *et al.,* 2018).

6.4 STEATOSIS INCREASED BY TMAO AND PAA CAN BE REVERSED

Gut microbiome composition is highly variable and largely dependable on the diet. Studies show that dietary alterations trigger microbiome shifts within 24 hours (Singh *et al.* 2017). The type and amount of gut bacteria metabolites measured in blood serum are altered constantly by diet. For instance, high red meat intake leads to increased levels of TMAO, while vegetarians and vegans present low levels of this metabolite (Abbasi, 2019). Turnbaugh *et al*. compared the gut bacteria of lean and obese mice and noticed that microbiome compositional changes were completely reversed after a return to a normal diet (Turnbaugh *et al*., 2008). The present study revealed that TMAO and PAA exacerbate lipid deposition in HepaRG cells, however this effect is reversible once these compounds are removed from the culture medium. Studies showing whether gut microbiome metabolite effects can be reversed are extremely limited.

6.5 DIFFERENTIATED HEPARG CELLS PRESENT A DISTINCT GENE EXPRESSION AND RESPONSE TO LIPID LOAD THAN PROLIFERATIVE HEPARG CELLS

Proliferative HepaRG cells were showed to be more susceptible to fatty acid load and the gut metabolites TMAO and PAA than differentiated HepaRG cells in this study. Interestingly, these findings were consistent with the described distinct gene expression

profile of HepaRG after differentiation. CYP3A4 expression was extremely increased in differentiated cells indicating that these cells perform better in xenobiotics removal.

Gerets *et al*. compared CYP3A4 expression from HepG2 and HepaRG cells. HepaRG cells presented CYP3A4 twenty times higher than the other hepatic cell line analysed (Gerets *et al*., 2012). Likewise, Aninat *et al*. measured the expression of a number of cytochrome P450 genes in differentiated HepaRG seeded at low and high densities. CYP3A4 was increased in high-density differentiated HepaRG cells (Aninat *et al.*, 2006). A study performed by Oeda *et al.* assessed the effect of 2% and 10% collagen coating in CYP3A4 expression of HepaRG cells. Intriguingly 2% collagen coating slightly increased CYP3A4 expression when compared to 10% coating (Oeda *et al.,* 2020). Collectively, the data supports that HepaRG is a unique cell line capable of expressing CYP3A4 at high levels. To this end, due to expressing CYP450 activity the HepaRG cell line is an appropriate alternative to primary hepatocytes. The CYP450 system in the liver plays a key role in drug metabolism. Fisher *et al.* found interesting data suggesting significant changes in hepatic P450 activity during progressive stages of NAFLD (Fisher *et al.,* 20019). Further studies could be done from a clinical perspective to speculate whether patients with CYP450 inhibition (e.g., by drugs) are more vulnerable to TMAO / PAA induced steatosis.

MRP2 is a hepatobiliary drug transporter responsible to conjugating xenobiotics to bile acids and eliminating them from the liver. MRP2 was downregulated in differentiated HepaRG cells, suggesting that the removal of components like TMAO and PAA do not occur via the bile acid route.

Furthermore, genes involved in fatty acid oxidation such as CPT1a and FXR were upregulated in differentiated cells in comparison to proliferative HepaRG cells. These results

enlighten why the HepaRG differentiation programme trigger cells to become more resistant to lipid build-up.

6.6 PROLIFERATIVE AND DIFFERENTIATED HEPARG CELLS PRESENT DISTINCT BIOENERGETIC PROFILES

The main difference observed in oxygen consumption between proliferative and differentiated HepaRG cultures was the lower rates presented by differentiated HepaRG cells (Figure 6.1). These findings are in accordance with Young & Young *et al*. who observed that HepaRG cells derived from proliferative and differentiated cultures showed unique bioenergetic parameters. HepaRG from proliferative cultures showed increased basal and ATP-linked respiration when compared to differentiated cells (Young & Young *et al*., 2019). Viale *et al.* noted that actively proliferating cancer cells demand mitochondrial respiration to continuously supply the high-energy molecules needed to maintain biologic pathways that enable proliferation (Viale *et al.*, 2014). Accordingly, Lewis *et al*. highlighted that in mammalian cells mitochondrial respiration is essential for rapid proliferation (Lewis *et al.,* 2014).

The reduced oxygen rates detected in cells after differentiation are equally observed in primary hepatocytes. Seki measured oxygen respiration in primary mouse hepatocytes using the XF24 analyser and mouse hepatocytes presented basal oxygen consumption rates of 100 pmol/min and maximal respiration of 200 pmol/min (Seki, 2016). In addition, Djafarzadeh *et al*. measured mitochondrial respiration in primary human hepatocytes and found basal respiration rates of 50 pmol/min (Djafarzadeh *et al*., 2012). Taken together these

results indicate that differentiated HepaRG cells present similar oxygen rates to primary hepatocytes as expected.

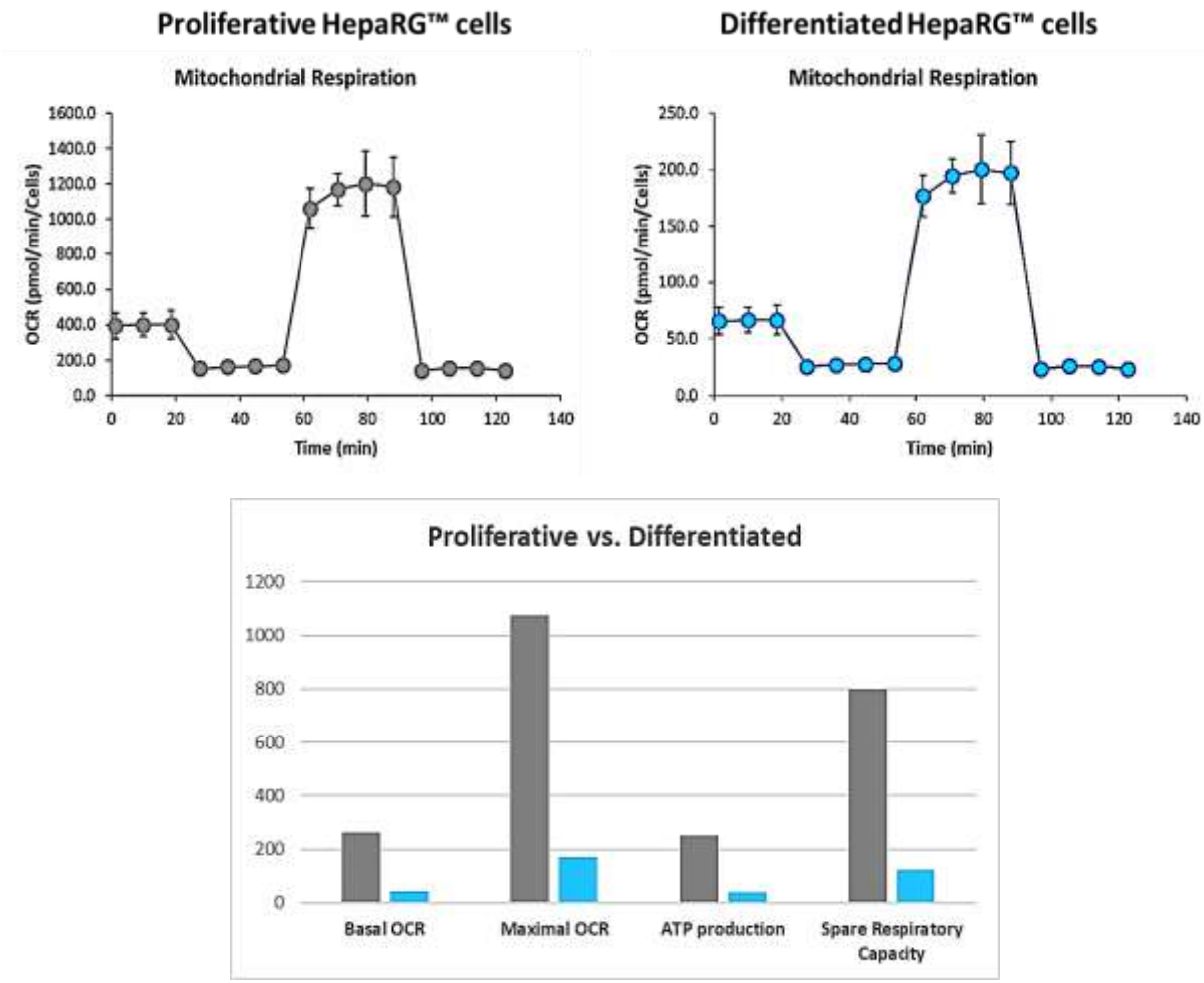

Figure 6.1. Comparison between bioenergetic profiles of proliferative and differentiated HepaRG cells. Results from representative Mito Stress tests (top). OCR measurements showing basal respiration, maximal respiration, ATP production and spare respiratory capacity. Data are presented as mean, n = 3.

6.7 GUT MICROBIOME METABOLITES ALTER MITOCHONDRIAL FUNCTION IN HEPARG CELLS

We observed that microbiome metabolites significantly altered mitochondrial function. The exposure to TMAO and PAA reduced maximal oxygen consumption, spare respiratory capacity and basal respiration in HepaRG cells. Various studies show evidence that there is a strong microbiome-mitochondria cross-talk, this communication between gut microbiome and host mitochondria during health and disease keeps rising as a major area of research (Han *et al*., 2019; Clark & Mach, 2017).

Liu *et al*. using *caenorhabditis elegans*, a transparent nematode worm, discovered that bacterial metabolites trigger a signalling cascade that modulates mitochondrial fission–fusion balance in the gut (Liu *et al*., 2019). Leschelle *et al*. demonstrated that bacteria metabolites inhibit cytochrome oxidase, one of the main complexes of the mitochondrial respiratory chain (Leschelle *et al.*, 2005). Moreover, Jiang *et al*. established that gut bacteria toxins lead to a deregulation of mitochondrial activity with increased ROS levels, and strong decrease in ATP levels (Jiang *et al*., 2012). A study published by MacFabe indicated that gut bacterial fermentation products induce mitochondrial dysfunction in the brain (MacFabe, 2012). Furthermore, Rodrigues *et al*. described the efficiency of two species of *Lactobacilli* in boosting hepatic mitochondria health leading to the improvement of lipid metabolism in high-fat fed mice (Rodrigues *et al.*, 2021). Microbiome-mitochondria cross-talk remains poorly understood and requires further investigation.

6.8 MITOCHONDRIAL DYSFUNCTION OCCURS PRIOR TO STEATOSIS IN HEPARG CELLS

Many questions remain about which "hit" occurs first triggering NAFLD development. An important finding in this study was that changes in mitochondrial function precede lipid accumulation. When HepaRG cells were exposed to fatty acids combined to TMAO and PAA for 24 hours no steatosis was established, however mitochondrial function began to decline.

Hepatic mitochondria are a major site of fatty acid β-oxidation; hence, it is consistent that lipids accumulate in hepatic cells in response to mitochondrial dysfunction (Figure 6.2).

Rector *et al*. published similar results in obese rats where a decrease in mitochondrial activity preceded steatosis. Reduced hepatic fatty acid oxidation and mitochondrial enzyme activity occurred prior to NAFLD onset; lowered hepatic mitochondrial function was present at 5 weeks of age, followed by hepatic steatosis by 8 weeks. NAFLD advanced to hepatocyte ballooning, fibrosis, inflammation, and elevated serum ALTs by 40 weeks of age (Rector *et al*., 2010). Nassir *et al.* described a mouse model with mitochondrial trifunctional protein knockout, mice with dysfunctional mitochondria developed NAFLD (Nassir *et al*., 2018).

Although the mechanisms responsible for NASH are still not fully elucidated, studies have shown that mitochondrial abnormalities are closely associated with NAFLD pathogenesis which raises the possibility that progression from healthy liver to steatosis or NASH is a mitochondrial disease (Serviddio *et al*., 2011). The mitochondrial abnormalities related to NAFLD include structural injury, depletion of mitochondrial DNA (mtDNA), reduced activity of respiratory chain complexes, and impaired mitochondrial β-oxidation. Abnormal morphology in liver mitochondria have been observed in patients and animal models with NASH (Pessayre & Fromenty, 2005). Electron microscopy revealed that mitochondria in NAFLD are swollen, limited in number, and present decreased matrix density. Liver biopsy of rats treated with

4,4'-diethylaminoethoxyhexestrol, a drug that inhibits mitochondrial respiratory chain activity and mitochondrial β-oxidation is associated with hepatic steatosis and steatohepatitis that is histologically indistinguishable from NAFLD in humans (Berson *et al*., 1998).

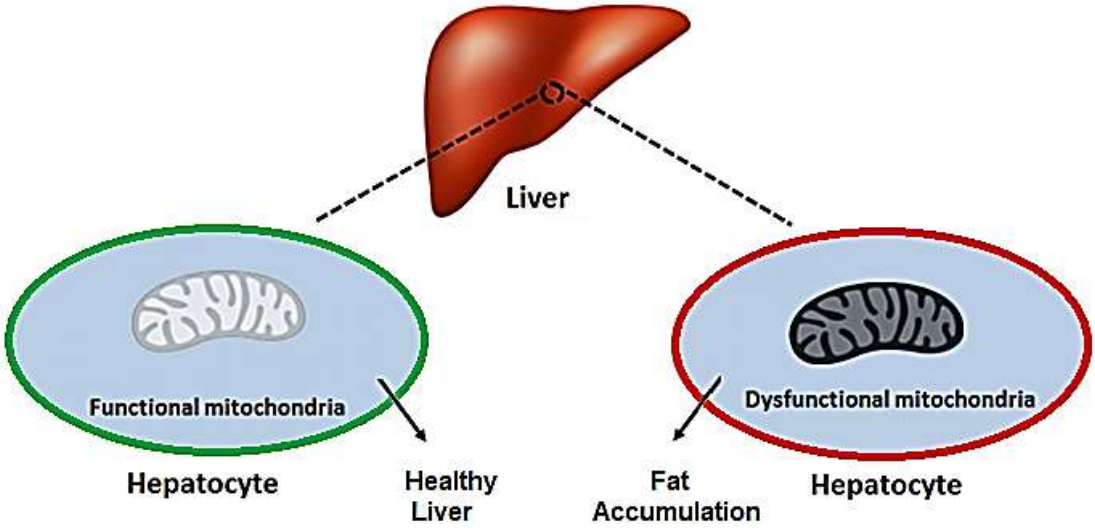

Figure 6.2. NAFLD/NASH as mitochondrial diseases. This study provided evidence that mitochondrial dysfunction occurs prior to hepatic accumulation. This finding strengthens the hypothesis of NAFLD and NASH being mitochondrial diseases.

6.9 MITOCHONDRIA AS A TARGET FOR NAFLD THERAPY

There are currently no approved therapies for the treatment of NALFD and NASH. Lifestyle changes and weight loss are essential for NAFLD therapy. A Mediterranean style diet is supported by some evidence, but which dietary factors and by which biological mechanisms this is of benefit are not well described (Yaskolka Meir *et al*., 2021). This study supports evidence that mitochondria is a promising target to treat these diseases. Accordingly, several

recent studies have been investigating specific agents targeting mitochondrial dysfunction for NAFLD therapy (Ajith, 2018).

Chacko *et al*. tested the effects of MitoQ, a mitochondria-targeted derivative of the antioxidant ubiquinone, with antioxidant and anti-apoptotic functions. MitoQ decreased hepatic steatosis in ethanol consuming animals but evidence in humans is still missing (Chacko *et al*., 2011). Likewise, Mao *et al*. examined the efficacy of MitoVit-E in thirty-two high-fat fed mice. MitoVit-E is a mitochondria-targeted antioxidant based on vitamin E. MitoVit-E upregulated CPT1a expression in the liver and inhibited hepatic fat deposition, suggesting that MitoVit-E is promising to treat NAFLD by enhancing mitochondrial fatty acid oxidation (Mao *et al*., 2010). Szeto-Schiller (SS) peptides are one of the most promising compounds for mitochondrial dysfunction. SS peptides selectively target the inner mitochondrial membrane, and it has been shown that SS prevents lipid peroxidation and inflammation being a good alternative for patients with NAFLD (Kelso *et al*., 2002). In addition, Rezazadeh *et al*. tested the effect of EUK-8 and 134 in rats with NASH. EUK-8 and 134 are salen manganese complexes that exhibit potent antioxidant activities. EUK-8 and EUK-134 reduced steatosis, ballooning degeneration and inflammation in liver of NASH rats without adverse effects (Rezazadeh *et al.*, 2012)

6.10 CONCLUSION

There is an urgent need for further understanding NAFLD and NASH pathogenesis. The gut metabolite hypothesis provides a mechanistic link to changes in microbiome and mitochondrial toxicity. One of our objectives was to develop a 3D cell culture model to study steatosis and mitochondrial bioenergetics in NASH. Unfortunately, lack of PHH viability, experimental variation, delivery of effectors and oxygen electrode sensitivity prevented the use of the Liverchip to interrogate TMAO and PAA in 3D during the time we had, therefore we performed our experiments in 2D cell culture. 2D cell culture holds many limitations and more robust NAFLD models are necessary.

This study investigated two different HepaRG cell populations. Differentiated HepaRG cells are a good model of 'healthy' hepatocytes with high capacity of clearing xenobiotics and showed to be resistant to steatosis and mitochondrial changes. Proliferative HepaRG cells were used as it is known that NASH patients present an overgrowth of liver progenitor cells, cells undergoing apoptosis and aged hepatocytes that display decreased CYP450 activity (Czerwinski *et al*., 2018).

This is the first time that a study assessed the effects of TMAO and PAA in mitochondrial bioenergetics in a steatosis model. This study provided crucial information to the hypothesis of NAFLD and NASH being mitochondrial diseases. Acquired data indicates that TMAO and PAA exacerbate hepatic lipid deposition by decreasing mitochondrial function.

Modulating the effects on mitochondrial bioenergetics mediated by microbiome derived metabolites is a promising target for NAFLD and NASH therapeutic intervention (Figure 6.3).

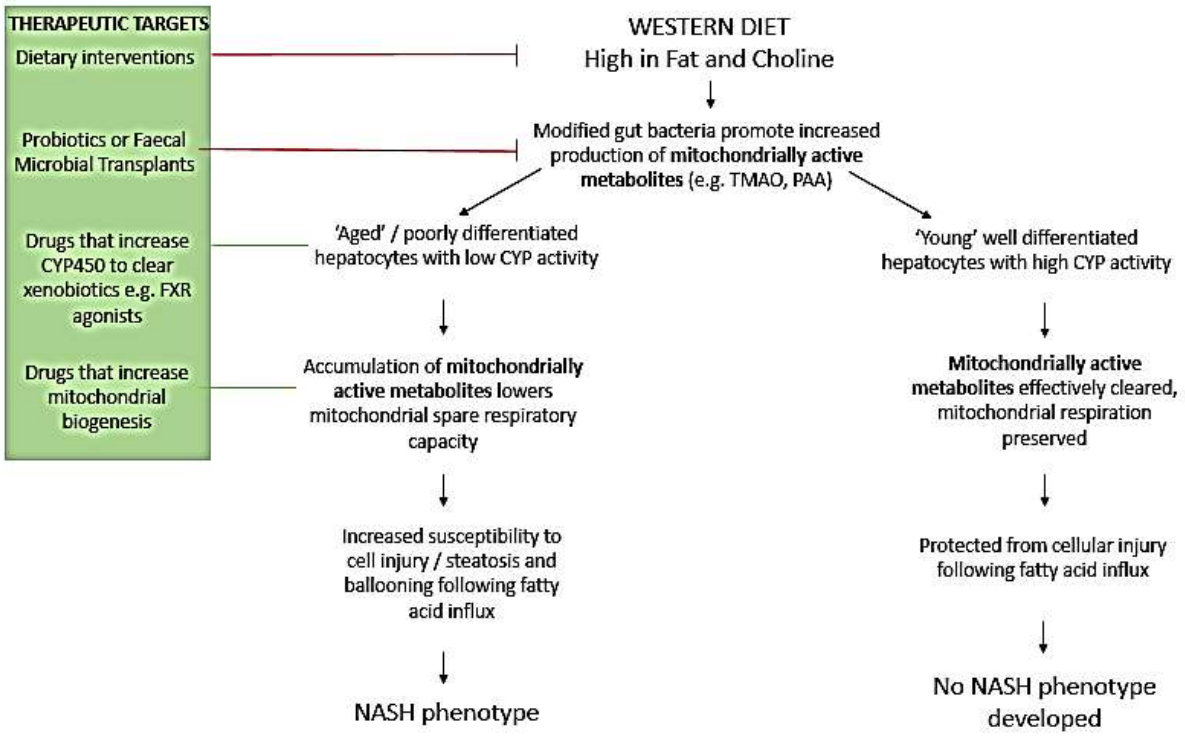

Figure 6.3. Poorly differentiated hepatocytes are susceptible to harmful effects of TMAO and PAA. TMAO and PAA exacerbate hepatic lipid accumulation by triggering mitochondrial dysfunction. Our findings suggest that drugs that increase CYP450 activity and drugs that enhance mitochondrial biogenesis are promising targets for NAFLD and NASH therapeutic intervention.

6.11 FUTURE WORK

Investigating TMAO and PAA association with NAFLD/NASH onset in a model that retains the complex physiological architecture of the liver is clearly needed. This study had interesting findings of the effects of TMAO and PAA in 2D cell culture but assessing the same effects in 3D remains a priority. As future work, we aim to interrogate the same research questions in other 3D models available. We will use precision cut liver slices to analyse the effects of TMAO and PAA in lipid deposition and mitochondrial bioenergetics (Palma *et al*.,

2019). In addition, co-culture models seem to be promising to better understand the link between gut microbiome and liver diseases. Liver organoids can be co-cultured with gut organoids to establish the direct link between the release of TMAO and PAA and the hepatic changes.

We intent to further explore the mechanistic links between TMAO and PAA and CYP450 metabolism by manipulating genes responsible for the clearance of xenobiotics, siRNA and CRISPR can be used to silence or knock-out genes such as CYP3A4.

Additionally, we aim to assess different NASH/NALFD therapeutic targets *in vivo*. Different trials can be performed in NAFLD patients with the purpose of ameliorating steatosis: dietary interventions where patients receive a diet low in TMAO and PAA, providing prebiotics and probiotics to patients to improve their gut microbiome composition and further investigating the effects of drugs that increase CYP450 activity and drugs that increase mitochondrial biogenesis in NAFLD patients.

BIBLIOGRAPHY

Abbasi J (2019). TMAO and Heart Disease: The New Red Meat Risk? JAMA.;321(22):2149–2151.

Ajith TA.(2018) Role of mitochondria and mitochondria-targeted agents in non-alcoholic fatty liver disease. Clin Exp Pharmacol Physiol. May;45(5):413-421.

Alisi, A., Panera, N., Agostoni, C. & Nobili, V. (2011) 'Intrauterine growth retardation and nonalcoholic Fatty liver disease in children'. Int J Endocrinol, 2011 pp. 269853.

Angulo, P., Kleiner, D. E., Dam-Larsen, S., Adams, L. A., Bjornsson, E. S., Charatcharoenwitthaya, P., Mills, P. R., Keach, J. C., Lafferty, H. D., Stahler, A., Haflidadottir, S. & Bendtsen, F. (2015) 'Liver Fibrosis, but No Other Histologic Features, Is Associated With Long-term Outcomes of Patients With Nonalcoholic Fatty Liver Disease'. Gastroenterology, 149 (2), pp. 389-397 e310.

Aninat C, Piton A, Glaise D, Le Charpentier T, Langouët S, Morel F, Guguen-Guillouzo C, Guillouzo A (2006). Expression of cytochromes P450, conjugating enzymes and nuclear receptors in human hepatoma HepaRG cells. Drug Metab Dispos. Jan;34(1):75-83.

Anstee, Q. M. & Day, C. P. (2015) 'The Genetics of Nonalcoholic Fatty Liver Disease: Spotlight on PNPLA3 and TM6SF2'. Semin Liver Dis, 35 (3), pp. 270-290.

Anstee, Q. M., McPherson, S. & Day, C. P. (2011) 'How big a problem is non-alcoholic fatty liver disease?'. BMJ, 343 pp. d3897.

Anthérieu S, Chesné C, Li R, Guguen-Guillouzo C, Guillouzo A (2012). Optimization of the HepaRG cell model for drug metabolism and toxicity studies. Toxicol In Vitro. Dec;26(8):1278-85.

Berson A, De Beco V, Lettéron P, Robin MA, Moreau C, El Kahwaji J, Verthier N, Feldmann G, Fromenty B, Pessayre D (1998). Steatohepatitis-inducing drugs cause mitochondrial dysfunction and lipid peroxidation in rat hepatocytes. Gastroenterology. Apr;114(4):764-74.

Boursier J, Mueller O, Barret M, Machado M, Fizanne L, Araujo-Perez F, Guy CD, Seed PC, Rawls JF, David LA, Hunault G, Oberti F, Calès P, Diehl AM (2016). The severity of nonalcoholic fatty liver disease is associated with gut dysbiosis and shift in the metabolic function of the gut microbiota. Hepatology. Mar;63(3):764-75.

Brand, M. D., & Nicholls, D. G. (2011). Assessing mitochondrial dysfunction in cells. The Biochemical journal, 435(2), 297–312.

Brunt, E. M., Kleiner, D. E., Wilson, L. A., Belt, P., Neuschwander-Tetri, B. A. & Network, N. C. R. (2011) 'Nonalcoholic fatty liver disease (NAFLD) activity score and the histopathologic diagnosis in NAFLD: distinct clinicopathologic meanings'. Hepatology, 53 (3), pp. 810-820.

Burton KJ, Krüger R, Scherz V, Münger LH, Picone G, Vionnet N, Bertelli C, Greub G, Capozzi F, Vergères G (2020). Trimethylamine-N-Oxide Postprandial Response in Plasma and Urine Is Lower After Fermented Compared to Non-Fermented Dairy Consumption in Healthy Adults. Nutrients. Jan 16;12(1):234.

Buzzetti E, Pinzani M, Tsochatzis EA (2016). The multiple-2d pathogenesis of non-alcoholic fatty liver disease (NAFLD). Metabolism. Aug;65(8):1038-48

Chacko, A. Kramer, Ravi, A. Benavides, Mitchell, P. Dranka, Ferrick, K. Singal, W. Ballinger, M. Bailey, W. Hardy, Zhang, Di Zhi, Darley-Usmar. (2014) The Bioenergetic Health Index: a new concept in mitochondrial translational research. Clin Sci (Lond) 1 September; 127.

Chacko, B. K., Srivastava, A., Johnson, M. S., Benavides, G. A., Chang, M. J., Ye, Y., Jhala, N., Murphy, M. P., Kalyanaraman, B., & Darley-Usmar, V. M. (2011). Mitochondria-targeted ubiquinone (MitoQ) decreases ethanol-dependent micro and macro hepatosteatosis. Hepatology (Baltimore, Md.), 54(1), 153–163.

Chalasani, N., Younossi, Z., Lavine, J. E., Charlton, M., Cusi, K., Rinella, M., Harrison, S. A., Brunt, E. M. & Sanyal, A. J. (2018) 'The diagnosis and management of nonalcoholic fatty liver disease: Practice guidance from the American Association for the Study of Liver Diseases'. Hepatology, 67 (1), pp. 328-357.

Chen MX, Wang SY, Kuo CH, Tsai IL (2019). Metabolome analysis for investigating host-gut microbiota interactions. J Formos Med Assoc. Mar;118 Suppl 1:S10-S22.

Chen, T., Li, R., & Chen, P. (2021). Gut Microbiota and Chemical-Induced Acute Liver Injury. Frontiers in physiology, 12, 688780.

Chen, Ym., Liu, Y., Zhou, Rf. et al (2016). Associations of gut-flora-dependent metabolite trimethylamine-N-oxide, betaine and choline with non-alcoholic fatty liver disease in adults. Sci Rep 6, 19076.

Clark A, Mach N (2017). The Crosstalk between the Gut Microbiota and Mitochondria during Exercise. Front Physiol. May 19;8:319.

Clarke, G., Stilling, R. M., Kennedy, P. J., Stanton, C., Cryan, J. F., & Dinan, T. G. (2014). Minireview: Gut microbiota: the neglected endocrine organ. Molecular endocrinology (Baltimore, Md.), 28(8), 1221–1238.

Corbin, D. R., Schwarz, S. & Sonnichsen, G. C. (1997) 'Methylamines synthesis: A review'. Catalysis Today, 37 (2), pp. 71-102.

Day, Christopher P (2011). Non-alcoholic fatty liver disease: a massive problem. Clinical Medicine Apr. 11 (2) 176-178.

Dehne, E. M., Hasenberg, T. & Marx, U. (2017) 'The ascendance of microphysiological systems to solve the drug testing dilemma'. Future Sci OA, 3 (2), pp. FSO185.

Delgado, J. S. (2008) 'Evolving trends in nonalcoholic fatty liver disease'. Eur J Intern Med, 19 (2), pp. 75-82.

Di Cocco S, Belloni L, Nunn ADG, Salerno D, Piconese S, Levrero M, Pediconi N (2019). Inducing and Characterizing Vesicular Steatosis in Differentiated HepaRG Cells. J Vis Exp. Jul 18;(149).

Divakaruni, A. S., Rogers, G. W., & Murphy, A. N. (2014). Measuring mitochondrial function in permeabilized cells using the seahorse XF analyzer or a clark-type oxygen electrode. Current protocols in toxicology, 60(1), 25-2.

Djafarzadeh S, Vuda M, Takala J, Jakob SM. Effect of remifentanil on mitochondrial oxygen consumption of cultured human hepatocytes. PLoS One. 2012;7(9):e45195.

Dufour JF, Caussy C, Loomba R (2020). Combination therapy for non-alcoholic steatohepatitis: rationale, opportunities and challenges. Gut. Oct;69(10):1877-1884.

Durand, François & Pavesi, Marco & Cheung, Ramsey. (2019). Liver transplantation for non-alcoholic steatohepatitis in Europe: Where do we stand?. Journal of Hepatology. 71.

Duval, K., Grover, H., Han, L. H., Mou, Y., Pegoraro, A. F., Fredberg, J. & Chen, Z. (2017) 'Modeling Physiological Events in 2D vs. 3D Cell Culture'. Physiology (Bethesda), 32 (4), pp. 266-277.

Dyson, J. K., Anstee, Q. M. & McPherson, S. (2014) 'Non-alcoholic fatty liver disease: a practical approach to diagnosis and staging'. Frontline Gastroenterol, 5 (3), pp. 211-218.

Edmondson, R., Broglie, J. J., Adcock, A. F. & Yang, L. (2014) 'Three-dimensional cell culture systems and their applications in drug discovery and cell-based biosensors'. Assay Drug Dev Technol, 12 (4), pp. 207-218.

Fazel, Y., Koenig, A. B., Sayiner, M., Goodman, Z. D. & Younossi, Z. M. (2016) 'Epidemiology and natural history of non-alcoholic fatty liver disease'. Metabolism, 65 (8), pp. 1017-1025.

Feng Li, Li Cao, Sweta Parikh, Rongjun Zuo. (2020) Three-Dimensional Spheroids With Primary Human Liver Cells and Differential Roles of Kupffer Cells in Drug-Induced Liver Injury, Journal of Pharmaceutical Sciences, Volume 109, Issue 6, Pages 1912-1923, ISSN 0022-3549.

Fennema, D., Phillips, I. R., & Shephard, E. A. (2016). Trimethylamine and Trimethylamine N-Oxide, a Flavin-Containing Monooxygenase 3 (FMO3)-Mediated Host-Microbiome Metabolic Axis Implicated in Health and Disease. Drug metabolism and disposition: the biological fate of chemicals, 44(11), 1839–1850.

Fey, S. J., & Wrzesinski, K. (2012). Determination of drug toxicity using 3D spheroids constructed from an immortal human hepatocyte cell line. Toxicological sciences : an official journal of the Society of Toxicology, 127(2), 403–411.

Fisher, J. Lickteig, M. Augustine, Ranger-Moore, P. Jackson, S. Ferguson and J. Cherrington (2009). Drug Metabolism and Disposition October 1, 37 (10) 2087-2094.

Ganz, M., Bukong, T. N., Csak, T., Saha, B., Park, J. K., Ambade, A., Kodys, K. & Szabo, G. (2015) 'Progression of non-alcoholic steatosis to steatohepatitis and fibrosis parallels cumulative accumulation of danger signals that promote inflammation and liver tumors in a high fat-cholesterol-sugar diet model in mice'. J Transl Med, 13 pp. 193.

Gerets, H. H., Tilmant, K., Gerin, B., Chanteux, H., Depelchin, B. O., Dhalluin, S., & Atienzar, F. A. (2012). Characterization of primary human hepatocytes, HepG2 cells, and HepaRG cells at the mRNA level and CYP activity in response to inducers and their predictivity for the detection of human hepatotoxins. Cell biology and toxicology, 28(2), 69–87.

Hagström H, Nasr P, Ekstedt M, Kechagias S, Stål P, Bedossa P, Hultcrantz R (2017). SAF score and mortality in NAFLD after up to 41 years of follow-up. Scand J Gastroenterol. Jan;52(1):87-91.

Han, B., Lin, C. J., Hu, G., & Wang, M. C. (2019). 'Inside Out'- a dialogue between mitochondria and bacteria. The FEBS journal, 286(4), 630–641.

Hoyles L, Fernández-Real JM, Federici M, Serino M, Abbott J, Charpentier J, Heymes C, Luque JL, Anthony E, Barton RH, Chilloux J, Myridakis A, Martinez-Gili L, Moreno-Navarrete JM, Benhamed F, Azalbert V, Blasco-Baque V, Puig J, Xifra G, Ricart W, Tomlinson C, Woodbridge M, Cardellini M, Davato F, Cardolini I, Porzio O, Gentileschi P, Lopez F, Foufelle F, Butcher SA, Holmes E, Nicholson JK, Postic C, Burcelin R, Dumas ME (2018). Molecular phenomics and metagenomics of hepatic steatosis in non-diabetic obese women. Nat Med. Jul;24(7):1070-1080.

Ibrahim, S. H., Hirsova, P. & Gores, G. J. (2018) 'Non-alcoholic steatohepatitis pathogenesis: sublethal hepatocyte injury as a driver of liver inflammation'. Gut, 67 (5), pp. 963-972.

Ingelman-Sundberg, M, Lauschke, VM (2021). 3D human liver spheroids for translational pharmacology and toxicology. Basic Clin Pharmacol Toxicol.; 00: 1– 11.

Janeiro, M. H., Ramírez, M. J., Milagro, F. I., Martínez, J. A., & Solas, M. (2018). Implication of Trimethylamine N-Oxide (TMAO) in Disease: Potential Biomarker or New Therapeutic Target. Nutrients, 10(10), 1398.

Jankowski J, van der Giet M, Jankowski V, Schmidt S, Hemeier M, Mahn B, Giebing G, Tolle M, Luftmann H, Schluter H, Zidek W, Tepel M (2003). Increased plasma phenylacetic acid in patients with end-stage renal failure inhibits iNOS expression. J Clin Invest. Jul;112(2):256-64.

Jastroch, M., Divakaruni, A. S., Mookerjee, S., Treberg, J. R., & Brand, M. D. (2010). Mitochondrial proton and electron leaks. Essays in biochemistry, 47, 53–67.

Jiang JH, Tong J, Gabriel K (2012). Hijacking mitochondria: bacterial toxins that modulate mitochondrial function. IUBMB Life. May;64(5):397-401.

Kanuri, G. & Bergheim, I. (2013) 'In vitro and in vivo models of non-alcoholic fatty liver disease (NAFLD)'. Int J Mol Sci, 14 (6), pp. 11963-11980.

Kaur, G. & Dufour, J. M. (2012) 'Cell lines: Valuable tools or useless artifacts'. Spermatogenesis, 2 (1), pp. 1-5.

Kelso GF, Porteous CM, Hughes G, Ledgerwood EC, Gane AM, Smith RA, Murphy MP (2002). Prevention of mitochondrial oxidative damage using targeted antioxidants. Ann N Y Acad Sci. Apr;959:263-74.

Kenwood BM, Weaver JL, Bajwa A, Poon IK, Byrne FL, Murrow BA, Calderone JA, Huang L, Divakaruni AS, Tomsig JL, Okabe K, Lo RH, Cameron Coleman G, Columbus L, Yan Z, Saucerman JJ, Smith JS, Holmes JW, Lynch KR, Ravichandran KS, Uchiyama S, Santos WL, Rogers GW,

Okusa MD, Bayliss DA, Hoehn KL (2013). Identification of a novel mitochondrial uncoupler that does not depolarize the plasma membrane. Mol Metab. Nov 28;3(2):114-23.

Kostrzewski, T., Cornforth, T., Snow, S. A., Ouro-Gnao, L., Rowe, C., Large, E. M. & Hughes, D. J. (2017) 'Three-dimensional perfused human in vitro model of non-alcoholic fatty liver disease'. World J Gastroenterol, 23 (2), pp. 204-215.

Kozyra, M., Johansson, I., Nordling, Å. et al (2018). Human hepatic 3D spheroids as a model for steatosis and insulin resistance. Sci Rep 8, 14297.

Kwon B, Lee HK, Querfurth HW (2014). Oleate prevents palmitate-induced mitochondrial dysfunction, insulin resistance and inflammatory signaling in neuronal cells. Biochim Biophys Acta.Jul;1843(7):1402-13.

Lau, J. K., Zhang, X. & Yu, J. (2017) 'Animal models of non-alcoholic fatty liver disease: current perspectives and recent advances'. J Pathol, 241 (1), pp. 36-44.

Le Roy, T., Llopis, M., Lepage, P., Bruneau, A., Rabot, S., Bevilacqua, C., Martin, P., Philippe, C., Walker, F., Bado, A., Perlemuter, G., Cassard-Doulcier, A. M. & Gerard, P. (2013) 'Intestinal microbiota determines development of non-alcoholic fatty liver disease in mice'. Gut, 62 (12), pp. 1787-1794.

Leschelle X, Goubern M, Andriamihaja M, Blottière HM, Couplan E, Gonzalez-Barroso MD, Petit C, Pagniez A, Chaumontet C, Mignotte B, Bouillaud F, Blachier F (2005). Adaptative metabolic response of human colonic epithelial cells to the adverse effects of the luminal compound sulfide. Biochim Biophys Acta Sep 15;1725(2):201-12.

Lewis, C.A., Parker, S.J., Fiske, B.P., McCloskey, D., Gui, D.Y., Green, C.R., Vokes, N.I., Feist, A.M., Vander Heiden, M.G., and Metallo, C.M. (2014). Tracing compartmentalized NADPH metabolism in the cytosol and mitochondria of mammalian cells. Molecular cell 55, 253-263.

Lin, J. K. & Ho, Y. S. (1992) 'Hepatotoxicity and hepatocarcinogenicity in rats fed squid with or without exogenous nitrite'. Food Chem Toxicol, 30 (8), pp. 695-702.

Liu, P., Li, D., Li, W., & Wang, D. (2019). Mitochondrial unfolded protein response to microgravity stress in nematode Caenorhabditis elegans. Scientific reports, 9(1), 1-9.

Lombardo, M.; Aulisa, G.; Marcon, D.; Rizzo, G.; Tarsisano, M.G.; Di Renzo, L.; Federici, M.; Caprio, M.; De Lorenzo, A (2021). Association of Urinary and Plasma Levels of Trimethylamine N-Oxide (TMAO) with Foods. Nutrients, 13, 1426.

Macfabe D. F. (2012). Short-chain fatty acid fermentation products of the gut microbiome: implications in autism spectrum disorders. Microbial ecology in health and disease, 23, 10.3402/mehd.v23i0.19260.

Magee N, Zou A, Zhang Y (2016). Pathogenesis of Nonalcoholic Steatohepatitis: Interactions between Liver Parenchymal and Nonparenchymal Cells. Biomed Res Int.5170402.

Mahdieh, A F (2020). Gut microbiota-dependent trimethylamine N-oxide and all-cause mortality: Findings from an updated systematic review and meta-analysis, Nutrition, Volume 78, 110856, ISSN 0899-9007.

Mao G, Kraus GA, Kim I, Spurlock ME, Bailey TB, Zhang Q, Beitz DC (2010). A mitochondria-targeted vitamin E derivative decreases hepatic oxidative stress and inhibits fat deposition in mice. J Nutr. Aug;140(8):1425-31.

Marchetti, P, Fovez, Q, Germain, N, Khamari, R, Kluza, J (2020). Mitochondrial spare respiratory capacity: Mechanisms, regulation, and significance in non-transformed and cancer cells. The FASEB Journal. 34: 13106– 13124.

Marion MJ, Hantz O, Durantel D (2010). The HepaRG cell line: biological properties and relevance as a tool for cell biology, drug metabolism, and virology studies. Methods Mol Biol.640:261-72.

Marra, F. & Svegliati-Baroni, G. (2018) 'Lipotoxicity and the gut-liver axis in NASH pathogenesis'. J Hepatol, 68 (2), pp. 280-295.

Metaboprolife: Absolute quantitative detection of TMAO is coming. Available at https://metaboprofile.biomart.cn/news/2972685.htm (Accessed: 11.01.2021).

Miele, L., Valenza, V., La Torre, G., Montalto, M., Cammarota, G., Ricci, R., Masciana, R., Forgione, A., Gabrieli, M. L., Perotti, G., Vecchio, F. M., Rapaccini, G., Gasbarrini, G., Day, C. P. & Grieco, A. (2009) 'Increased intestinal permeability and tight junction alterations in nonalcoholic fatty liver disease'. Hepatology, 49 (6), pp. 1877-1887.

Misra A, Khurana L (2008). Obesity and the metabolic syndrome in developing countries. J Clin Endocrinol Metab. 93:S9-30.

Nassir F, Arndt JJ, Johnson SA, Ibdah JA (2018). Regulation of mitochondrial trifunctional protein modulates nonalcoholic fatty liver disease in mice. J Lipid Res. Jun;59(6):967-973.

Nassir, F. & Ibdah, J. A. (2014) 'Role of mitochondria in nonalcoholic fatty liver disease'. Int J Mol Sci, 15 (5), pp. 8713-8742.

Neuschwander-Tetri, B. A. (2010) 'Hepatic lipotoxicity and the pathogenesis of nonalcoholic steatohepatitis: the central role of nontriglyceride fatty acid metabolites'. Hepatology, 52 (2), pp. 774-788.

Nunn, A., Scopigno, T., Pediconi, N. et al (2016). The histone deacetylase inhibiting drug Entinostat induces lipid accumulation in differentiated HepaRG cells. Sci Rep 6, 28025.

O'Hara et al. (2020). Cost of non-alcoholic steatohepatitis in Europe and the USA: The GAIN study. JHEP reports : innovation in hepatology, 2(5), 100142.

Onzi G, Moretti F, Balbinot SS, Balbinot RA, Soldera J (2019). Hepatocellular carcinoma in non-alcoholic fatty liver disease with and without cirrhosis. Hepatoma Res ;5:7.

Oeda, K., Kubiura-Ichimaru, M., Tsuji, S., Okuyama, S., Yamashita, M., Mine, A., Kawamura, F., Ueyama, T., & Tada, M. (2020). A two-dimensional multiwell cell culture method for the production of CYP3A4-expressing hepatocyte-like cells from HepaRG cells. Pharmacology research & perspectives, 8(5), e00652.

Ortega-Prieto, A. M., Skelton, J. K., Wai, S. N., Large, E., Lussignol, M., Vizcay-Barrena, G., Hughes, D., Fleck, R. A., Thursz, M., Catanese, M. T. & Dorner, M. (2018) '3D microfluidic liver cultures as a physiological preclinical tool for hepatitis B virus infection'. Nat Commun, 9 (1), pp. 682.

Osellame, L. D., Blacker, T. S. & Duchen, M. R. (2012) 'Cellular and molecular mechanisms of mitochondrial function'. Best Pract Res Clin Endocrinol Metab, 26 (6), pp. 711-723.

P. León-Mimila, H. Villamil-Ramírez, X.S. Li, D.M. Shih, S.T. Hui, E. Ocampo-Medina, B. López-Contreras, S. Morán-Ramos, M. Olivares-Arevalo, P. Grandini-Rosales, L. Macías-Kauffer, I. González-González, R. Hernández-Pando, F. Gómez-Pérez, F. Campos-Pérez, C. Aguilar-Salinas, E. Larrieta-Carrasco, T. Villarreal-Molina, Z. Wang, A.J. Lusis, S.L. Hazen, A. Huertas-Vazquez, S. Canizales-Quinteros (2021). Trimethylamine N-oxide levels are associated with NASH in obese subjects with type 2 diabetes, Diabetes & Metabolism, Volume 47, Issue 2, 101183.

Paish HL, Reed LH, Brown H, Bryan MC, Govaere O, Leslie J, Barksby BS, Garcia Macia M, Watson A, Xu X, Zaki MYW, Greaves L, Whitehall J, French J, White SA, Manas DM, Robinson SM, Spoletini G, Griffiths C, Mann DA, Borthwick LA, Drinnan MJ, Mann J, Oakley F (2019). A Bioreactor Technology for Modeling Fibrosis in Human and Rodent Precision-Cut Liver Slices. Hepatology.Oct;70(4):1377-1391.

Palma, E., Doornebal, E. & Chokshi, S (2019). Precision-cut liver slices: a versatile tool to advance liver research. Hepatol Int 13, 51–57.

Pant A, Rondini EA, Kocarek TA (2019). Farnesol induces fatty acid oxidation and decreases triglyceride accumulation in steatotic HepaRG cells. Toxicol Appl Pharmacol. Feb 15;365:61-70.

Pessayre D, Fromenty B (2005). NASH: a mitochondrial disease. J Hepatol. Jun;42(6):928-40.

Pheasant, H (2019). Understanding NAFLD Referral Pathways in the UK and Ireland. PHAST Associates Meeting.

Popkin, B. M., Adair, L. S., & Ng, S. W. (2012). Global nutrition transition and the pandemic of obesity in developing countries. Nutrition reviews, 70(1), 3–21.

Prior N, Inacio P, Huch M (2019). Liver organoids: from basic research to therapeutic applications. Gut. Dec;68(12):2228-2237.

Rector RS, Thyfault JP, Uptergrove GM, Morris EM, Naples SP, Borengasser SJ, Mikus CR, Laye MJ, Laughlin MH, Booth FW, Ibdah JA (2010). Mitochondrial dysfunction precedes insulin

resistance and hepatic steatosis and contributes to the natural history of non-alcoholic fatty liver disease in an obese rodent model. J Hepatol. May;52(5):727-36

Rezazadeh A, Yazdanparast R, Molaei M (2012). Amelioration of diet-induced nonalcoholic steatohepatitis in rats by Mn-salen complexes via reduction of oxidative stress. J Biomed Sci. Feb 29;19(1):26.

Rinella, M. E. (2015) 'Nonalcoholic fatty liver disease: a systematic review'. JAMA, 313 (22), pp. 2263-2273.

Rodrigues, R.R., Gurung, M., Li, Z. et al (2021). Transkingdom interactions between Lactobacilli and hepatic mitochondria attenuate western diet-induced diabetes. Nat Commun 12, 101.

Roncal, C., Martínez-Aguilar, E., Orbe, J. et al (2019). Trimethylamine-N-Oxide (TMAO) Predicts Cardiovascular Mortality in Peripheral Artery Disease. Sci Rep 9, 15580.

Schattenberg, J.M., Ekstedt, M (2019). Assessing the disease burden of non-alcoholic fatty liver disease in the real world – big data and big numbers. BMC Med 17, 123.

Schulz H (1991). Beta oxidation of fatty acids, Biochimica et Biophysica Acta (BBA) - Lipids and Lipid Metabolism, Volume 1081, Issue 2, Pages 109-120.

'Seahorse XF Analyzers'. (2018). [Online]. Available at: https://www.agilent.com/en/products/cell-analysis/seahorse-analyzers (Accessed: 21.04.2021).

Seki E (2016). HEDGEHOG Signal in hepatocytes mediates macrophage recruitment: A new mechanism and potential therapeutic target for fatty liver disease. Hepatology. Apr;63(4):1071-3

Serviddio G, Bellanti F, Vendemiale G, Altomare E (2011). Mitochondrial dysfunction in nonalcoholic steatohepatitis. Expert Rev Gastroenterol Hepatol. Apr;5(2):233-44.

Seyfried,Thomas N. Gabriel Arismendi-Morillo, Purna Mukherjee, Christos Chinopoulos (2020). On the Origin of ATP Synthesis in Cancer, iScience, Volume 23, Issue 11, 101761, ISSN 2589-0042.

Singh, R. K., Chang, H. W., Yan, D., Lee, K. M., Ucmak, D., Wong, K., Abrouk, M., Farahnik, B., Nakamura, M., Zhu, T. H., Bhutani, T., & Liao, W. (2017). Influence of diet on the gut microbiome and implications for human health. Journal of translational medicine, 15(1), 73.

Takahashi, Y., Soejima, Y. & Fukusato, T. (2012) 'Animal models of nonalcoholic fatty liver disease/nonalcoholic steatohepatitis'. World J Gastroenterol, 18 (19), pp. 2300-2308.

Tan X, Liu Y, Long J, Chen S, Liao G, Wu S, Li C, Wang L, Ling W, Zhu H (2019). Trimethylamine N-Oxide Aggravates Liver Steatosis through Modulation of Bile Acid Metabolism and Inhibition of Farnesoid X Receptor Signaling in Nonalcoholic Fatty Liver Disease. Mol Nutr Food Res.

Tang, W. H., Kitai, T., & Hazen, S. L. (2017). Gut Microbiota in Cardiovascular Health and Disease. Circulation research, 120(7), 1183–1196.

Tateishi, R. & Koike, K. (2017) 'Epidemiology and risk factors of nonalcoholic fatty liver disease (NAFLD) and nonalcoholic steatohepatitis (NASH)'. Nihon Shokakibyo Gakkai Zasshi, 114 (5), pp. 813-818.

Turnbaugh PJ, Bäckhed F, Fulton L, Gordon JI (2008). Diet-induced obesity is linked to marked but reversible alterations in the mouse distal gut microbiome. Cell Host Microbe. Apr 17;3(4):213-23.

Usmar, Darley Victor (2015). Cellular Bioenergetics as a Predictor of Diabetic Nephropathy. Diabetic Complications Consortium Report 2015.

Van Herck, M. A., Vonghia, L. & Francque, S. M. (2017) 'Animal Models of Nonalcoholic Fatty Liver Disease-A Starter's Guide'. Nutrients, 9 (10).

Vayalil P. K. (2019). Mitochondrial oncobioenergetics of prostate tumorigenesis. Oncology letters, 18(5), 4367–4376.

Viale, A., Pettazzoni, P., Lyssiotis, C. et al (2014). Oncogene ablation-resistant pancreatic cancer cells depend on mitochondrial function. Nature 514, 628–632.

Wagner, A.O., Prem, E.M., Markt, R. et al (2019). Formation of phenylacetic acid and phenylpropionic acid under different overload conditions during mesophilic and thermophilic anaerobic digestion. Biotechnol Biofuels 12, 26.

Wan H T, Y.G. Zhao, X. Wei, K.Y. Hui, J.P. Giesy, Chris K.C. Wong (2012). PFOS-induced hepatic steatosis, the mechanistic actions on β-oxidation and lipid transport, Biochimica et Biophysica Acta (BBA) - General Subjects, Volume 1820, Issue 7.

Wieland, A., Frank, D.N., Harnke, B. and Bambha, K. (2015), Systematic review: microbial dysbiosis and nonalcoholic fatty liver disease. Aliment Pharmacol Ther, 42: 1051-1063.

Williams, R. & Taylor-Robinson, S. D. (2016) Clinical Dilemmas in Non-Alcoholic Fatty Liver Disease.

Williamson, R. M., Price, J. F., Glancy, S., Perry, E., Nee, L. D., Hayes, P. C., Frier, B. M., Van Look, L. A., Johnston, G. I., Reynolds, R. M., Strachan, M. W. & Edinburgh Type 2 Diabetes Study, I. (2011) 'Prevalence of and risk factors for hepatic steatosis and nonalcoholic Fatty liver disease in people with type 2 diabetes: the Edinburgh Type 2 Diabetes Study'. Diabetes Care, 34 (5), pp. 1139-1144.

Wilson, D. F. (2017) 'Oxidative phosphorylation: unique regulatory mechanism and role in metabolic homeostasis'. J Appl Physiol (1985), 122 (3), pp. 611-619.

Wu, M., Neilson, A., Swift, A. L., Moran, R., Tamagnine, J., Parslow, D., Armistead, S., Lemire, K., Orrell, J., Teich, J., Chomicz, S. & Ferrick, D. A. (2007) 'Multiparameter metabolic analysis reveals a close link between attenuated mitochondrial bioenergetic function and enhanced glycolysis dependency in human tumor cells'. Am J Physiol Cell Physiol, 292 (1), pp. C125-136.

Yaskolka Meir A, Rinott E, Tsaban G, et al (2021). Effect of green-Mediterranean diet on intrahepatic fat: the DIRECT PLUS randomised controlled trial, Gut.

Young CKJ, Young MJ (2019). Comparison of HepaRG cells following growth in proliferative and differentiated culture conditions reveals distinct bioenergetic profiles. Cell Cycle. Feb;18(4):476-499.

Younossi, Z., Anstee, Q. M., Marietti, M., Hardy, T., Henry, L., Eslam, M., George, J. & Bugianesi, E. (2018) 'Global burden of NAFLD and NASH: trends, predictions, risk factors and prevention'. Nat Rev Gastroenterol Hepatol, 15 (1), pp. 11-20.

Yuzefovych L, Wilson G, Rachek L (2010). Different effects of oleate vs. palmitate on mitochondrial function, apoptosis, and insulin signaling in L6 skeletal muscle cells: role of oxidative stress. Am J Physiol Endocrinol Metab. Dec;299(6):E1096-105.

Zelber-Sagi, S., Ivancovsky-Wajcman, D., Fliss Isakov, N., Webb, M., Orenstein, D., Shibolet, O. & Kariv, R. (2018) 'High red and processed meat consumption is associated with non-alcoholic fatty liver disease and insulin resistance'. J Hepatol, 68 (6), pp. 1239-1246.

Zhang, D. Y., Zhu, L., Liu, H. N., Tseng, Y. J., Weng, S. Q., Liu, T. T., Dong, L., & Shen, X. Z. (2019). The protective effect and mechanism of the FXR agonist obeticholic acid via targeting gut microbiota in non-alcoholic fatty liver disease. Drug design, development and therapy, 13, 2249–2270.

Zhu, L., Baker, S. S., Gill, C., Liu, W., Alkhouri, R., Baker, R. D., & Gill, S. R. (2013). Characterization of gut microbiomes in nonalcoholic steatohepatitis (NASH) patients: a connection between endogenous alcohol and NASH. Hepatology, 57(2), 601-609.

Zhu W, Buffa JA, Wang Z, Warrier M, Schugar R, Shih DM, Gupta N, Gregory JC, Org E, Fu X, Li L, DiDonato JA, Lusis AJ, Brown JM, Hazen SL (2018). Flavin monooxygenase 3, the host hepatic enzyme in the metaorganismal trimethylamine N-oxide-generating pathway, modulates platelet responsiveness and thrombosis risk. J Thromb Haemost. Sep;16(9):1857-1872.

APPENDIX

HONOURS & AWARDS

1st place winner three-minute thesis competition

University of Plymouth, 2019

Best Poster Presentation Prize at Plymouth Annual Research Event

University of Plymouth, 2019

PhD Studentship

Plymouth University Peninsula Schools of Medicine and Dentistry, 2017

CONFERENCE PRESENTATIONS

BASL Basic Science Meeting, Seale Hayne Conference centre, Devon, June 2017: Developing a 3D cell culture model for progression to non-alcoholic steatohepatitis. Paula Boeira, Daniel Felmlee, Doha Hegazy, Matthew Cramp, Charles Affourtit, David Sheridan - Oral presentation

BASL Basic Science Meeting, The Hayes Conference Centre, Derbyshire, June 2019: Investigation of microbiome metabolites and mitochondrial function in non-alcoholic steatohepatitis. Paula Boeira, Daniel Felmlee, Matthew Cramp, Charles Affourtit, David Sheridan – Oral presentation

10th World Congress on Targeting Mitochondria in Berlin, October 2019: Investigation of microbiome metabolites and mitochondrial function in non-alcoholic steatohepatitis. Paula Boeira, Daniel Felmlee, Charles Affourtit, David Sheridan – Oral presentation

European Association for the Study of the Liver meeting - August 2020: Boeira P, Affourtit C, Felmlee D, Sheridan D. Investigation of microbiome metabolites and mitochondrial function in non-alcoholic fatty liver disease. Journal of Hepatology: vol 73 Suppl. 1, Aug 2020 – Poster